Inorganic Chemistry Laboratory

Department of Chemistry

University of Oxford

Solid Acid Zeolite Catalysts for Benzene/ Ethylene Alkylation Reactions

A Thesis Submitted for the Degree of

Master of Science (by research), 2011

Saud Aldrees

Pembroke College, Oxford




بسم الله الرحمن الرحيم

Dedication

In the name of Allah, most merciful, most gracious

I would like to dedicate this work to,

The spirit of my father (God have mercy), who was the first to encourage and support me in my life.

My dear beloved mother, may Allah preserves her, who was praying Allah for me every day.

All my brothers and sisters, who have always encouraged and supported me for my further study.

Lastly, I dedicate this work to my beloved wife, who provides me with unlimited care, support and encouragement to achieve my goal and success; and to my dearest children Abdulaziz and Ashry who have suffered as a result of me not spending sufficient time with them during the period of my study.

Acknowledgements

All the praise goes to Allah for his generous blessings, without which I would not have completed this work.

I gratefully acknowledge to his highness Dr. Turki bin Saud bin Mohammad Al-Saud the vice president for research institutes at King Abdulaziz City for Science and Technology (KACST), for his unlimited encouragement and support during my study.

My utmost deep and sincere gratitude to Prof. Peter P. Edwards, my supervisor, teacher and friend. I have learnt a lot from you, from your intelligence, creativity, patience and attention to detail. Thanks for your invaluable support and encouragement since day one in Oxford. I am grateful to have been part of your group, working amongst dedicated scientists, in an excellent scientific environment of learning and exchange. I thank you for the confidence you have in me and in the work I do. Thank you very much Prof. Peter for one of a kind supervision.

I like to express my gratitude and thanks to Dr. Hamid Almegren the director of petrochemical institute at KACST, who generously gave me this chance to complete my studies.

I would like to thank Dr. Tiancun Xiao for his support, helpful discussions and for his encouragement during my study.

I am grateful for the invaluable help of Dr. Mohammad Alkinany, and for all his advice, support and guidance.

Special thanks go to Dr. Asel Sartbaeva. She spent many hours introducing me to zeolite structure and characterization. Thanks for sharing with me your knowledge and experience.

I would like also to thank Dr. Martin Jones, Dr. Vladimir Kuznetsov and Dr. Liam France for their support and helpful discussions.

Thanks to our NMR specialist Dr. Nick Rees and Dr. David Apperley (Durham University), for their help with the MAS NMR measurements.

Thanks to all the member of the Edward's group for many interesting discussions.

Finally, I would like to thank my family, my wife and my children, for giving me love, happiness and joy; and for their endless support, encouragement and patience; the "thank you" word does not express this enough.

Many thanks to all again and to Oxford, where all this has happened!

Saud, Oxford
November 2011

Abstract

Alkylation of benzene with ethylene to ethylbenzene is widely used in the petrochemical industry. Ethylbenzene is an important raw material in the petrochemical industry. It is used as feedstock for the production of styrene, an important material for plastic and rubber production [12,43,48,51,66].

The conventional catalyst for this alkylation process is $AlCl_3$, which still accounts for 24% of the worldwide ethylbenzene production in 2009 [8,12,49].

As utilization of this catalyst involves problems of separation, handling, safety and corrosion, immense efforts have been devoted to the development of new catalysts for ethylbenzene production [8,12,45].

Compared with $AlCl_3$, zeolites possess advantages in easy separation, low corrosion, high surface area as well as uniform microporous structure coupled to shape selectivity, and thus they are better acidic catalysts when applied in petrochemical industry [11,40].

In this thesis, zeolite catalysts based on Y, ZSM-5 and HBeta were prepared and characterized by several techniques (XRD, MAS NMR, BET and SEM). The catalytic performance of these zeolite catalysts has been studied in benzene/ethylene alkylation reaction in a gas phase using fixed bed reactor at reaction temperature of 250ºC and a 5 bar pressure with a 0.5 h^{-1} ethylene space velocity (WHSV) and different benzene to ethylene feed ratio. The products were identified by GC/MS and quantified by gas chromatography.

These studies highlight the importance of ion-exchange with rare earth cations as a powerful method to control the local structural and catalytic properties of zeolites, and also to enhance the acid properties upon rare earth exchange.

Most notable is the significant enhancement in product selectivity – viz, ethylbenzene selectivity- for La and Ce ion-exchanged HZSM-5 zeolite catalysts, showing a 30% + increase in selectivity for the alkylation reaction after rare-earth ion exchange.

This work done at KACST-Oxford Petrochemical Research Center (KOPRC) in the Inorganic Chemistry Laboratory, Oxford Universiry.

Table of contents

Dedication ……..…….. iii

Acknowledgements ……..…… iv

Abstract …… vi

Table of contents …… viii

List of figures …….. xi

List of tables ……..…….. xiv

Abbreviations ……. xv

Chapter One: Introduction ……..…….. 1

1.1 Preface …….…… 1

1.2 Solid acid catalysts ……..…….…….. 2

1.3 Zeolites ……..…… 4

1.3.1 What is a zeolite? …… 4

1.3.2 Zeolites properties ……. 5

1.3.3 Zeolites structures ……..…… 5

1.3.4 Zeolites applications …….. 7

1.4 Alkylation of aromatics ……..…… 10

1.4.1 Alkylation of benzene with ethylene ……..…….. 10

1.4.2 Importance of ethylbenzene …….. 12

1.4.3 World demand and capacities of ethylbenzene ……...…. 13

1.5 Aim of thesis …….…… 14

Chapter Two: Characterization and analytical techniques ....…..… 15

2.1 Characterization of zeolite catalysts ……. 15

2.1.1 Solid state nuclear magnetic resonance (SSNMR) ……... 18

2.1.2 X-ray powder diffraction (XRD) ……. 20

2.1.3 Scanning electron microscope …..…… 22

2.1.4 Nitrogen physisorption …… 24

2.2 Product analysis ……...… 24

2.2.1 Gas chromatography (GC) …….. 26

2.2.2 Gas chromatography/mass spectrometry (GC/MS) ….....… 28

Chapter Three: Experimental methods ……..… 28

3.1. Zeolites used ……..… 28

3.2. Synthesis of NaY zeolite ……...… 28

3.3 Preparation of the solid acid catalysts: HY and HZSM-5 ……. 29

3.4 Rare-earth ion-exchange on H-zeolite catalysts. ……. 29

3.4.1 Preparation of 5% and 10% Ce …….……. 29

3.4.2 Preparation of 5% and 10% La ……...…. 30

3.5 Characterization of zeolite samples ……. 30

3.5.1. X-ray powder diffraction (XRD) ……..…..…. 30

3.5.2. Solid state NMR ……..…… 31

3.5.3. Scanning electron microscopy (SEM) ……. 32

3.5.4. Nitrogen physisorption …… 33

3.6 Zeolite catalysts evaluation …….……...….. 34

3.7 Products distribution identification ……...…….……. 37

3.7.1 Gas chromatography (GC) …… 37

3.7.2 Gas chromatography/mass spectrometry (GC/MS) …..…. 38

3.8 Calibration of reactants flowrates …….. 38

3.8.1 Calibration of ethylene mass flowmeters …… 39

3.8.2 Calibration of HPLC pump ……. 40

Chapter Four: Results and discussion……..…. 41

4.1. X-ray powder diffraction …….……. 41

4.2. Zeolite morphology studied by SEM ……. . 47

4.3. Solid state MAS NMR ……. 48

4.3.1. ^{29}Si NMR spectra …….……. 48

4.3.2. ^{27}Al NMR spectra ……. 56

4.4. Nitrogen physisorption …… 62

4.5. Catalyst performance …… ……..…. 64

4.5.1 The effect of time-on-stream ……..…. 66

4.5.2 The effect of feed ratio ……..…… 66

4.5.3 The effect of rare-earth ion-exchange in HZSM-5 …….. 69

Chapter Five: Conclusions …….……. 75

References …… . 78

Appendix A: XRD peak position……..……. 85

Appendix B: Unit-cell parameters……..……...… 87

Appendix C: GC/MS data……..…….…… 88

List of figures

Figure 1.1	A schematic representation of the generation of acid sites in zeolites.	3
Figure 2.1	Representations of $[SiO_4]^{4-}$ or $[AlO_4]^{5-}$ tetrahedra.	4
Figure 3.1	Framework structure for: (a) FAU, (b) MFI and (c) BEA.	6
Figure 4.1	Representation of (a) reactant shape selectivity in zeolite channel (rejection of branched chain hydrocarbons), (b) product shape selectivity (*p*-xylene diffuses preferentially out of the channels and (c) transition state shape selectivity in zeolite channels.	8
Figure 5.1	Primary alkylation and transalkylation reactions for ethylbenzene production.	12
Figure 6.1	World capacities of ethylbenzene in 2010 (metric tons).	13
Figure 7.1	World actual and forecast demand of ethylbenzene.	14
Figure 1.2	Magic-angle spinning.	17
Figure 2.2	Electrons produces a magnetic field which opposes the applied field.	18
Figure 3.2	Scattering of X-rays from a parallel set of crystal planes.	20
Figure 4.2	Schematic of scanning electron microscopy.	22
Figure 5.2	Forms of experimental adsorption isotherms.	23
Figure 6.2	A schematic representation of a typical gas chromatography.	24
Figure 7.2	A schematic representation of a typical gas chromatography/mass spectrometer.	27
Figure 1.3	PW3040/60 X'pert PRO Console diffractometer.	31
Figure 2.3	Varian VNMRS spectrometer.	32
Figure 3.3	FEI-NNL200 scanning electron microscope.	33
Figure 4.3	Micromeritics ASAP 2020.	34
Figure 5.3	MicroReactor 10A benchtop pilot plant.	35
Figure 6.3	Schematic diagram of the reaction system.	36
Figure 7.3	Shimadzu GC-2014.	37
Figure 8.3	Shimadzu GC/MS-QP 2010 SE.	38

Figure 9.3	Mass flowmeter calibration using ethylene gases under different reactor pressures: (a) atmospheric, (b) 2.5 bar, (c) 5 bar and (d) 7.5 bar.	39
Figure 10.3	HPLC pumb calibration for liquid benzene.	40
Figure 1.4	XRD patterns of (a) NaY, (b) ZSM-5 and (c) HBeta zeolites.	43
Figure 2.4	XRD patterns of various ion-exchanged form of zeolite catalysts (a) Y, (b) ZSM-5 and (c) HBeta.	46
Figure 3.4	SEM images of (a) NaY, (b) ZSM-5 and (c) HBeta.	47
Figure 4.4	^{29}Si MAS NMR spectra for (a) NaY, (b) ZSM-5 and (c) HBeta.	50
Figure 5.4	^{29}Si MAS NMR spectra for (a) HY and (b) HZSM-5.	51
Figure 6.4	^{29}Si MAS NMR spectra for (a) 5%Ce-HY and (b) 10%Ce-HY.	54
Figure 7.4	4 ^{29}Si MAS NMR spectra for (a) 5%Ce-HZSM-5 and (b) 10%Ce-HZSM-5.	54
Figure 8.4	^{29}Si MAS NMR spectra for (a) 5%Ce-HBeta and (b) 10%Ce-HBeta.	54
Figure 9.4	^{29}Si MAS NMR spectra for (a) 5%La-HY and (b) 10%La-HY.	55
Figure 10.4	^{29}Si MAS NMR spectra for (a) 5%La-HZSM-5 and (b) 10%La-HZSM-5.	55
Figure 11.4	^{29}Si MAS NMR spectra for (a) 5%La-HBeta and (b) 10%La-HBeta.	55
Figure 12.4	^{27}Al MAS NMR spectra for (a) NaY, (b) ZSM-5 and (c) HBeta.	57
Figure 13.4	^{27}Al MAS NMR spectra for (a) HY and (b) HZSM-5.	58
Figure 14.4	Representation of the location of octahedral extra-framework Al species in HY zeolite.	59
Figure 15.4	^{27}Al MAS NMR spectra for (a) 5%Ce-HY and (b) 10%Ce-HY.	60
Figure 16.4	^{27}Al MAS NMR spectra for (a) 5%Ce-HZSM-5 and (b) 10%Ce-HZSM-5.	60
Figure 17.4	^{27}Al MAS NMR spectra for (a) 5%Ce-HBeta and (b) 10%Ce-HBeta.	60
Figure 18.4	^{27}Al MAS NMR spectra for (a) 5%La-HY and (b) 10%La-HY.	61
Figure 19.4	^{27}Al MAS NMR spectra for (a) 5%La-HZSM-5 and (b) 10%La-HZSM-5.	61

Figure 20.4	^{27}Al MAS NMR spectra for (a) 5%La-HBeta and (b) 10%La-HBeta.	61
Figure 21.4	Nitrogen adsorption and desorption isotherms (relative N_2 pressure P/P_0 against adsorbed volume) for (a) NaY, (b) ZSM-5 and (c) HBeta.	63
Figure 22.4	Effect of time-on-stream on benzene conversion over HY, HZSM-5 and HBeta. (a) 250°C, 5 bar, ethylene WHSV=0.5h^{-1}, feed ratio 1:1 (B:E). (b) 250°C, 5 bar, ethylene WHSV=0.5h^{-1}, feed ratio 3:1 (B:E).	67
Figure 23.4	Effect of time-on-stream on selectivity for EB over HY, HZSM-5 and HBeta. (a) 250°C, 5 bar, ethylene WHSV=0.5h^{-1}, feed ratio 1:1 (B:E). (b) 250°C, 5 bar, ethylene WHSV=0.5h^{-1}, feed ratio 3:1 (B:E).	67
Figure 24.4	Effect of feed ratio on benzene conversion over HY, HZSM-5 and HBeta. At 250°C, 5 bar, ethylene WHSV=0.5h^{-1}, TOS=120min.	68
Figure 25.4	Effect of feed ratio on selectivity for EB over HY, HZSM-5 and HBeta. At 250°C, 5 bar, ethylene WHSV=0.5h^{-1}, TOS=120min.	60
Figure 26.4	Effect of rare-earth ion-exchange of HZSM-5 on: (a) the conversion of benzene and (b) the selectivity of EB. At 250°C, 5 bar, ethylene WHSV=0.5h^{-1}, feed ratio 1:1 (B:E).	70
Figure 27.4	Representation of the location of the $La(OH)_2^+$ cluster in ZSM-5 zeolite.	73

List of tables

Table 1.1	Types of commercial processes using FAU, BEA and MFI zeolite-based catalyst.	9
Table 2.1	Licensed process technologies for ethylbenzene manufacture.	11
Table 1.2	Comparison of characteristics of GC detectors.	25
Table 1.4	Derived cell parameters for NaY, ZSM-5 and HBeta zeolites.	42
Table 2.4	Ranges of ^{29}Si MAS NMR chemical shifts for aluminosilicate zeolites.	49
Table 3.4	Si/Al ratios and chemical shifts from ^{29}Si NMR data for Na-Y, ZSM-5 and HBeta zeolites.	51
Table 4.4	Comparison of Si/Al ratio from 29Si NMR data for different modified zeolite catalysts.	53
Table 5.4	^{27}Al NMR chemical shift in rare earth exchange zeolite catalysts.	59
Table 6.4	Physical properties of NaY, ZSM-5 and HBeta zeolites.	62
Table 7.4	Reaction performance comparison between zeolite catalysts in benzene/ethylene alkylation reaction[a].	72
Table A1	Peak position of zeolite Y catalysts.	85
Table A2	Peak position of ZSM-5 zeolite catalysts.	85
Table A3	Peak position of HBeta zeolite catalysts.	86
Table B1	Unit-cell parameters of zeolite Y catalysts.	87
Table B2	Unit-cell parameters of ZSM-5 zeolite catalysts.	87
Table B3	Unit-cell parameters of HBeta zeolite catalysts.	87
Table C1	GC/MS retention time of the B/E alkylation products.	88

Abbreviations

Abbreviation	*Full name*
ABS	Acrylonitrile-Butadiene-Styrene
B	Benzene
BET	Brunauer-Emmett-Teller
BJH	Barret-Joyner-Halenda
DEB	Diethylbenzene
DFT	Density functional theory
E	Ethylene
EB	Ethylbenzene
FID	Flame Ionization Detector
GC	Gas Chromatography
GC/MS	Gas Chromatography/Mass Spectrometry
HPLC	High Performance Liquid Chromatography
IZA-SC	International Zeolite Association-Structure Commission
MAS	Magic Angle Spinning
MS	Mass Spectrometry
NMR	Nuclear Magnetic Resonance
PP	Polypropylene
SAN	Styrene-Acrylonitrile
SEM	Scanning Electron Microscopy
SSNMR	Solid State Nuclear Magnetic Resonance
TCD	Thermal Conductivity Detector
TEB	Triethylbenzene
TOS	Time-on-Stream
WHSV	Weight Hourly Space Velocity
XRD	X-ray powder Diffraction

Chapter One: Introduction

1.1 Preface

Catalysis has played a central role during the second half of the 20th century in the development of the refining and petrochemical industries [1]. Today over 90% of all industrial chemicals are produced with the aid of catalysts. In 1991 it was estimated that the total value of fuels and chemicals derived from catalysts exceeded $900 billion/year. World catalyst demand is forecast to grow to $16.3 billion through 2012 [2,3].

Zeolites are widely used throughout the petrochemical industry in a range of acid catalyzed processes. The analysis of the catalyst market and the position of zeolites therein is a striking indication of their continued strategic importance [4,5].

The focus on cleaner fuels, lower cost petrochemicals the issue of global sustainability has catalysed the refining and petrochemical industries towards improvements in the performance of conventional catalysts. Zeolites offer the basis of many of these technological solutions building on efficient and balanced cooperation between industry and academia [4,6].

The alkylation of aromatic hydrocarbons with olefins is applied on a large scale in the chemical industry. One of the major products produced via alkylation is ethylbenzene. Nearly all ethylbenzene produced in the world is used in the manufacture of styrene. Other applications include paint solvents and pharmaceuticals [6,7].

1.2 Solid acid catalysts

Acid catalysts are widely used in the petrochemical industry, including oil refining, the production of petrochemicals and fine chemicals [8]. Among the first commonly-used acid catalysts, were HF, H_2SO_4, $HClO_4$ and H_3PO_4 (in liquid form or supported on solid form such as Kieselguhr). Since 1940 the tendency, worldwide, has been to replace, wherever possible, such liquid acid catalysts by solid acid catalysts, which present clear advantages, including; ease of handling, simplicity and versatility of process engineering, catalyst regeneration, decreasing reactor and plant corrosion problems, and environmentally-safe disposal [9]. Perhaps the main characteristic of solid acids compared to liquid acids, is that solid acids possess specific acid sites differing markedly in their nature and strength, thus allowing a high degree of control of catalytic reactions [10,11].

Solid acid catalysts are generally categorized by a combination of their Brønsted and/or Lewis acidity, the strength and number of their catalytic sites, and the morphology of the supporting material (e,g., surface area, pore size, chemical structure). The synthesis of pure Brønsted and pure Lewis acid catalysts continues to attract a great deal of academic and industrial interest [5].

A Brønsted acid site is able to *transfer* a proton from the catalytic solid to the adsorbed molecule, whilst the Lewis acid site is able to *accept* an electron pair from the adsorbed molecule and a coordinative bond with the surface is thereby formed [12]. These active sites in solid acid catalysts are usually formed either by ammonium or polyvalent cation exchange followed by calcinations [13] (Figure 1.1).

Among the wide range of solid acid catalysts, zeolites have found many large-scale applications [14]. Their success is based on the ability to routinely and consistently function as high-volume, high-performance catalysts with strong Brønsted acidity that can be carefully controlled, and which can robustly withstand high reaction temperatures and catalyst regeneration conditions [9].

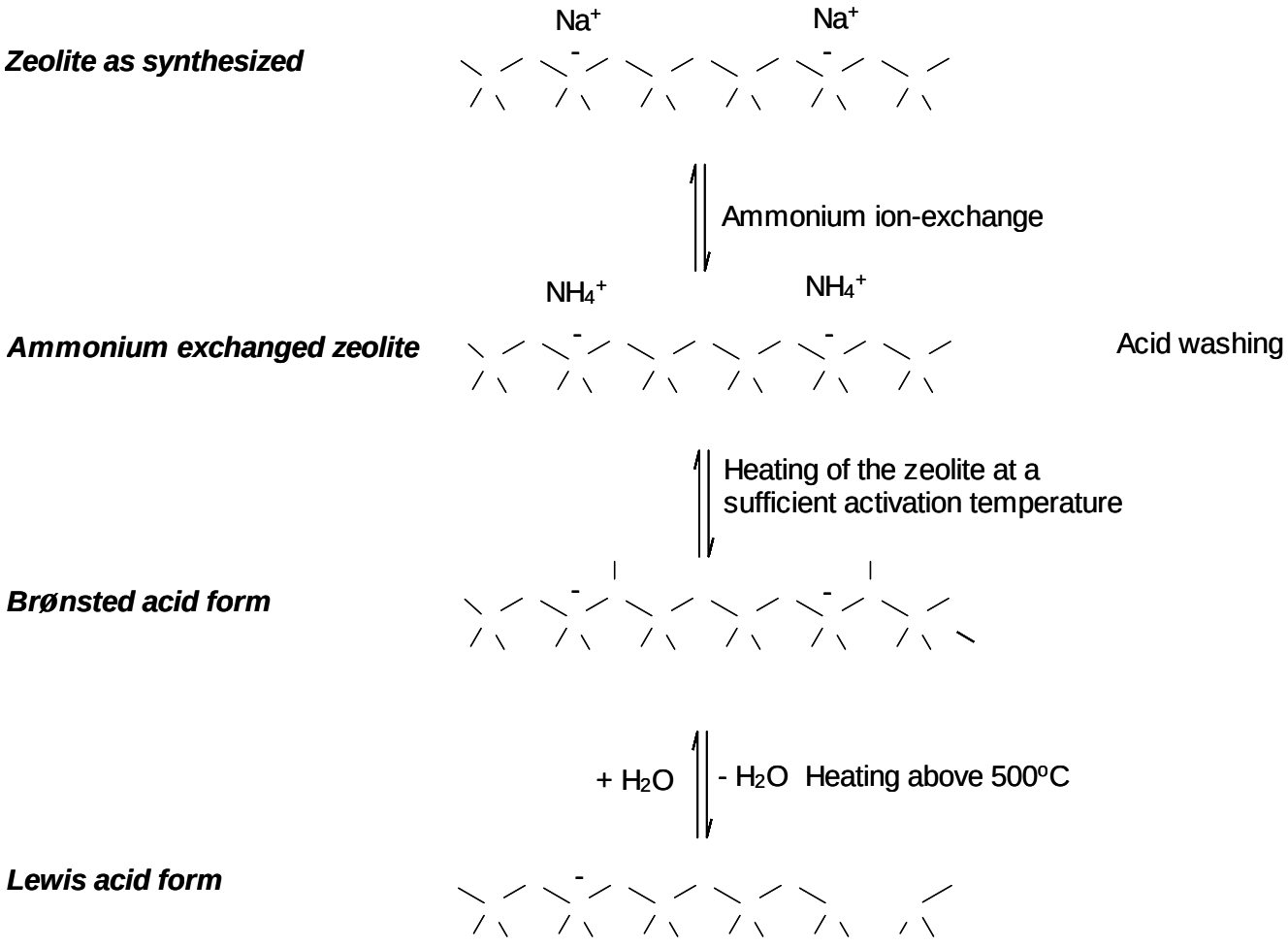


Figure 1.1 A schematic representation of the generation of acid sites in zeolites [15].

1.3 Zeolites

1.3.1 What is a zeolite?

A zeolite is best defined as a hydrated aluminosilicate that possesses a three-dimensional framework structure, formed by $[SiO_4]^{4-}$ and $[AlO_4]^{5-}$ tetrahedra that are connected by sharing an oxygen atom (Figure 2.1). When an AlO_4 tetrahedron is substituted for a SiO_4 tetrahedron, a negative charge appears over the framework structure which is neutralized by the incorporation of extra framework cationic species (Na^+,NH_4^+, K^+, Ca^{2+}, Mg^{2+}… etc) [16,17]

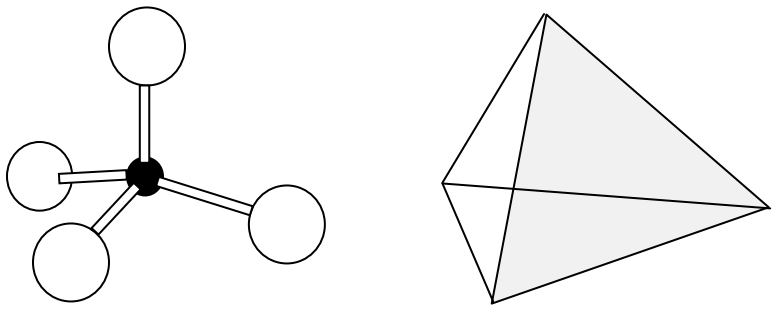


Figure 2.1 Representations of $[SiO_4]^{4-}$ or $[AlO_4]^{5-}$ tetrahedra.

Chemically, zeolites are represented by the empirical formula:

$$[M_{x/n}O.(AlO_2)_x.\ (SiO_2)_y.wH_2O]$$

Where *n* is the valence of cation M, *x+y* is the total number of tetrahedral sites per unit cell and *y/x* the atomic Si/Al ratio [6,13,16].

1.3.2 Zeolites properties

The word ‘zeolite’ has Greek roots, (*zéo*), meaning "to boil" and (*líthos*) meaning "stone", an allusion to the visible loss of water noted when natural zeolites are heated [16].

In general, zeolites have the following properties that make them particularly useful for a wide range of applications [17,18]:

- *Low cost.*
- *High surface area.*
- *High thermal and chemical stability.*
- *High selectivity of sorption.*
- *Tremendous diversity: >190 frameworks type are known and each can be further modified by introducing other elements, metal cations and molecular species.*
- *Uniform size and high density of pores.*
- *Possibility of modifying the electronic properties of the active sites.*
- *Non-toxic and environmentally friendly; recyclable.*

1.3.3 Zeolite structures

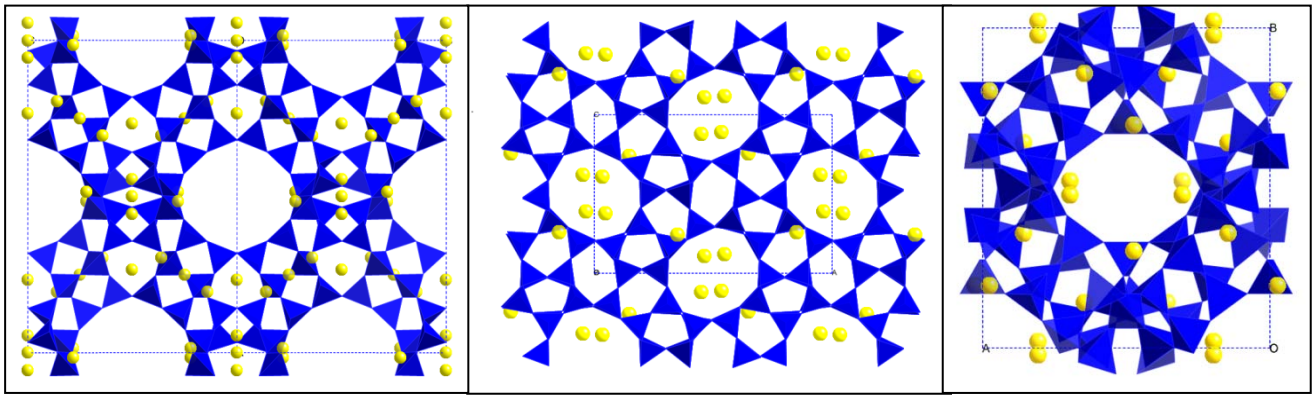
From both industrial and academic perspectives, the three widely studied and used zeolites are zeolite Y, ZSM-5 and Beta. This is due to their unique crystal structure, their high thermal stability, their acidity and shape-selective properties, all of the properties match the requirements for many applications in oil refining, the petrochemical industry and environmental catalysis. Their properties can be tuned to the specific processes of

diverse industrial applications [19,20]. We briefly summarize the major feature of the three zeolites investigated in this thesis.

- Zeolite Y has the faujasite **(FAU)** framework; built by linking sodalite cages through double six-rings (Figure 3.1a). This creates a large cavity called the supercage which is accessible by a three-dimensional 12-ring pore system [13].

- ZSM-5 zeolite **(MFI)** framework; built from five-rings. The pore structure consist of two-dimensional 10 rings pore system, contains cavities and comprises two different pore system, one consisting of zig-zag channels of near-circular cross-section and another of straight channels of elliptical shape (Figure 3.1b) [13,21].

- Zeolite Beta **(BEA)** framework; a large pore, high-silica zeolite. The pore structure consists of channels of three-dimensional 12 rings pore system interconnected by cages constituted by the intersections of the channels (Figure 3.1c) [12,22].



(a) (b) (c)

Figure 3.1 Framework structure for: (a) **FAU**, (b) **MFI** and (c) **BEA** [23]. Blue tetrahedral – Si/Al; dashed lines – one unit cell and yellow spheres are the extra framework cations.

1.3.4 Zeolites applications

A wide variety of industrial applications now exist for zeolites, the most important being catalysis, but others include gas separation and ion exchange:

- *Catalysis*

Several important organic reactions are catalyzed by zeolites; the most significant being cracking, alkylation and hydrocarbon synthesis. A diverse range of catalytic reactions including acid-base and metal- induced reactions can be promoted by zeolites. The reactions occur within the zeolite pores, which through steric influence, give the property of high selectivity towards the reactants, the transition state and the product molecules which overall improve the yield of a desired isomeric product. A schematic representation of these situations is shown in figure 4.1 [24,25]. In Table 1.1 we illustrate the various applications of Y, ZSM-5 and Beta zeolites in three main industrial fields [4].

- *Adsorption and Separation*

A widely used property of zeolites is that of gas separation. The shape-selective properties are also the basis for their use in molecular adsorption. This property can be fine tuned by variating the structure by changing the size and number of cations around the pores [6,25].

- *Ion Exchange*

The loosely-bound nature of extra-frame work cations (Figure 3.1) can readily exchange with other cations when in aqueous media. Applications of this can be seen in water softening devices, and the use of zeolites in detergents and soaps [6,25].

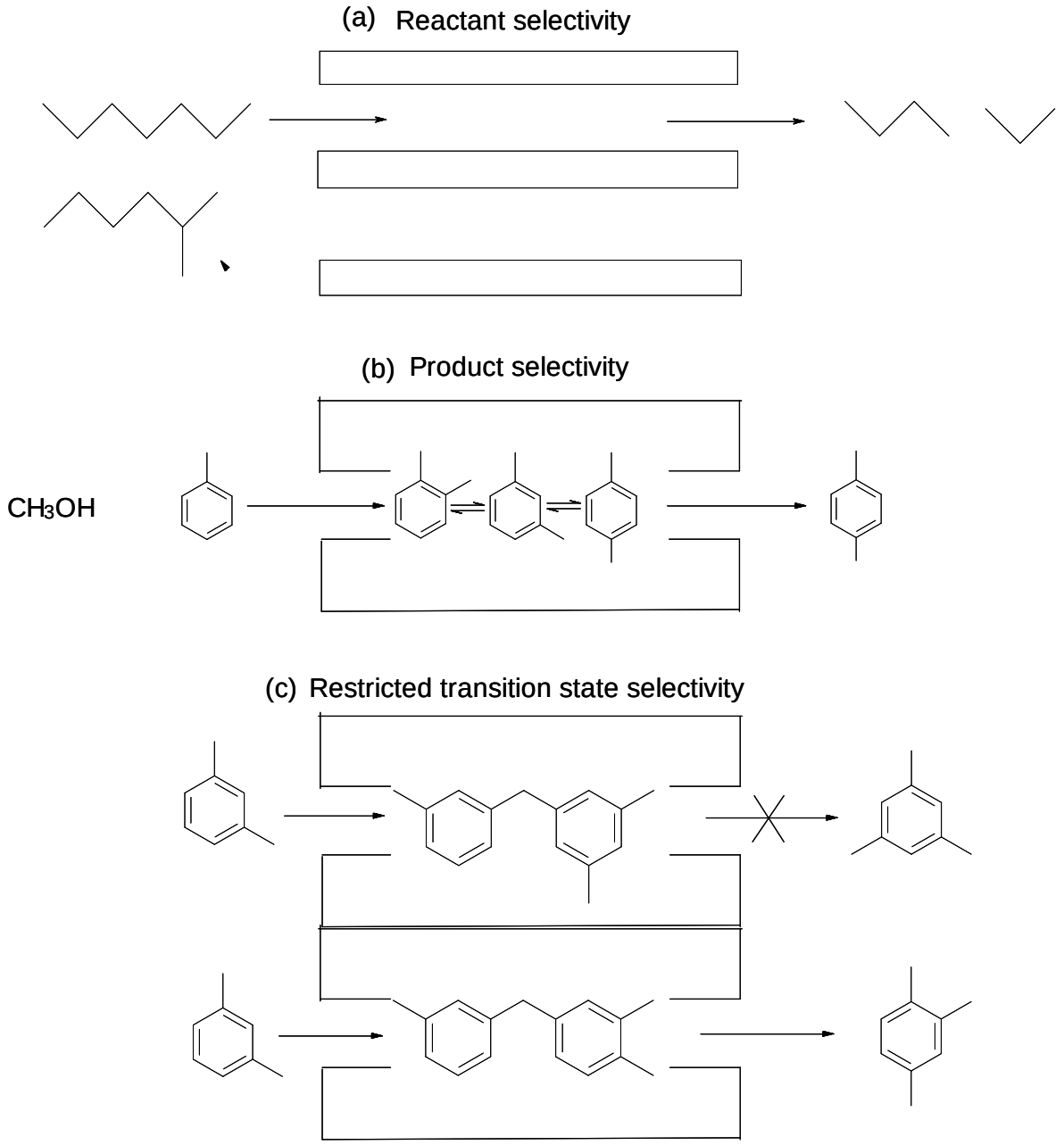


Figure 4.1 Representation of (a) reactant shape selectivity in zeolite channel (rejection of branched chain hydrocarbons), (b) product shape selectivity (*p*-xylene diffuses preferentially out of the channels and (c) transition state shape selectivity in zeolite channels [16].

Table 1.1 Types of commercial processes using **FAU**, **BEA** and **MFI** zeolite-based catalyst.

Zeolite structure code	**FAU**	**BEA**	**MFI**	Area
Zeolite name	Y, USY	Beta	ZSM-5, TS-1	
Process				
Iso-dewaxing			B	Refining
Dewaxing			M	
Hydro-cracking	B			
Hydro-dearomatisation	B			
FCC	M		M	
Olefin oligomerisation			M	
Ethylbenzene			M	Petrochemicals
Cumene	M	M		
C_2, C_3-transalkylation	M	M		
p-Ethyltoluene			M	
Xylene isomerisation			M/B	
Toluene disproportionation			B	
LPG or olefin aromatisation			B	
Amination			M	Chemicals
Hydration			M	
Chlorination/isomerisation			M	
Beckmann rearrangment			M	
Oxidation			M	
Acylation	M	M		

M stands for monofunctional catalyst and **B** stands for biofunctional catalyst [4].

1.4 Alkylation of aromatics

The alkylation of aromatic hydrocarbons with olefins is the main commercial route for the production of important petrochemical intermediates, such as ethylbenzene, subsequently converted to styrene for polymer use; isopropylbenzene (cumene), a precursor to important solvents and chemical intermediates such as acetone and phenol; alkali benzene sulfonates, used extensively in detergent building; and alkylnapthalenes, precursors to advanced high strength polymers [6,26].

1.4.1 Alkylation of benzene with ethylene

Alkylation of benzene with ethylene to produce ethylbenzene is widely used in the petrochemical industry [27]. Nearly 40% of the world's ethylbenzene capacity still utilizes the $AlCl_3$-based Friedel-Crafts alkylation process first introduced in the 1950s [6,28]. The continued use of $AlCl_3$ has caused an increasing number of environmental and sustainability problems concerning handling, safety, corrosion, and waste disposal. An immense effort is being directed toward developing alternative catalytic systems. The $AlCl_3$-based processes have been progressively substituted, worldwide, with solid acid zeolite-based processes [29].

Several technologies using zeolites are now available for the production of ethylbenzene. Zeolite catalyzed processes are licensed by Mobil-Badger, Lummus-UOP, CDTech, and Dow Chemical. Table 2.1 summarizes the manufacturing volume share of each of the licensed process technologies for ethylbenzene manufacture [27,28].

Table 2.1 Licensed process technologies for ethylbenzene manufacture [27].

Process (year)	***Alkylation***					***Transalkylation***		***Yield (%)***
	T(°C)	Catalyst	Phase	Feed ratio	Life (year)	Catalyst	Phase	
Monsanto-Lummus (<1975)	160	$AlCl_3$	Liquid	2.5	-	-		99.7
Mobile-Badger (1980)	390-440	ZSM-5	Vapor	7.6	0.25	-		98.1
Lummus/Unocal/UOP (1989)	240-270	Y	Liquid	7.2	1	Y	Liquid	98.2
Mobile-Badger (1994)	390-440	ZSM-5	Vapor	7.6	1	ZSM-5	Vapor	99.2
CDTECH EB (1994)	-	Y	-	-	5	Y	Liquid	99.7
Mobile-Raytheon EBMax (1995)	-	MCM-22	Liquid	4	3	ZSM-5	Vapor	99.6
Lummus/UOP EBOne (1996)	-	EBZ-500	Liquid	4-6	2	EBZ-100	Liquid	99.6

The majority product in the reaction of ethylene with benzene is ethylbenzene. Meanwhile, some undesirable byproducts are generated including diethylbenzene (DEB), tri-ethylbenzene (TEB) and xylene. The DEB and TEB mixture can be transformed into ethylbenzene via a transalkylation reactor system [30]. Figure 5.1 shows the major reactions associated with ethylbenzene synthesis [28].

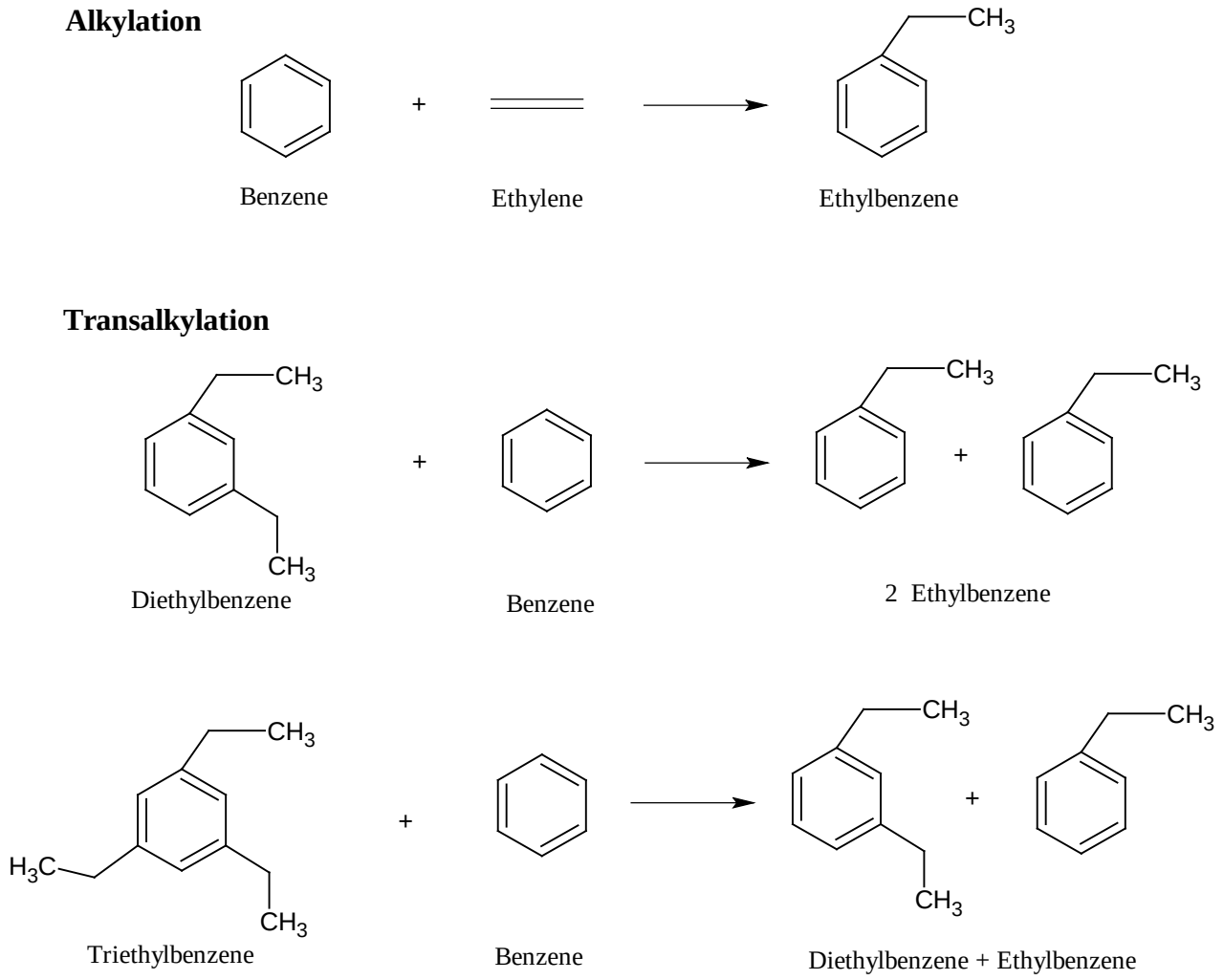


Figure 5.1 Primary alkylation and transalkylation reactions for ethylbenzene production.

1.4.2 Importance of ethylbenzene

Ethylbenzene is important in the petrochemical industry as an intermediate in the production of styrene [6,27,31], which in turn is used mostly in polymer production for poly styrene, acrylonitrile-butadiene-styrene (ABS) and styrene-acrylonitrile (SAN)

resins, styrene-butadiene elastomers and latexes, and unsaturated polyester resins. The major styrene markets include packaging, electrical/electronic/appliances, construction and consumer products [32]. The 90% of EB world's production is employed in the production of styrene, the other 10% is used is used in other applications like paint solvents and pharmaceuticals [31].

1.4.3 World demand and capacities of ethylbenzene

The worldwide capacity for ethylbenzene is currently estimated to be 36 million metric tons/ year (1 metric ton = 1000 kg) [33]. The following pie chart shows world average annual capacities of ethylbenzene in 2010 (Figure 6.1).

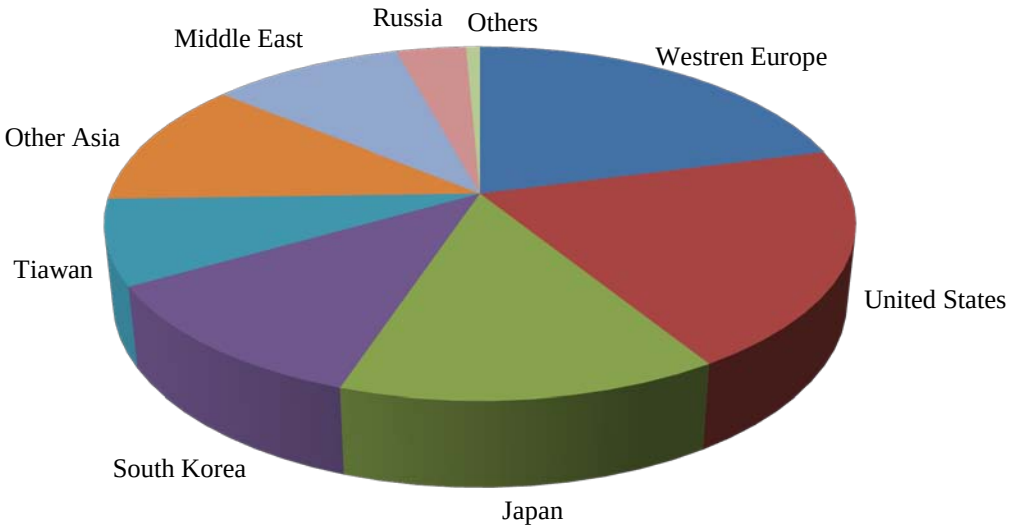


Figure 6.1 World capacities of ethylbenzene in 2010 (metric tons) [33].

Figure 7.1 shows the world actual and forecast demand of ethylbenzene; it is expected to grow an average 3.5% per year from 2010 to 2015 [33].

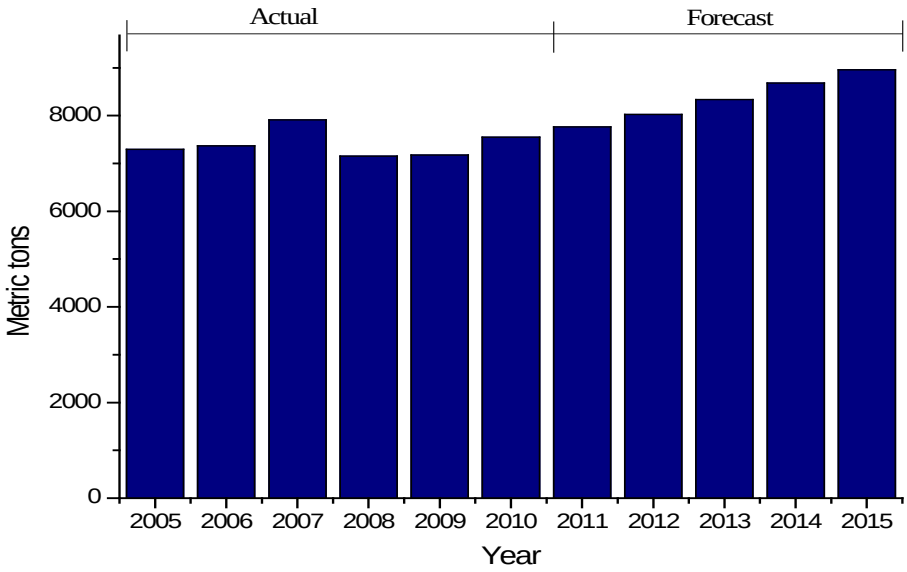


Figure 7.1 World actual and forecast demand of ethylbenzene.

1.5 Aim of thesis

The ultimate aim of this thesis is to develop new and higher performance solid acid zeolite catalysts for the benzene/ethylene alkylation reaction. To achieve this aim, I have synthesized and also investigated the structure and physical/chemical properties of acid zeolites by using a combination of characterization techniques in order to develop a detailed understanding of the key features that create high acidity, catalytic activity and high selectivity in these materials. These characterization studies form the basis to directly investigate also the catalytic performances for benzene / ethylene alkylation of a variety of zeolites whose structural and catalytic reactivities were modified by ion-exchange and other chemical treatments.

Chapter Two: Characterization and analytical techniques

The purpose of this chapter is to provide a briefly describe on the characterization and analytical techniques which used in this work including X-ray powder diffraction (XRD), solid state nuclear magnetic resonance (SSNMR), scanning electron microscopy (SEM), nitrogen physisorption, gas chromatography (GC) and gas chromatography-mass spectrometry (GC/MS).

2.1 Characterization of zeolite catalysts

The total characterization is an essential part for the development of new zeolites and for the development and commercialization of zeolitic catalysts before, during, and after their catalytic evaluation. A combination of selective characterization techniques is required to understanding and solving a specific problem in order to achieve commercial success [13,34].

2.1.1 Solid state nuclear magnetic resonance (SSNMR)

NMR is one of the most versatile of the spectroscopic techniques because it embraces the widest range of materials: liquids and solids, organic and inorganic molecules, pure compounds and complex reaction mixtures can all be studied [35]. Liquid phase NMR is a common technique applied to many molecular compounds on a routine basis [34]. The big difference between a solid sample and liquid sample that in solution the molecules are

free to rotate rapidly and isotropically whereas in a solid the molecules are more or less rigidly fixed in the lattice. In a solution averaging to the "intend" interaction experienced by nuclei results in narrow spectral lines. The absence of such averaging in the solid state results in very broad lines [34,36] .

Important line broadening internal interactions affecting the NMR spectrum in the solid state are [36]:

(i) *Shielding interactions*: modification of the interaction with the applied magnetic field by electrons.

(ii) *Dipolar interactions*: direct, through space interaction section of magnetic nuclei.

(iii) *Quadropolar interactions*: interaction of electric quadropole moments with electric field gradients.

- Magic angle spinning (MAS)

  Fortunately, the line broadening can be reduced or removed by an experimental technique called magic angle spinning (MAS), by spinning the sample (usually at a frequency of 1 to 70 kHz) at the magic angle θm (ca. 54.74°, where $\cos^2\theta m=1/3$) with respect to the direction of the magnetic field (Figure 1.2), the normally broad lines become narrower, increasing the resolution for better identification and analysis of the spectrum [34,36,37].

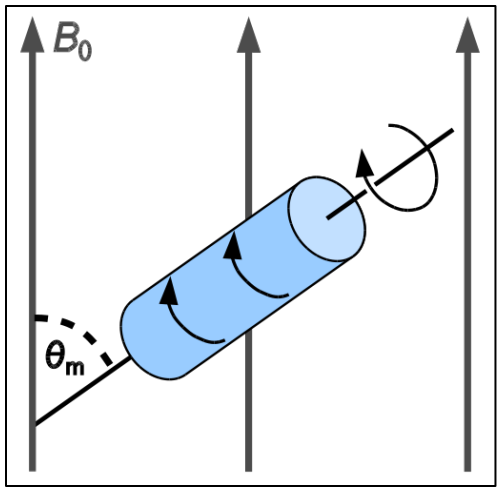


Figure 1.2 Magic-angle spinning: The sample (blue) is rotating with high frequency inside the main magnetic field (B_0). The axis of rotation is tilted by the magic angle θ_m with respect to the direction of B_0.

- Cross polarization

Is a technique which involves transfer of polarization from one NMR active nucleus to another when the nucleus under study has low natural abundance to enhance its signal [13,36].

- Nuclear spin relaxation

Relaxation refers to the processes which allow nuclear spins to lose energy and drop from the excited state to the ground state. Ideally, the NMR spectroscopist would like relaxation rates to be fast – but not too fast. If the relaxation rate is fast, then saturation is reduced. If the relaxation rate is too fast, line- broadening in the resultant NMR spectrum is observed [36,38].

- Nuclear shielding and chemical shift

All nuclei are surrounded by electrons. The movement of electrons round the nucleus produces a tiny, localised magnetic field which opposes the applied field (Figure 2.2). As a result, the nucleus experiences a reduced overall field and is described as *shielded.* The extent of the shielding depends on the nature of the electron density in that region [36].

Spectrometers are sensitive enough to show the amount of shielding a nucleus experiences and this can be seen on a spectrum as the chemical shift. It is convenient to give the chemical shift (δ) as a fraction of the applied magnetic field, in parts per million, from a standard reference to remove the effect of spectrometer magnetic field strength. Chemical shift increase as shielding decreases as shown in the equation 1.2 [38]

$$\delta = \frac{v\,(observed) - v\,(reference)}{v\,(reference)} \qquad (1.2)$$

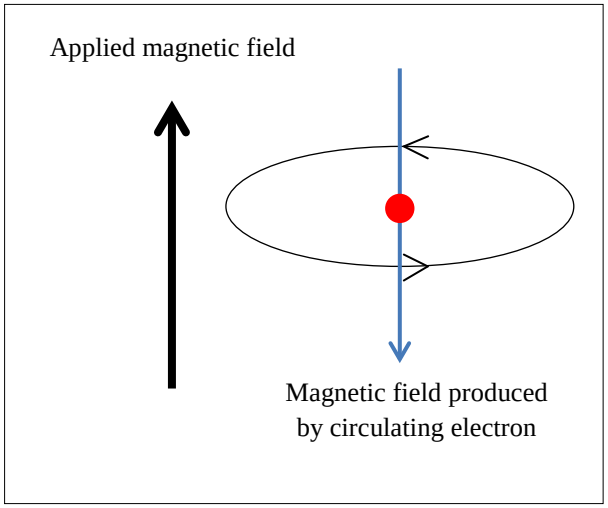


Figure 2.2 Electrons produces a magnetic field which opposes the applied field.

2.1.2 X-ray powder diffraction (XRD)

Powder X-ray diffraction (XRD) is one of the primary and widely techniques used to solid reveal detailed information about the chemical composition and crystallographic structure of natural and manufactured zeolitic materials [13,39].

These techniques are based on observing the scattered intensity of an X-ray beam hitting a sample as a function of incident and scattered angle, polarization, and wavelength of energy [34].

- Principles of X-ray diffraction

X-rays interact with electrons in atoms. When x-ray photons collide with electron clouds of the atoms, it is scattered in various directions. If the wavelength of these scattered x-rays did not change, the process is called elastic scattering (Thompson Scattering). These are the x-rays that we measure in diffraction experiments, as the scattered x-rays carry information about the electron distribution in materials [34,38].

- Bragg's law

Diffracted waves from different atoms can interfere with each other and the resultant intensity distribution is strongly modulated by this interaction. If the atoms are arranged in a periodic fashion, as in crystals, the diffracted waves will consist of sharp interference peaks with the same symmetry as in the distribution of atoms. Measuring the diffraction pattern therefore allows us to deduce the distribution of atoms in a material.

The peaks in an X-ray diffraction pattern are directly related to the atomic distances. When an X-ray beam interacting with the atoms arranged in a periodic manner as shown in figure 3.2, the atoms can be viewed as forming different sets of planes in the crystal. For a given set of lattice planes with an inter-plane distance of d, the condition for a diffraction (peak) to occur can be simply written as

$$2\,d\,\sin\theta = n\,\lambda \qquad (2.2)$$

Where n is an integer, and λ is the X-ray wavelength. Which this equation is known as the Bragg's law [34,38].

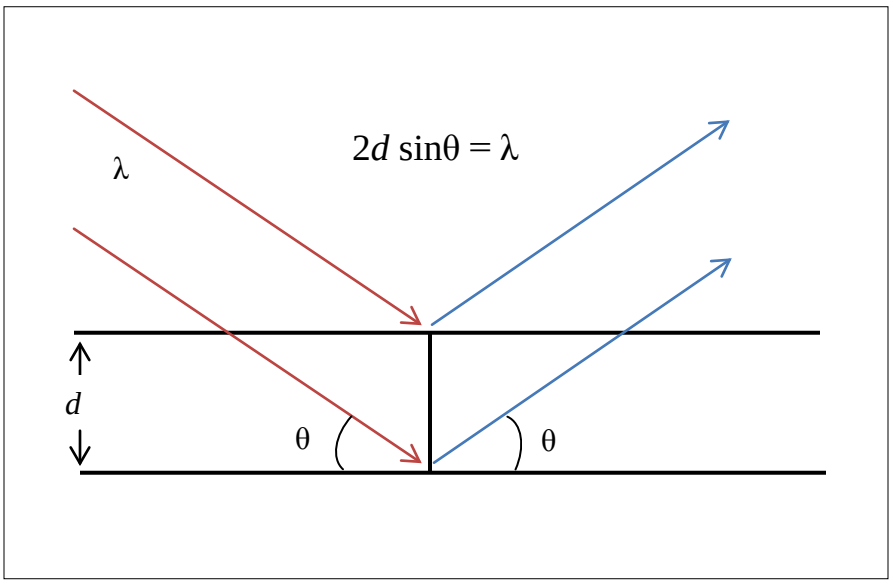


Figure 3.2 Scattering of X-rays from a parallel set of crystal planes.

2.1.3 Scanning electron microscope (SEM)

The electron microscope has become a very important part of materials structure determination, yielding information on the morphology, surface structure and element composition of new or known phases [13].

The SEM uses a beam of electrons to scan the surface of a sample to build a three-dimensional image of the specimen. The electron gun is housed on the top of the column and generates the beam of electrons that rushes towards the sample housed in the specimen chamber. The electron beam follows a vertical path through the microscope, which is held within a vacuum. The beam travels through electromagnetic fields and

lenses, which focus the beam down toward the sample. Once the beam hits the sample, electrons and X-rays are ejected from the sample (Figure 4.2) [13,34].

Because the SEM utilizes vacuum conditions and uses electrons to form an image, special preparations must be done to the sample. All water must be removed from the samples because the water would vaporize in the vacuum. All metals are conductive and require no preparation before being used. All non-metals need to be made conductive by covering the sample with a thin layer of conductive material. This is done by using a device called a "sputter coater."

The sputter coater uses an electric field and argon gas. The sample is placed in a small chamber that is at a vacuum. Argon gas and an electric field cause an electron to be removed from the argon, making the atoms positively charged. The argon ions then become attracted to a negatively charged gold foil. The argon ions knock gold atoms from the surface of the gold foil. These gold atoms fall and settle onto the surface of the sample producing a thin gold coating [12].

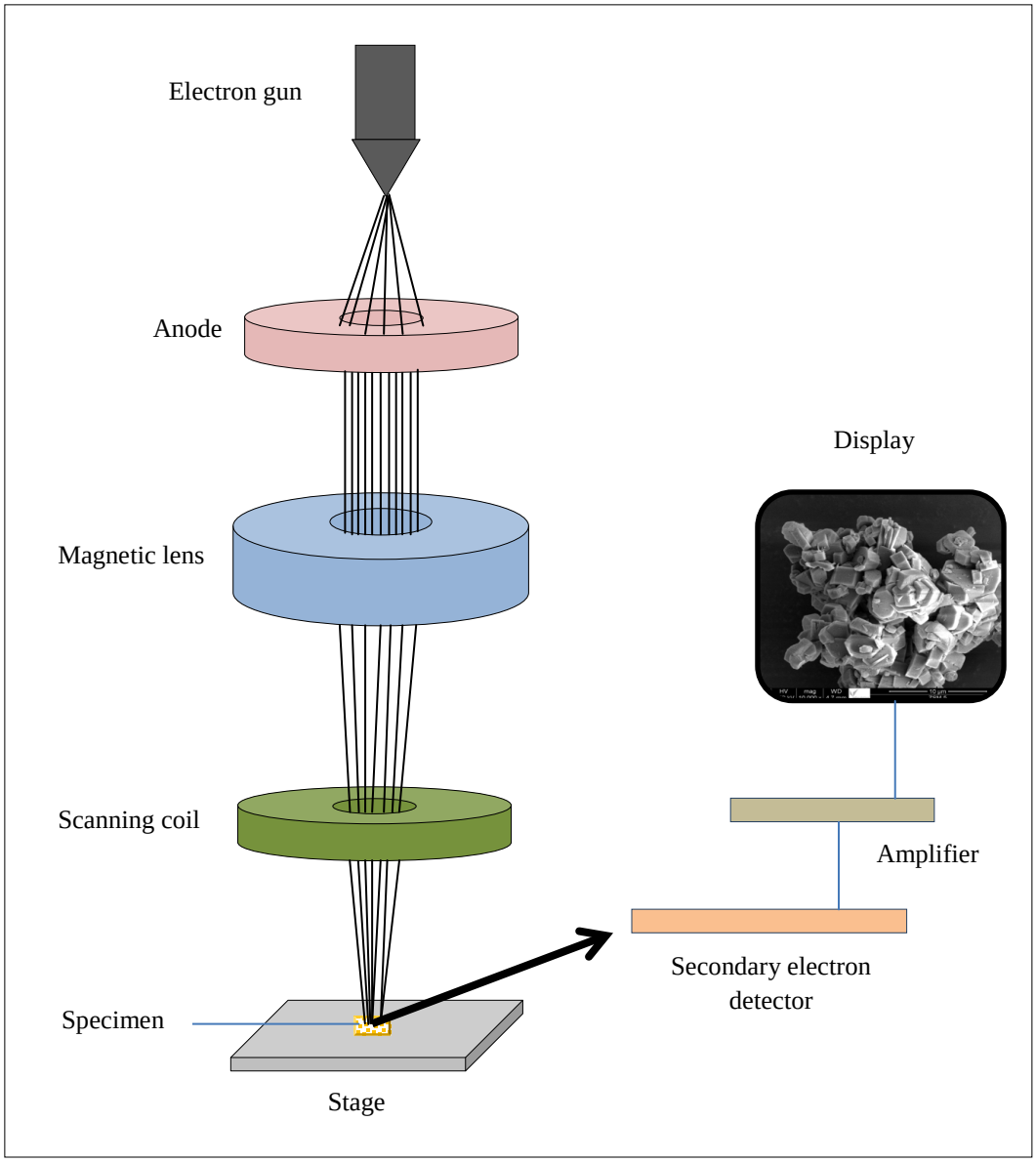


Figure 4.2 Schematic of scanning electron microscopy [90].

2.1.4 Nitrogen physisorption

Nitrogen adsorption is widely used for the determination of the surface area and pore size distribution of various porous materials. Gas adsorption by a solid surface is expressed quantitatively as a gas volume adsorbed by the adsorbent per unit mass or unit surface of the adsorbent [13,40].

The diversity of experimental adsorption isotherms is depicted in Figure 5.2. The Type I isotherm is typical of microporous solids and chemisorption isotherms. Type II is shown by finely divided non-porous solids. Type III and Type V are typical of vapor adsorption (i.e. water vapor on hydrophobic materials). Type VI and V feature a hysteresis loop generated by the capillary condensation of the adsorbate in the mesopores of the solid. Finally, the rare Type VI step-like isotherm is shown by nitrogen adsorbed on special carbon.

Once the isotherm is obtained, a number of calculation models can be applied to different regions of the adsorption isotherm to evaluate the specific surface area (i.e. BET, Dubinin, Langmuir, etc.) [40].

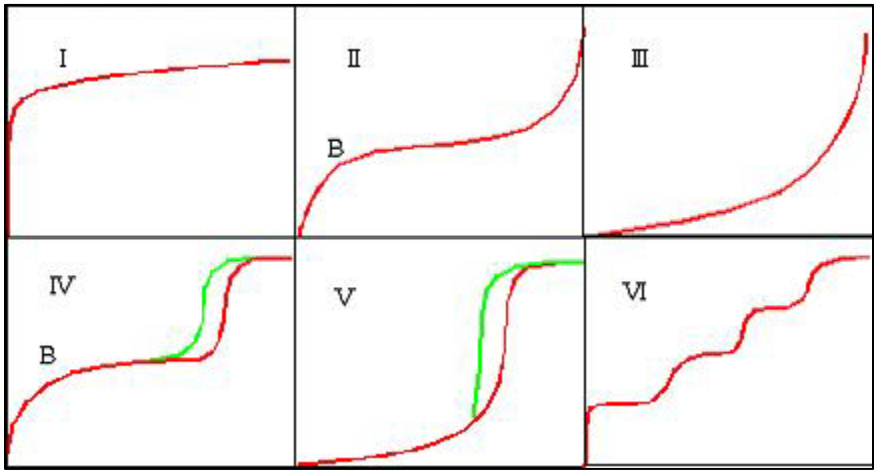


Figure 5.2 Forms of experimental adsorption isotherms [91].

- BET method

Brunauer, Emmett and Teller (BET) method is widely used in surface science for the calculation of surface areas of solids by physical adsorption of gas molecules. The concept of the theory is an extension of the Langmuir theory, which is a theory for monolayer molecular adsorption, to multilayer adsorption with the following hypotheses:

(a) gas molecules physically adsorb on a solid in layers infinitely; (b) there is no interaction between each adsorption layer; and (c) the Langmuir theory can be applied to each layer [13,41,42].

2.2 Product analysis

2.2.1 Gas chromatography (GC)

Gas chromatography (GC) is a commonly used analytic technique, in many research and industrial laboratories, for separating compounds based primarily on their volatilities. The sample is transported through the column by the flow of inert, gaseous mobile phase. The column itself contains a liquid stationary phase which is adsorbed onto the surface of an inert solid. The main reason why different compounds can be separated in GC is the interaction of the compound with the stationary phase. The stronger interaction remains the compound attached longer to the stationary phase, and takes more time to go through the column (longer retention time) (Figure 6.2). [43,44]

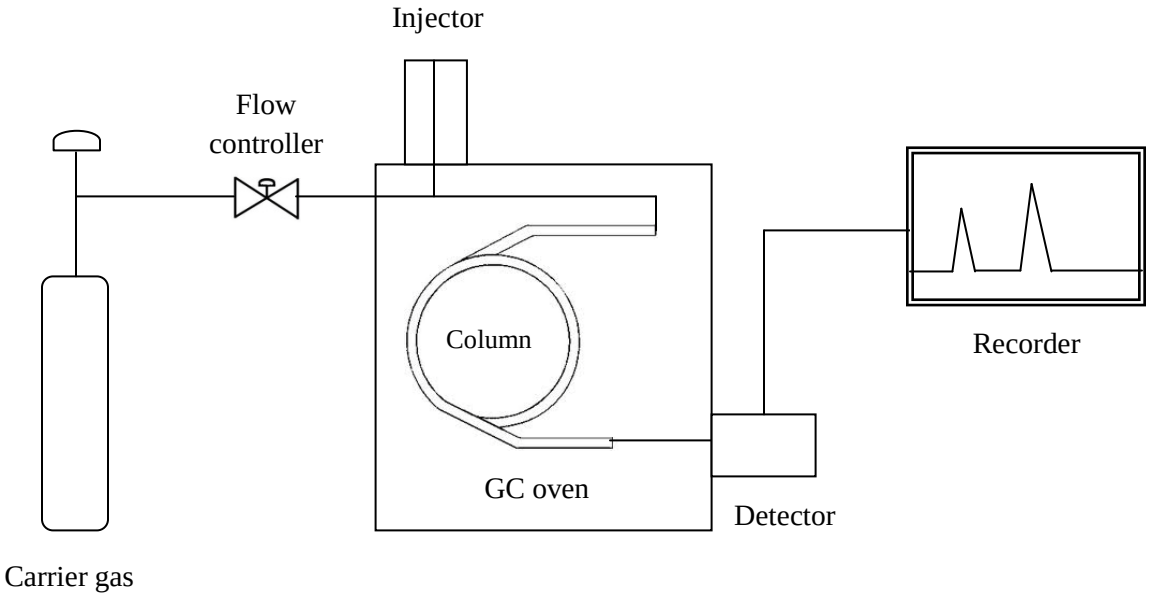


Figure 6.2 Schematic representation of a typical gas chromatography.

- Carrier gas

  The carrier gas must be chemically inert. Commonly used gases include nitrogen, helium, argon, and carbon dioxide. The choice of carrier gas is often dependent upon the type of detector which is used [43,44].

- Columns

  GC columns most widely used fall into two distinct categories: *packed* and *capillary*. Packed columns are typically a glass or stainless steel coil (typically 1-5 m total length and 5 mm inner diameter) that is filled with the stationary phase, or a packing coated with the stationary phase. Capillary columns are a thin fused-silica (purified silicate glass) capillary (typically 10-100 m in length and 250 µm inner diameter) that has the stationary phase coated on the inner surface. The choice of column depends on the sample and the active measured [43,44].

- Detectors

  There are many detectors which can be used in gas chromatography. The most common are the flame ionization detector (FID) and the thermal conductivity detector (TCD). Both are sensitive to a wide range of components, and both work over a wide range of concentrations. Their characteristics are outlined in Table 1.2

Table 1.2 Comparison of characteristics of GC detectors [43,44].

Detector	**Principle**	**Selectivity**	**Sensitivity (g/s)**
TCD	Measures difference in thermal conductivity of gases	Universally respond to all compounds	10^{-10}
FID	Burns compounds in H_2/O_2 flame at 2000°C and measures ion created	Responds to all oxidizable carbon compounds	10^{-12}

2.2.2 Gas chromatography/mass spectrometry (GC/MS)

Gas chromatography mass spectrometry (GC/MS) is an instrumental technique. GC can separate volatile and semivolatile compounds with great resolution, but it cannot identify them. MS can provide detailed structural information on must compounds such that they can be exactly identified, but it cannot readily separate them. By combining the two techniques, an analytical chemist can both qualitatively and quantitatively evaluate a solution containing a number of chemicals. The capabilities of that system are not merely the sum of the two instruments; the increase in analytical capabilities is exponential. [43,44].

Figure 7.2 show the MS component of a GC/MS system includes a sample inlet into a vacuum-sealed chamber that houses an ionization source, a mass analyzer, and an ion detector. In a GC/MS system, the input sample is always a chemically-homogenous gas produced by the GC component that can be introduced directly to the ionizer. Once ionized, the partitioned compound moves into the mass analyzer where the ions travel through an electrical or magnetic field that sorts them according to their m/z ratios (mass of the fragment divided by the charge is called the mass to charge). The detector measures the beam of now-separated ions arriving at the end of the analyzer, and converts changes in its intensity to produce the mass spectrum. A sample's mass spectrum is then displayed, catalogued, and compared to a library of known mass spectra by a computer data system [43,44].

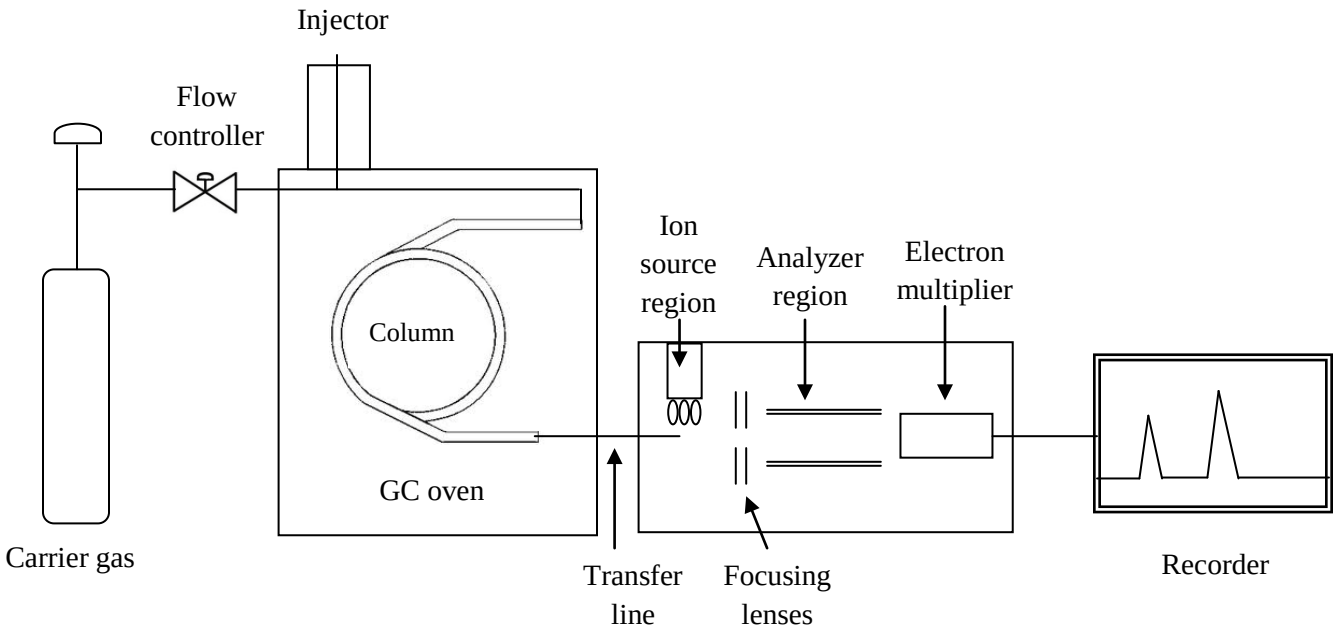


Figure 7.2 Schematic representation of a typical gas chromatography/mass spectrometer.

Chapter Three: Experimental methods

3.1 Zeolites used

Both synthesised and commercially supplied zeolite catalysts with different Si/Al ratios were used in this work. NaY zeolite was synthesized as described in the following section 3.2, HBeta was supplied by Alfa Aesar and ZSM-5 was supplied by Beijing Balvin-kalvin Co., LTD.

3.2 Synthesis of NaY zeolite

Zeolite Y was synthesized from a seed gel and feedstock gel following the detailed procedure given by Ginter et al. [45]. The major difference between seed gel and feedstock gel is that the feedstock gel was prepared and used immediately without aging. Briefly, the seed gel having a molar ratio of $10.67Na_2O:Al_2O_3:10SiO_2:180H_2O$ was prepared by adding Na_2SiO_3 solution to the solution of $NaAlO_2$. The mixture was stirred until homogeneous and transferred into a polypropylene (PP) bottle, capped, and aged at room temperature for 24 h. The feedstock gel with molar ratio $4.30Na_2O:Al_2O_3:10SiO_2:180H_2O$ was prepared in similar fashion to that of the seed gel. The NaY synthesis was carried out by a slow addition of the seed gel into the feedstock gel while stirring. The mixture was transferred into a PP bottle, capped, and crystallized at 100°C for 5 h. After the crystallization, the sample was left to cool to room temperature. The solid product was separated by filtration, washed thoroughly with deionised water, and dried at 110°C. [46].

3.3 Preparation of the solid acid catalysts: HY and HZSM-5

Aqueous ion exchange was carried out with a solution of 10^{-1} mol/L concentration of ammonium nitrate (Aldrich chemical, ≥99.0%) to produce NH_4-zeolites. NaY and ZSM-5 samples (10 g of each) were added to the ammonium nitrate solution and stirred at room temperature for 24 h; the exchanged samples were separated by filtration and dried in oven at 80°C overnight. This procedure was repeated three times to produce a high degree of exchange [47]. The exchanged samples were then calcined in a tubular furnace at 500°C for 1h in air to produce the protonated form of the zeolites [48].

3.4 Rare-earth ion-exchange on H-zeolite catalysts

3.4.1 Preparation of 5% and 10% Ce

The cerium incorporation in the zeolites was performed by ion exchange using aqueous solution of cerium (III) nitrate hexahydrate [$Ce(NO_3)_3.6H_2O$] (Aldrich, 99.9% purity). For 5% Ce on zeolite, 0.775g of $Ce(NO_3)_3.6H_2O$ was dissolved in deionised water and stirred at room temperature for 2 h until a clear solution obtained. Zeolites samples (5 g of each) were impregnated with the solution, the resultant mixture was stirred for 60 min and ultrasonated for 2 h at room temperature until a homogeneous mixture obtained. The exchange was followed by filtering, drying and calcination in air 4 h at 550°C. For 10% Ce on zeolite the quantity of [$Ce(NO_3)_3.6H_2O$] was doubled [49].

3.4.2 Preparation of 5% and 10% La

The lanthanum incorporation in the zeolites was performed by ion exchange using aqueous solution of lanthanum nitrate solution [$La(NO_3)_3$] (Fluka, 0.1 mol/l). For 5% La, zeolites samples (5 g of each) were impregnated in 18 ml of [$La(NO_3)_3$]. The resultant mixture was stirred for 60 min and ultrasonated for 2 h at room temperature until a homogeneous mixture obtained. The exchange was followed by filtering, drying and calcination in air 4 h at 550°C. For 10% La on zeolite the quantity of [$La(NO_3)_3$] was doubled [49].

3.5 Characterization of zeolite samples

Characterization is an integral tool for the development of new zeolites and for the development and commercialization of zeolitic catalysts and adsorbents [13]. A variety of physical techniques were utilized to fully characterise the samples.

3.5.1 X-ray powder diffraction (XRD)

Powder XRD patterns were collected on a PW3040/60 X'pert PRO Console diffractometer (Figure 1.3) using Cu-Kα1 (1.5406 Å) as incident radiation. The tube voltage was 45 mV and tube current was 40 mA. The scan diffraction angle is from 5º to 70º and the samples were scanned at 0.008°/min in 2θ. The cell parameters were determined from the powder diffraction data using the program UnitCell are outlined in chapter 4.



Figure 1.3 PW3040/60 X'pert PRO Console diffractometer.

3.5.2 Solid state NMR

Solid state ^{29}Si spectra were record at 79.435 MHz using a Varian VNMRS spectrometer (Figure 2.3) and a 6 mm (rotor o.d.) magic angle spinning probe. They were obtained using direct excitation with a 300 s recycle delay, at ambient probe temperature (~25°C) and at a sample spin rate of 6.8 kHz. Spectral referencing was with respect to an external sample of neat tetramethylsilane.

Solid state ^{27}Al spectra were record at 104.199 MHz using a same spectrometer and a 4 mm (rotor o.d.) magic angle spinning probe. They were obtained using direct excitation with a 0.2 s recycle delay, at ambient probe temperature (~25°C) and at a sample spin rate of 12 kHz. Spectral referencing was with respect to an external sample of aqueous 1M $AlCl_3$.



Figure 2.3 Varian VNMRS spectrometer.

3.5.3. Scanning electron microscopy (SEM)

To determine the morphology of zeolite samples, the scanning electron microscopy images of gold-coated zeolite samples were obtained using a FEI-NNL200 microscope (Figure 3.3).



Figure 3.3 FEI-NNL200 scanning electron microscope.

3.5.4 Nitrogen physisorption

Textural properties such as surface area, pore volume and pore size measurements studies were carried out by using physisorption technique. The adsorption –desorption isotherm for nitrogen was measured at 77K. Prior to the experiments, the samples were degassed at 200ºC for 10 h. The isotherm was measured using a Micrometrics ASAP 2010 system (Figure 4.3). The surface area was calculated using the Brunauer-Emmett-Teller (BET) equation based on adsorption data. The pore size distributions were calculated using the Barrett–Joyner– Halenda (BJH) model applied to the adsorption branch of the isotherm, assuming cylindrical pore geometry. The statistical film thickness (t) was calculated by means of the Harkins–Jura equation. Pore volumes were determined from the nitrogen adsorbed volume at P/P0 = 0.98. Micropore volume and external surface area were calculated by application of the t-plot method in the selected range of the adsorption branch of the isotherm.



Figure 4.3 Micromeritics ASAP 2020.

3.6 Zeolite catalysts evaluation

The alkylation of benzene with ethylene was carried out in a benchtop pilot plant (MicroReactor 10A, Beijing Brighty Instrument Co., LTD) as shown in Figure 5.3, equipped with a stainless-steel fixed bed down-flow reactor. In a typical run, 250 mg of catalyst was located in the center of the reactor and pretreated at 550°C for 1 h in Argon. After the reactor was cooled down to 250°C, benzene (Sigma-Aldrich, HPLC grade 99.9%) was pumped into the reactor to fully fill the bed before ethylene was introduced. The reaction conditions were as follows: 5 bar of pressure, 250°C of temperature, 0.5 h^{-1} of weight hourly space velocity (WHSV) of ethylene, 1:1 and 3:1 of benzene/ethylene molar ratio. A schematic diagram of the reaction system is shown in Figure 6.3.



Figure 5.3 MicroReactor 10A benchtop pilot plants.

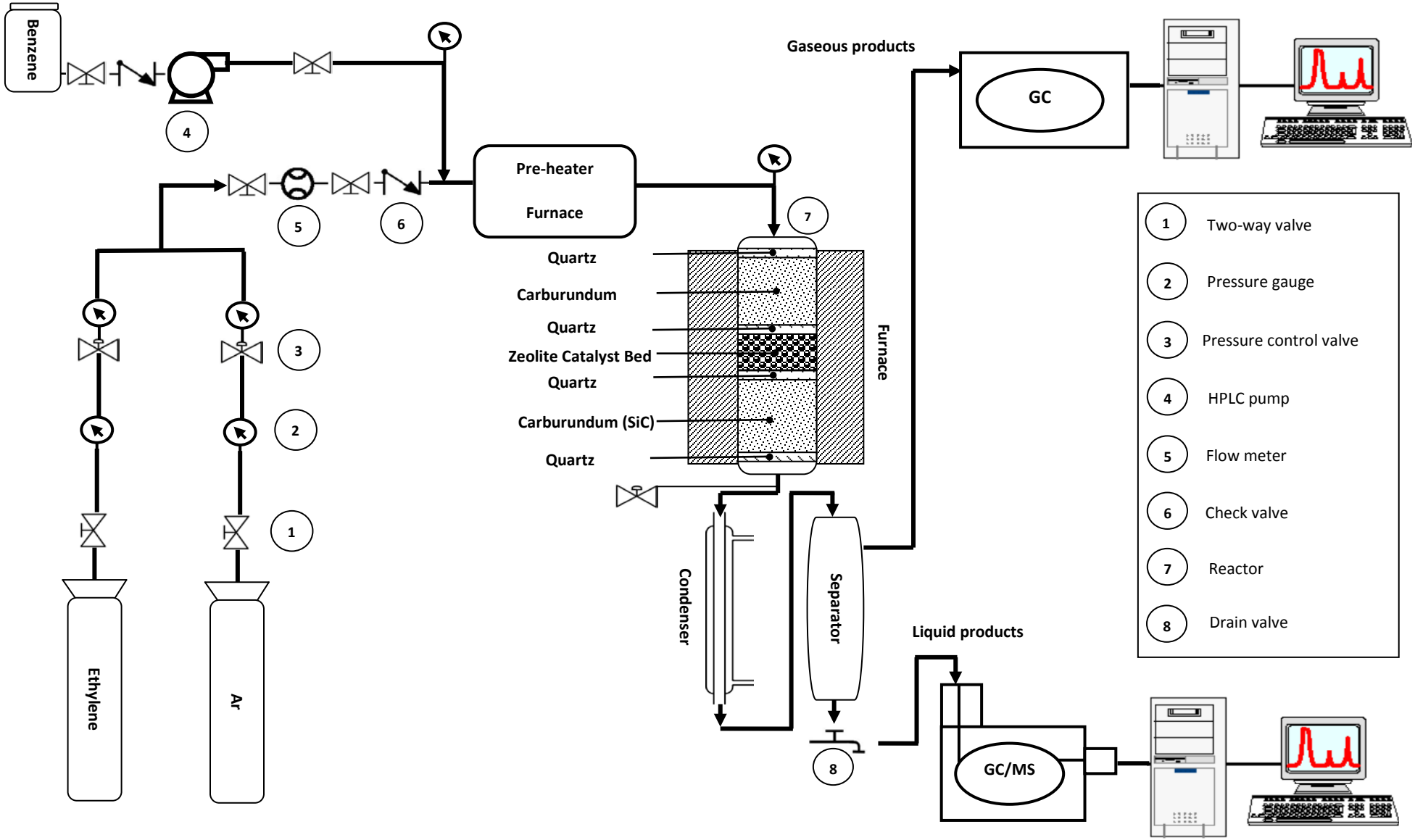


Figure 6.3 Schematic diagram of the reaction system.

3.7 Products distribution identification

3.7.1 Gas chromatography (GC)

Gas products were analyzed by gas chromatography (Shimadzu GC-2014) (Figure 7.3) equipped with a FID and TCD detectors and a concentric packed column (CTR I); the outer column dimension is 6ft X 1/4" packed with activated molecular sieve, and the inner column dimension is 6ft X 1/8" packed with porous polymer mixture. The carrier gas is argon and the analyzing temperature is 35°C.



Figure 7.3 Shimadzu GC-2014.

3.7.2 Gas chromatography/mass spectrometry (GC/MS)

The liquid products were analyzed by gas chromatograph-mass spectrometer (Shimadzu GC/MS-QP 2010 SE) (Figure 8.3) equipped with a capillary column (SHIM-5MS) 30m X 0.25 mm ID. The ion source temperature is 250°C, interface temperature 250°C and detector voltage 0.7kV.



Figure 8.3 Shimadzu GC/MS-QP 2010 SE.

3.8 Calibration of reactants flowrates

To prepare the catalyst testing unit for the reaction, it is important to calibrate the reactant flow rate to get accurate feed ratios.

3.8.1 Ethylene mass flowmeters calibration

The mass flowmeter was calibrated by a cylindrical burette using ethylene gas (BOC, 99.9% purity) under deferent reactor pressure (atmospheric, 2.5, 5 and 7.5 bar) as shown in figure 9.3.

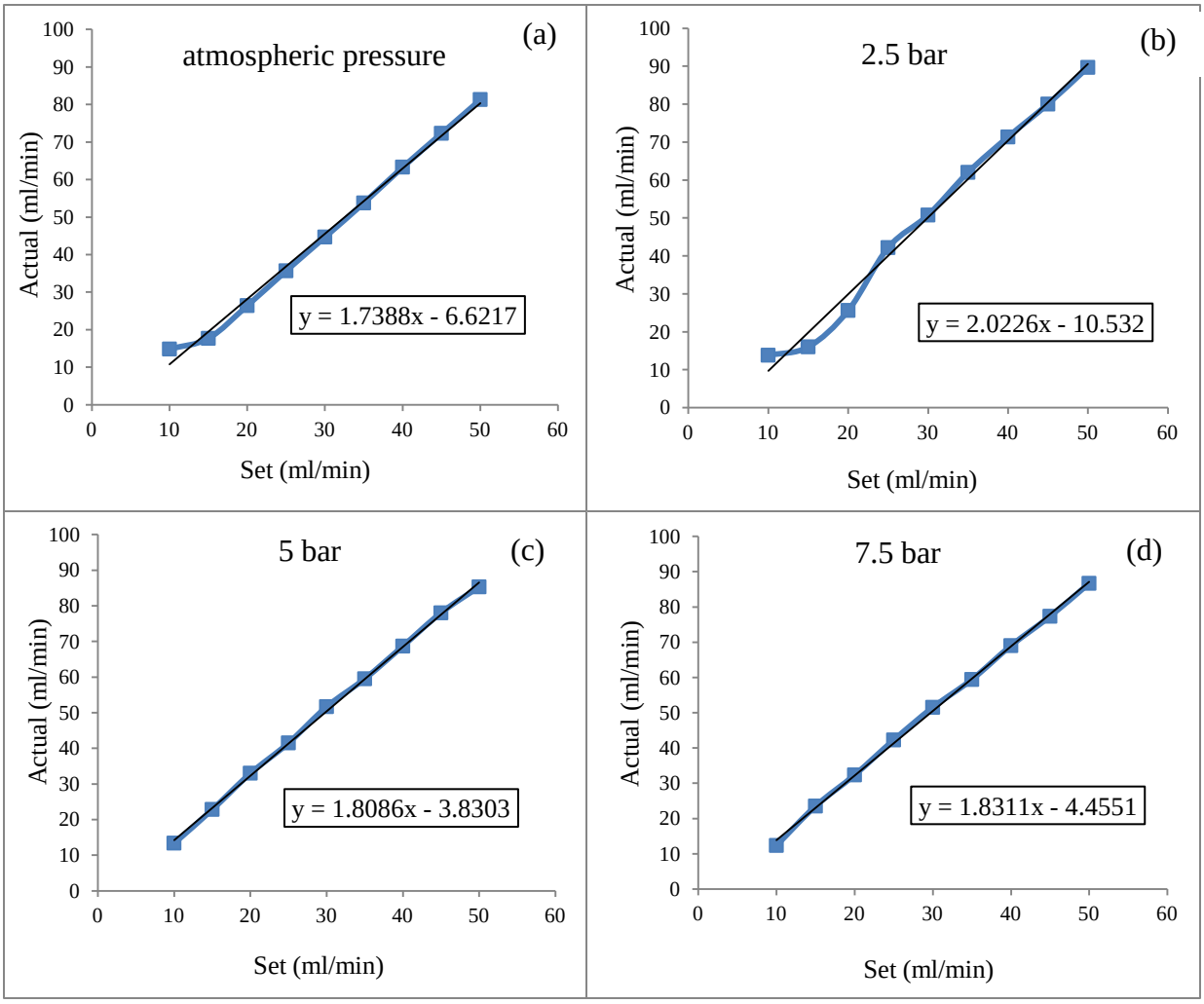


Figure 9.3 Mass flowmeter calibration using ethylene gases under different reactor pressures: (a) atmospheric, (b) 2.5 bar, (c) 5 bar and (d) 7.5 bar.

3.8.2 HPLC pump calibration

HPLC pumb was calibrated using methanol (Rathburn, HPLC grade) as shown in figure 10.3.

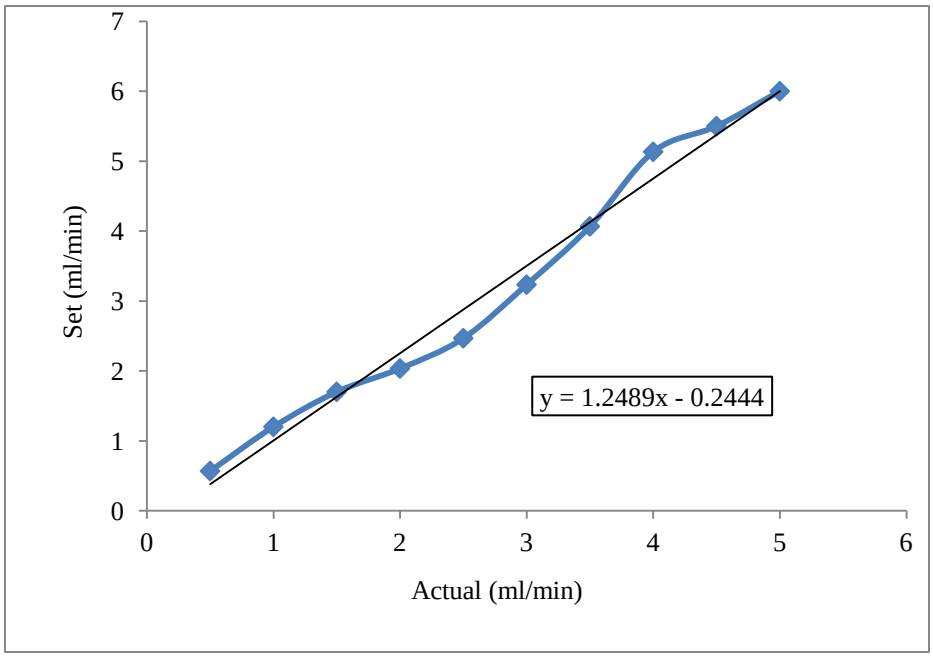


Figure 10.3 HPLC pumb calibration for liquid benzene.

Chapter Four: Results and discussion

4.1 X-ray powder diffraction

X-ray powder diffraction is a powerful analytical tool for the structural characterization of zeolites; it can be used to determine whether a new zeolite has been formed; it also provides direct information on the zeolites crystal structure and morphology.

Using diffraction methods, Lutz et al. [50] showed a very pure faujasite zeolite diffraction pattern with only a small non-crystalline contribution for the NaY sample. Chen et al. [21] made a comparison between the calculated results and the data supplied by the Structure Commission of the International Zeolite Association (IZA-SC); they observed that the locations of the peaks in the XRD patterns were consistent. This was supported by Morales et al. [31] for both NaY and ZSM-5 zeolites.

Figure 1.4 shows the XRD patterns for NaY, ZSM-5 and HBeta zeolites, and indicate to high crystallinity for both NaY and ZSM-5 zeolites, contained almost pure phases with a trace amount of NaP zeolite (indicated on the pattern by *) in NaY pattern. This is known to be a competing phase during synthesis of the **FAU**-type zeolites (Figure 1.4a, 1.4b). The XRD pattern for HBeta (Figure 1.4c) showed acceptable (but clearly not high) crystallinity and was similar to those reported in previous studies [48,52].

The cell parameters for the zeolites NaY, ZSM-5 and HBeta were determined from the powder diffraction data using the program UnitCell [53]. These were compared against literature values by Treacy and Higgins [54] (Table 1.4).

Table 1.4 Derived cell parameters for NaY, ZSM-5 and HBeta zeolites†.

Sample	***a* (Å)**		***b* (Å)**		***c* (Å)**	
	This data	*Data from ref. [54]*	*This data*	*Data from ref. [54]*	*This data*	*Data from ref. [54]*
NaY	24.60003 (0.00115)†	25.028	24.60003 (0.00115)	25.028	24.60003 (0.00115)	25.028
ZSM-5	20.21843 (0.00369)	20.002	20.05305 (0.00343)	19.899	13.21139 (0.00153)	13.383
HBeta	12.48165 (0.00095)	12.661	26.47509 (0.00280)	26.406	26.47509 (0.00280)	26.406

† Error estimates shown in brackets.

Considerable work has been done to relate the aluminium content of the hydrated zeolite structure to the unit cell size. In general, a linear relationship is derived where unit cell parameter increases with increased framework aluminium content and such relationships are commonly used to estimate framework aluminium content [55]

Appendix B shows in detail the influence of ion exchange processes on unit cell parameter for zeolites Y, ZSM-5 and HBeta. It is interesting to see the unit cell parameter increases with Na^+ was exchanged with NH_4 in Y and ZSM-5 zeolites. Such ammonium exchange can lead to an increased lattice parameter. In this work we observed also the decreasing in the unit cell parameter with increasing the rare-earth exchanged amount, this may to the effect of high Ce or La content lead to make some strain on the unit cell lead to a decreased lattice parameter.

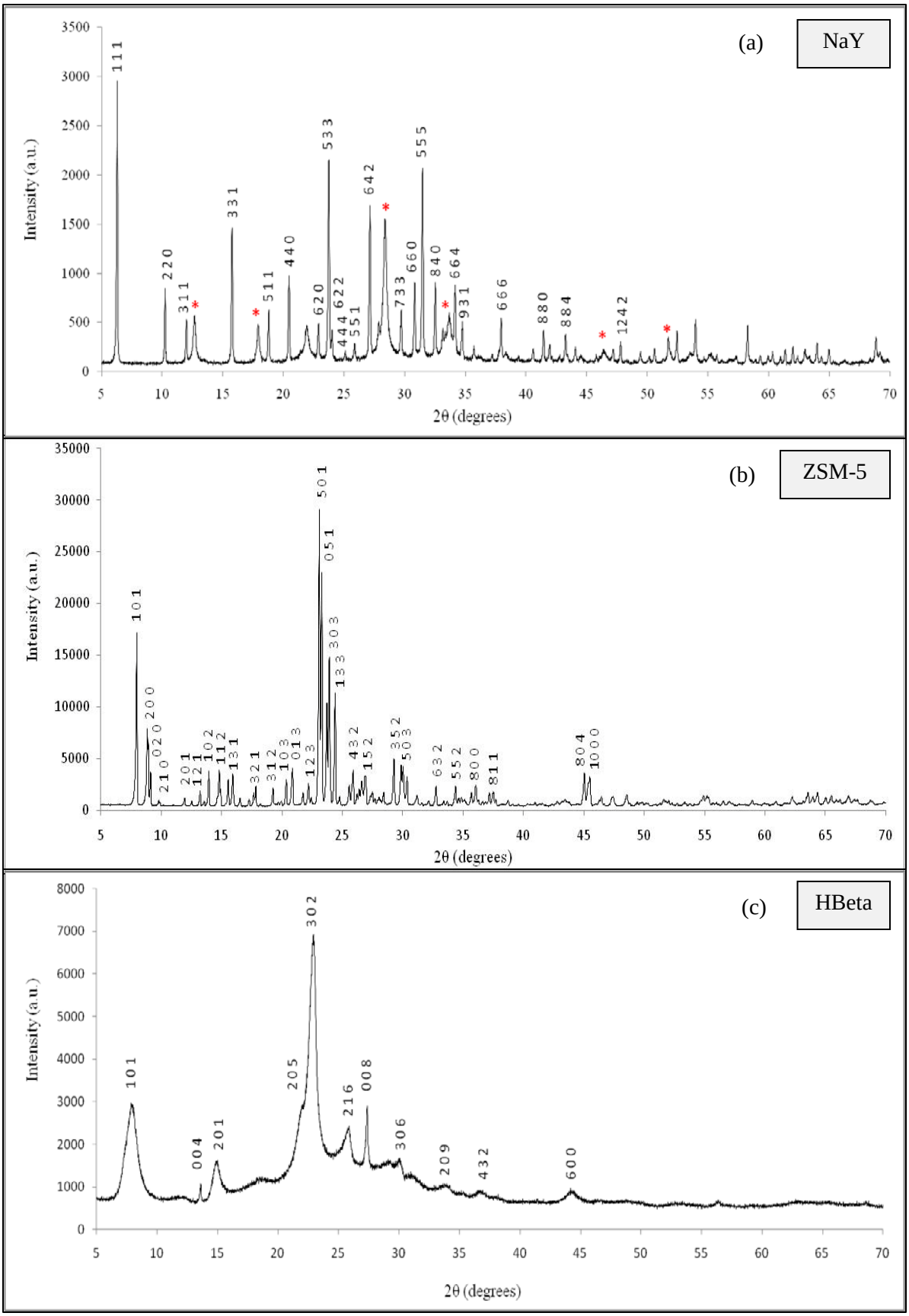


Figure 1.4 XRD patterns of (a) NaY, (b) ZSM-5 and (c) HBeta zeolites. Indexed to calculate cell parameter using UnitCell program, * indicate the observation of a trace amount of NaP zeolite in NaY pattern.

With respect to the influence of ion-exchanged rare-earth species on the crystallinity of zeolites, Zhang et al. [56] pointed out that crystallinity is not changed significantly following the ion-exchange of lanthanum in ZSM-5, and Ren et al. [57] confirmed that the ion-exchange of lanthanum would not drastically affect the framework structure of ZSM-5. In contrast, Wang et al. [58] reported that La^{3+} substitutes for Al^{3+} and this substitution noticeably affects the crystal structure and crystallinity of ZSM-5.

Figure 2.4 shows the XRD patterns of various ion exchanged samples of NaY, ZSM-5 and HBeta. In general, it is interesting to note that the resulting overall XRD patterns remained approximately same after cation exchange with both the number and position of peaks do not change noticeably following the ion-exchange and treatment processes (see Appendix A), and any dealumination treatments do not appear to lead to a significant destruction of the zeolite framework. This is suggestive that these zeolites appear to have a broad range of flexible crystal structure, which can accomodate a range of various cations (of varying composition also).

The XRD pattern of zeolite Y samples shows a general decrease in peak intensities of the two rare-earth HY materials (actually some of the diffraction peaks also broaden) when the rare-earth ion-exchange concentration is increased, reflecting both a possible local change in the zeolite structure and also a possible degree of disruption / local destruction of the crystallite structure. The peak intensity of HZSM-5 zeolite materials also decreased with the increase in the concentration of the ion exchange [82]. It is known also the low-angle XRD intensities are particularly sensitive to the presence of any extra-framework species inside the channels [56]. Therefore, the decrease of peak intensity of low-angle diffraction peaks in the XRD pattern of rare-earth ion-exchanged zeolites might also

suggest the location/movement of extra framework La or Ce (or other) cations into the host zeolite channels.

In the case of HBeta zeolites, the intensity of the peaks at angle about (2θ = 15°, 23°, 25° and 27°) decrease noticeably as the ion-exchange concentration is increased. In this particular zeolite it is clear that the crystal structure is noticeably destroyed when the (H^+) ion exchange concentration is too large, which leads to the decrease in the stability and crystallinity of the catalyst [83]. The relative low level of crystallinity is also immediately evident in figure 1.4 for the "parent" HBeta zeolite.

In both ZSM-5 and HBeta, the presence of four new peaks at angle about (2θ = 28°, 33°, 47° and 57°) appear after exchanged with Ce, and this peaks significantly increase as the impregnated amount is increased from, which may be due to the high Ce content inducing some plane changes.

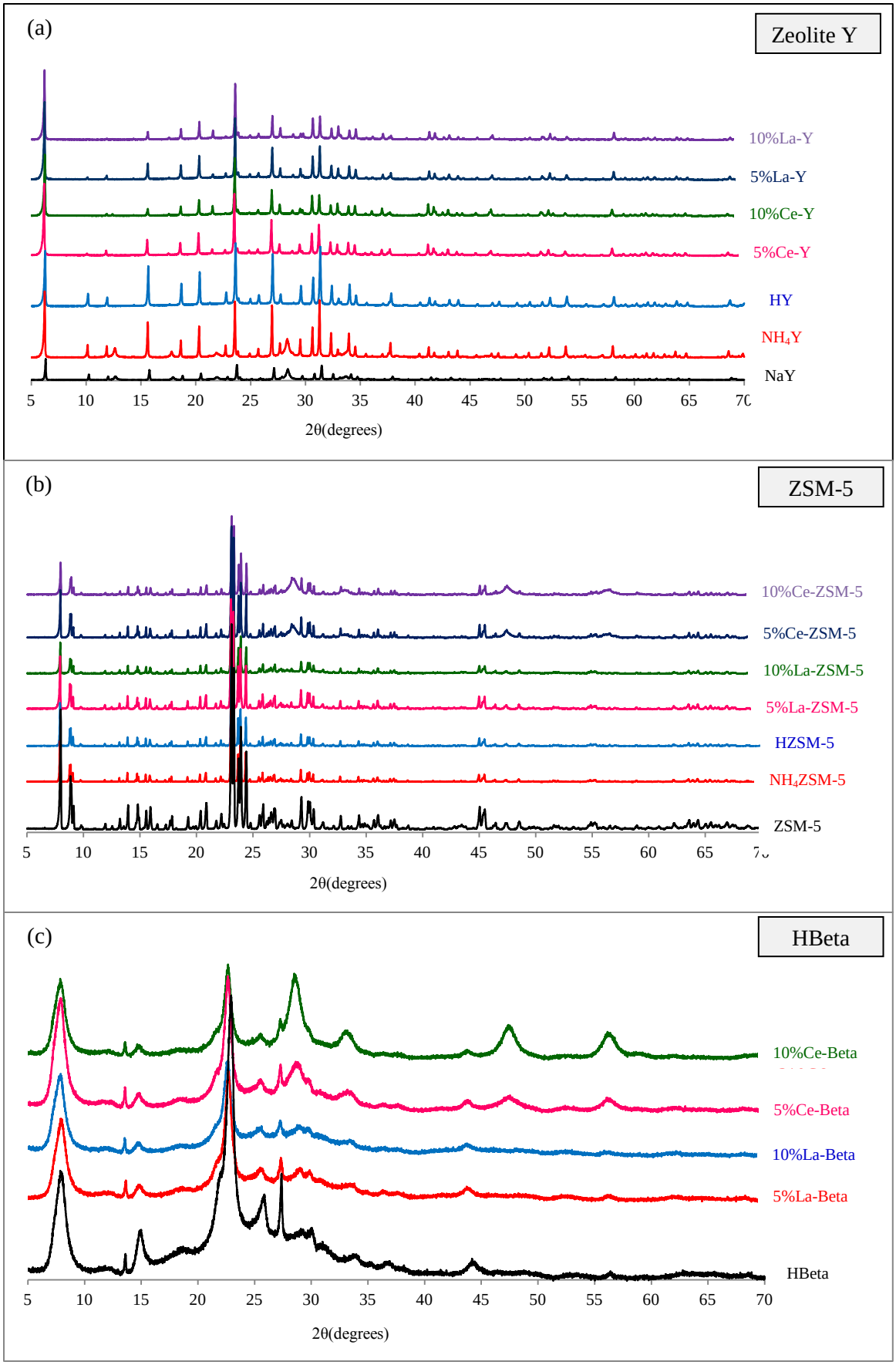


Figure 2.4 XRD patterns of various ion-exchanged forms of zeolite catalysts (a) Y, (b) ZSM-5 and (c) HBeta.

4.2 Zeolite morphology studied by SEM

Figure 3.4 shows the SEM images of NaY, ZSM-5 and HBeta with reveal a uniform particle size of the sample with a more-or-less regular shape, a very clear and sharp crystallinity and a narrow distribution of particle size, with average crystal size of <1 μm.

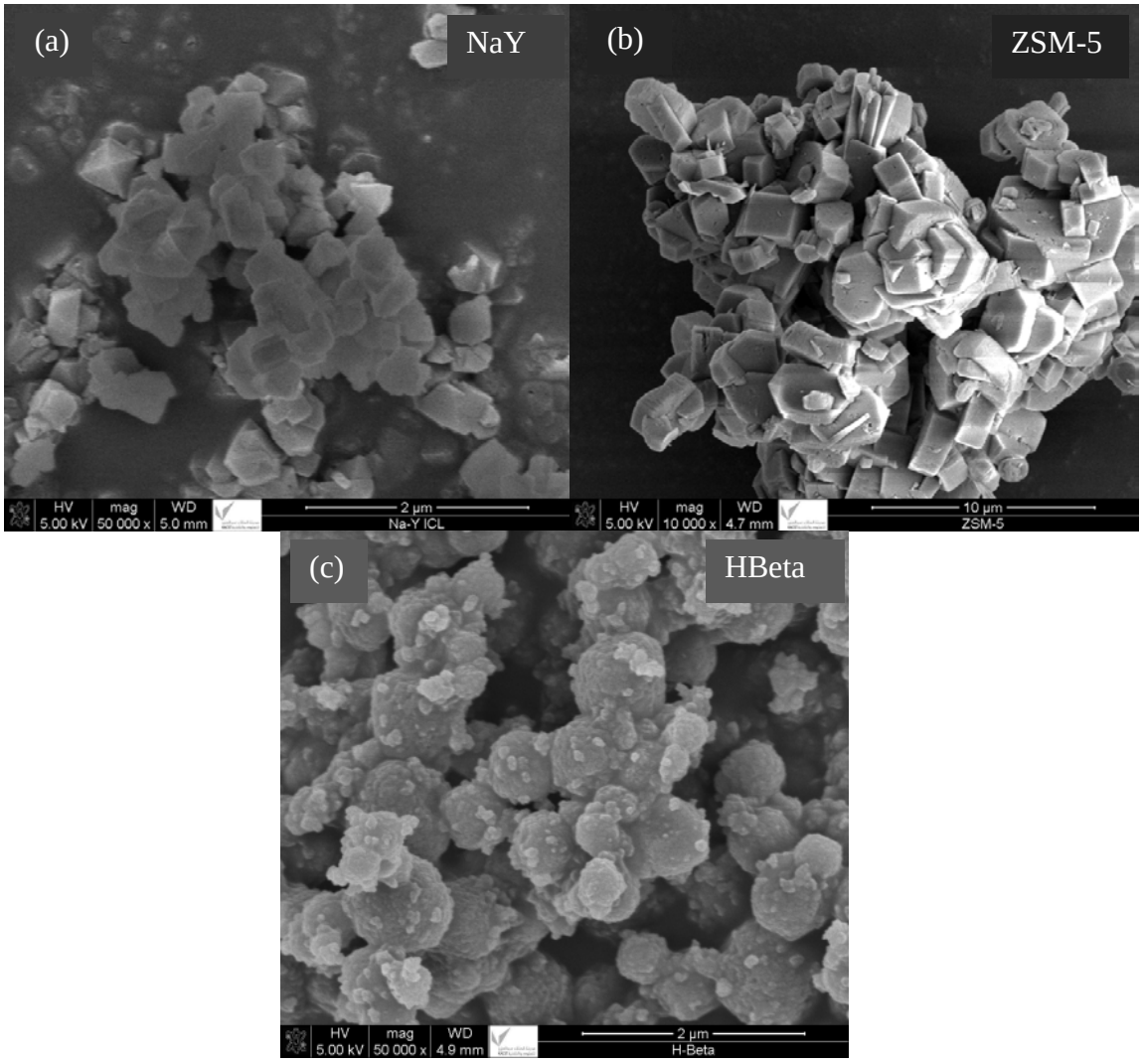


Figure 3.4 SEM images of (a) NaY, (b) ZSM-5 and (c) HBeta.

4.3 Solid state MAS NMR

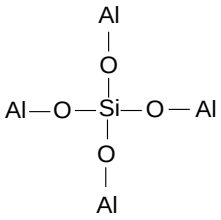
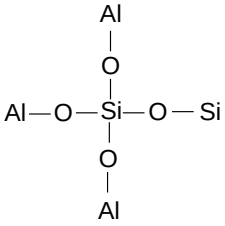
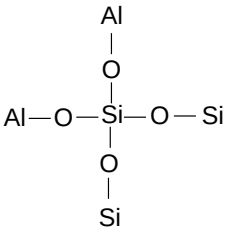
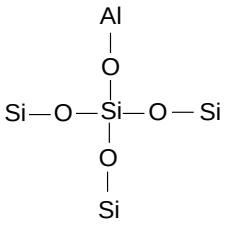
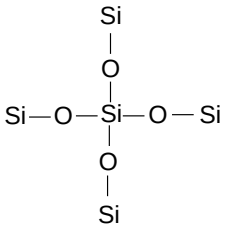
4.3.1 ^{29}Si NMR spectra

The Si framework ions in aluminosilicate zeolites are usually tetrahedrally coordinated, and thus in principle there can be five different possible local environments for a silicon atom, reflecting the various (combinatorial) possibilities for neighboring aluminium atoms. Certain zeolites can have all five local environments, while some only have one or two of local environments, depending on the Si/Al ratio (Table 2.4) [59-62,71].

Engelhardt et al. [63] found that the ^{29}Si spectra of NaY consists of two weak peaks for Si(3Al) and Si(0Al) and two strong peaks for Si(2Al) and Si(1Al) with Si/Al ratio equal to 2.5. Hannus et al. [64] showed that the NaY zeolite contains of all five Si environments for a Si/Al ratio equal to 2.44.

Figure 4.4 show ^{29}Si MAS NMR spectra for NaY, ZSM-5 and HBeta zeolites. The ^{29}Si spectrum for NaY (Figure 4.4a) nicely illustrates the presence of all five silicon environments, corresponding to Si(4Al), Si(3Al), Si(2Al), Si(1Al) and Si(0Al) in the range of chemical shift between -85 and -101 ppm. ^{29}Si MAS NMR spectrum for ZSM-5 (Figure 4.4b) shows two silicon environments, one at -105.5 ppm, which is generally attributed to silicon having one aluminium as neighbor Si(1Al) and other around -112 ppm is due to silicon without any aluminium in the surroundings Si(0Al). These results are similar with those published by Maijanen et al [65] where the authors observed two peaks, one at -106 ppm for Si(1Al) and another at around -112 ppm for Si(0Al). Figure 4.4c shows ^{29}Si MAS NMR spectrum for HBeta zeolite, where a large peak at 101.4 ppm is assigned to Si(1Al), and two peaks at -91 ppm and -112 ppm indicate the presence of Si(3Al) and Si(0Al) respectively. This is in agreement with the data of Kuehl et al. [66].

Table 2.4 Ranges of ^{29}Si MAS NMR chemical shifts for aluminosilicate zeolites [16].

Coordination	*Notation*	*Chemical shift (ppm)*
	Si (4Al)	-86 ⟶ -90.5
	Si (3Al)	-88 ⟶ -97
	Si (2Al)	-93 ⟶ -102
	Si (1Al)	-97.5 ⟶ -107
	Si (0Al)	-101.5 ⟶ -116.5

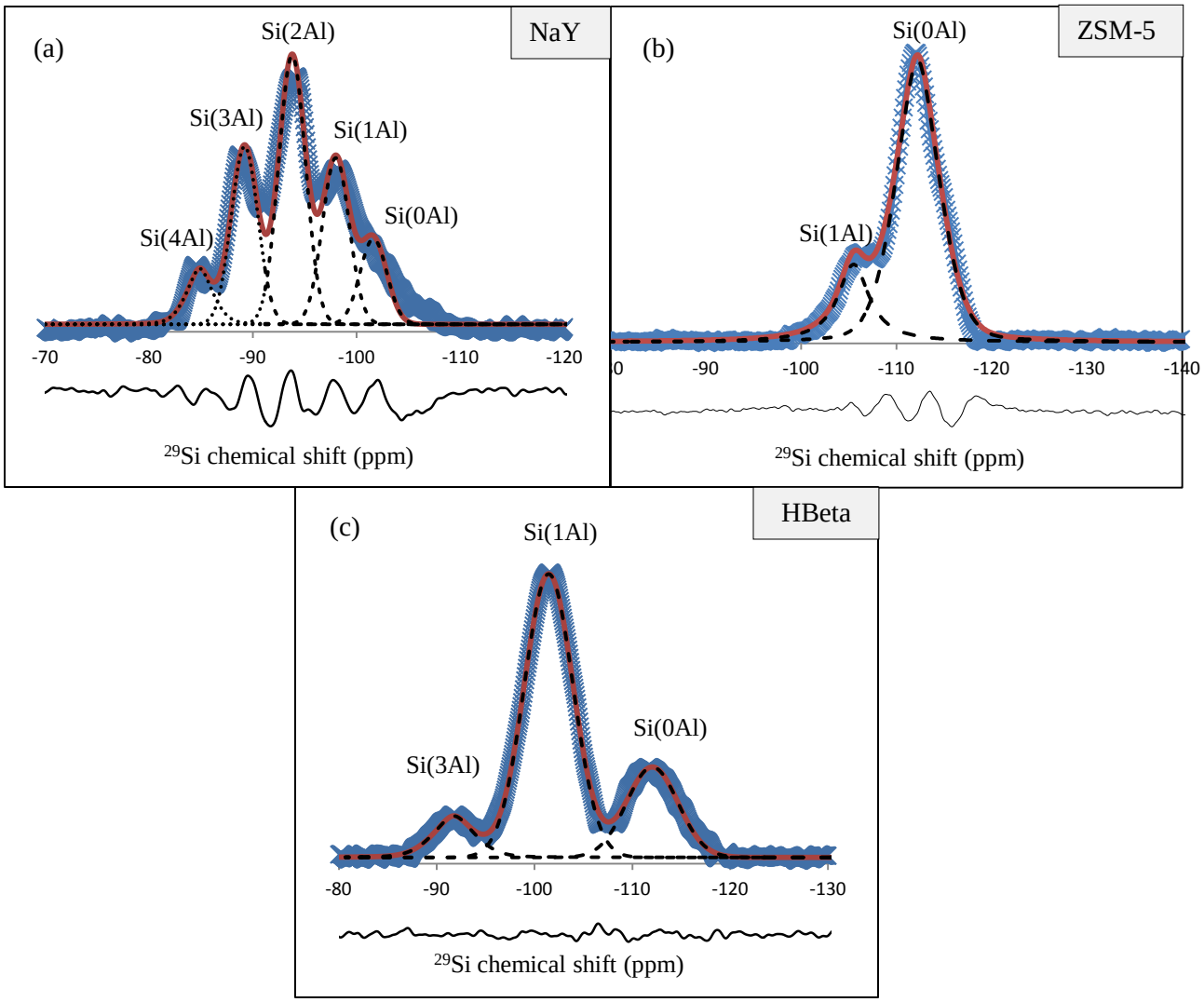


Figure 4.4 ^{29}Si MAS NMR spectra for (a) NaY, (b) ZSM-5 and (c) HBeta. Experimental spectrum-blue symbols, red line-computer simulated spectrum fitted with pseudo-Voigt profile, Individual deconvoluted peaks are shown as black dotted lines, solid black line- difference between experimental and simulated spectrum.

The Si/Al ratio in the aluminosilicate framework can therefore be calculated from the integrated intensities of the ^{29}Si MAS NMR spectrum using the formula:

$$Si/Al = \sum_{n=0}^{4} I_{Si(nAl)} \; / \; \sum_{n=0}^{4} \left(\frac{n}{4}\right) I_{Si(nAl)} \qquad (1.4)$$

Where *I* denotes the intensity (peak area) of the individual NMR peak corresponding to the Si(*n*Al) building unit, *n* varies between 0 and 4 [61].

Calculated Si/Al ratios and chemical shifts from our experimental ^{29}Si NMR spectra are listed in Table 3.4.

Table 3.4 Si/Al ratios and chemical shifts from ^{29}Si NMR data for NaY, ZSM-5 and HBeta zeolites.

Sample	***Si/Al ratio***	***δ (ppm)***				
		Si(4Al)	**Si(3Al)**	**Si(2Al)**	**Si(1Al)**	**Si(0Al)**
NaY	3.92	-84.53	-89.81	-93.76	-98.31	-101.45
ZSM-5	18.46	-	-	-	-105.5	-112.22
HBeta	22.64	-	-91	-	-101.4	-112

Figure 5.4 shows the ^{29}Si spectra of HY and HZSM-5 zeolites. Figure 5.4a indicates the effects on the NMR spectra of ion exchange and calcination processes on the silicon local environments. If one compares the corresponding spectrum for the Na form of zeolite Y (Figure 4.4a), we notice the absence of the Si peak from Si(4Al) in figure 5.4b, for HZSM-5 we see the same silicon environments as the Na form (Figure 4.4b) with only a minor change in the area under the peaks.

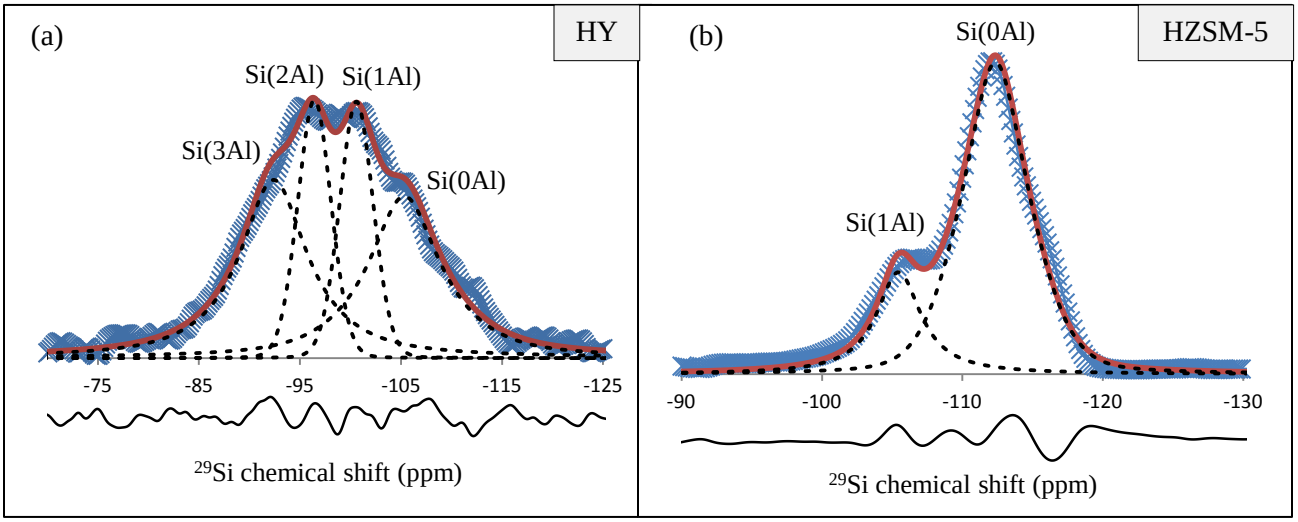


Figure 5.4 ^{29}Si MAS NMR spectra for (a) HY and (b) HZSM-5. Experimental spectrum-blue symbols, red line-computer simulated spectrum fitted with pseudo-Voigt profile, Individual deconvoluted peaks are shown as black dotted lines, solid black line- difference between experimental and simulated spectrum.

The ^{29}Si MAS NMR spectra of rare-earth ion-exchanged zeolite catalysts, to be discussed later in this thesis, we see a discernible high-field shift of the Si(*n*Al) signal also, the NMR detects a variation of the local structure of AlO_4 tetrahedra in the vicinity of the silicon atoms due to the presence of highly charged rare earth cations. We also observe theeffect of cationic extra-framework aluminium (hexa-coordinated aluminium formed via leaching from the framework) which have been widely reported [83]. Each rare earth cation satisfies single negative valency of 3 aluminium tetrahedra in the framework and this induce considerable strain in the zeolite framework. This nicely illustrate the ^{29}Si NMR is noticeably influenced by counter cations in the extra-framework cations locations.

^{29}Si MAS NMR spectra for zeolites Y, ZSM-5 and Beta in figures 6.4-11.4 show the effect of zeolites modification by various ion exchange and dealumination processes on silicon environments for the modified zeolites.

For H zeolite Y, one sees after H^+ ion-exchange presence of now four silicon environments corresponding to Si(3Al), Si(2Al), Si(1Al) and Si(0Al) in the range of chemical shift between -89 and -106 ppm (Figures 6.4 and 9.4).

^{29}Si MAS NMR spectrum for HZSM-5 modified catalysts (Figures 7.4 and 10.4) shows two silicon environments, one around -105 ppm, which is generally attributed to silicon having one aluminium as neighbor Si(1Al) and other around -112 ppm is due to silicon without any aluminium in the surroundings Si(0Al).

Figures 8.4 and 11.4 show also ^{29}Si MAS NMR spectrum for H-Beta modified zeolite, where a large peak around -111 ppm assign to Si(1Al), and two peaks at -106 ppm and -

115 ppm indicates to present of Si(2Al) and Si(0Al) respectively. The broad peak at -106 ppm may assign to the overlapping between two environments, Si(2Al) and Si(1Al).

These spectra are similar to those shown previously in figures 4.4 and 5.4, with observed changes in the area under the peaks due to the differences in aluminium distribution on the zeolite framework.

Table 4.4 shows the influence of rare-earth ion-exchanged process on the Si/Al ratio in different zeolite catalysts. We observe a decrease in the Si/Al ratio following the ion exchange process as the rare earth concentration increase. This decrease in the Si/Al ratio is due to the incorporation of rare-earth ions and the calcination step which deal to "loosing" of frame-work aluminiums. In the case of HZSM-5, it is particularly interestingly to observe that no effect of the rare earth concentration in the Si/Al ratio and this indicates to the ability in ZSM-5 zeolite to host high concentrations of Ce or La as extra framework cations.

Table 4.4 Comparison of Si/Al ratio from ^{29}Si NMR data for different modified zeolite catalysts.

	Si/Al ratio				
Catalyst	*H-form*	*5%Ce*	*10%Ce*	*5%La*	*10%La*
Y	3.69	3.21	2.79	3.60	2.33
ZSM-5	12.68	4.00	4.00	4.00	4.00
HBeta	22.64	4.70	4.48	4.65	4.50

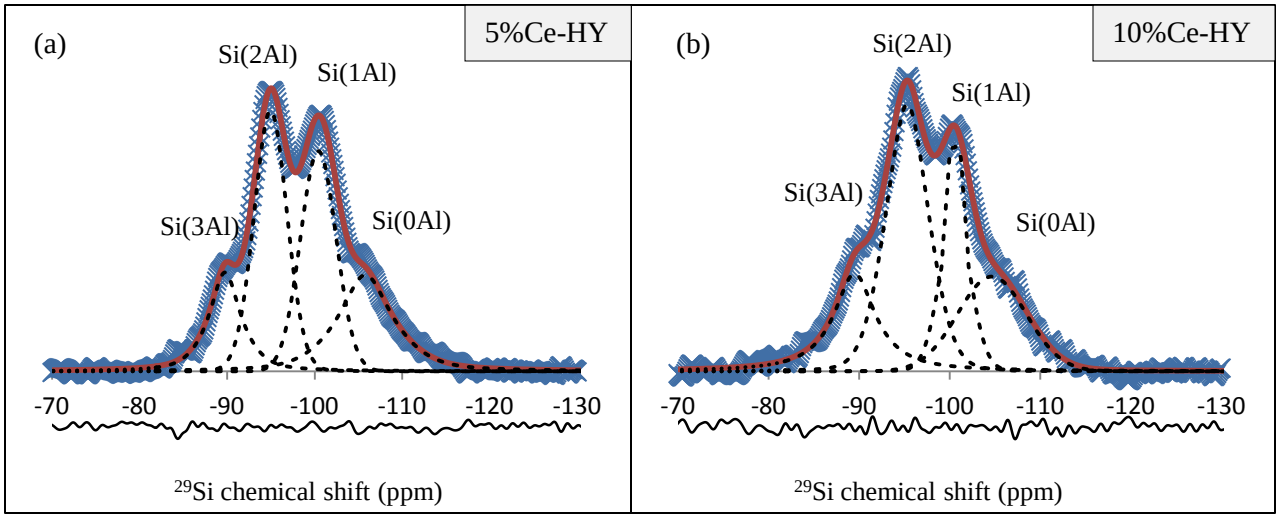


Figure 6.4 ^{29}Si MAS NMR spectra for (a) 5%Ce-HY and (b) 10%Ce-HY.

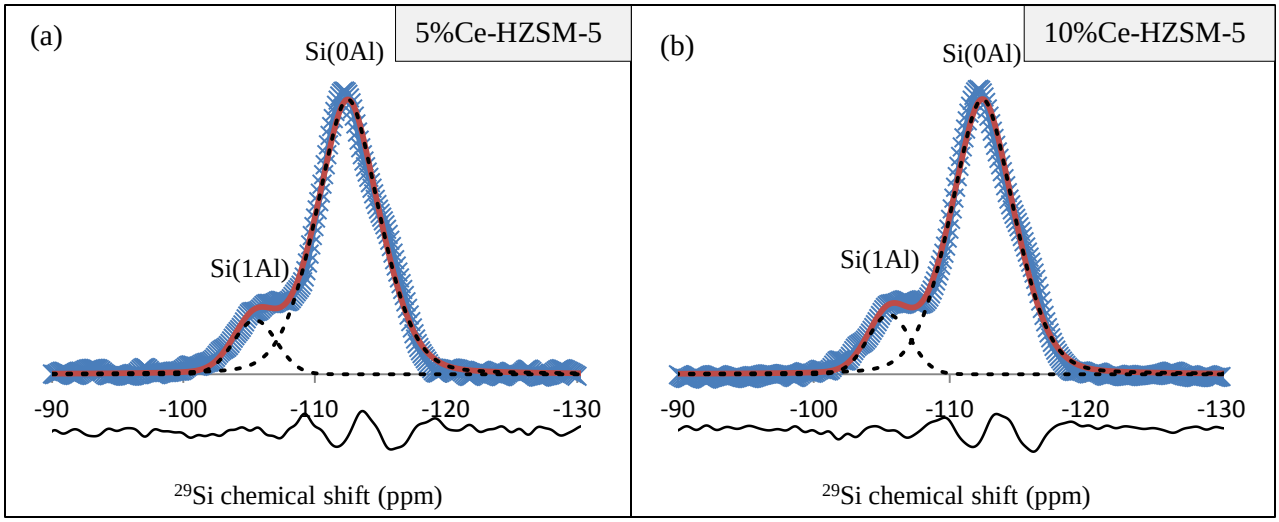


Figure 7.4 ^{29}Si MAS NMR spectra for (a) 5%Ce-HZSM-5 and (b) 10%Ce-HZSM-5.

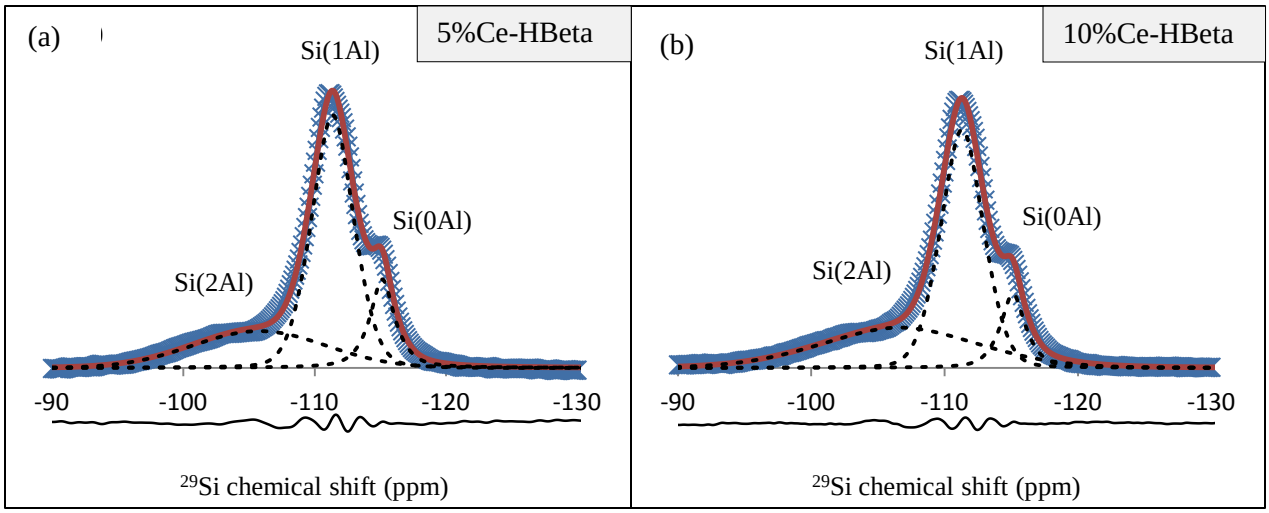


Figure 8.4 ^{29}Si MAS NMR spectra for (a) 5%Ce-HBeta and (b) 10%Ce-HBeta.

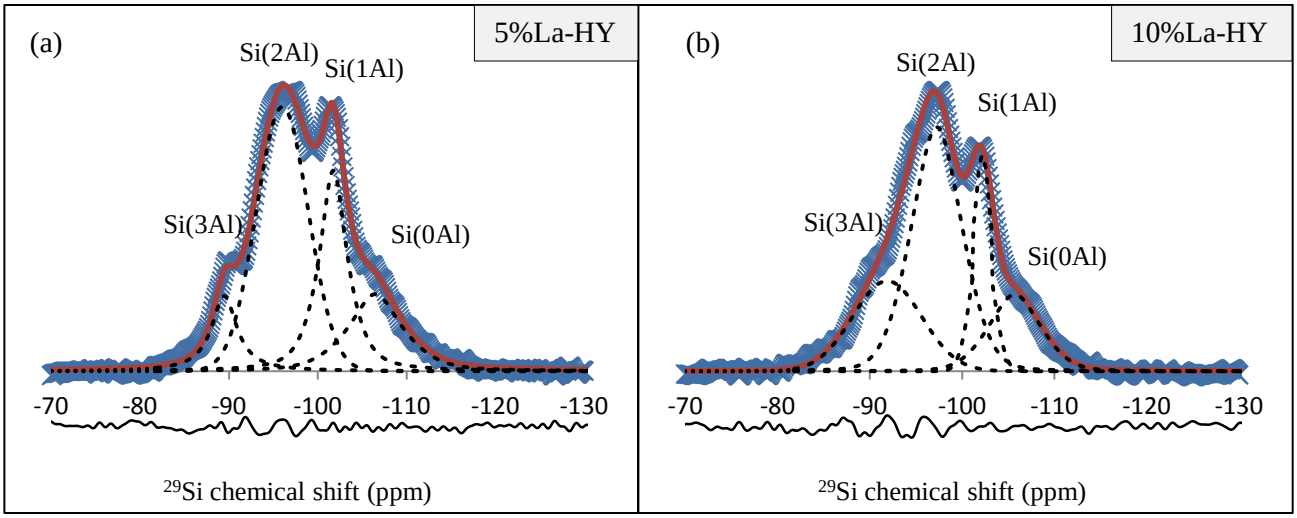


Figure 9.4 ^{29}Si MAS NMR spectra for (a) 5%La-HY and (b) 10%La-HY.

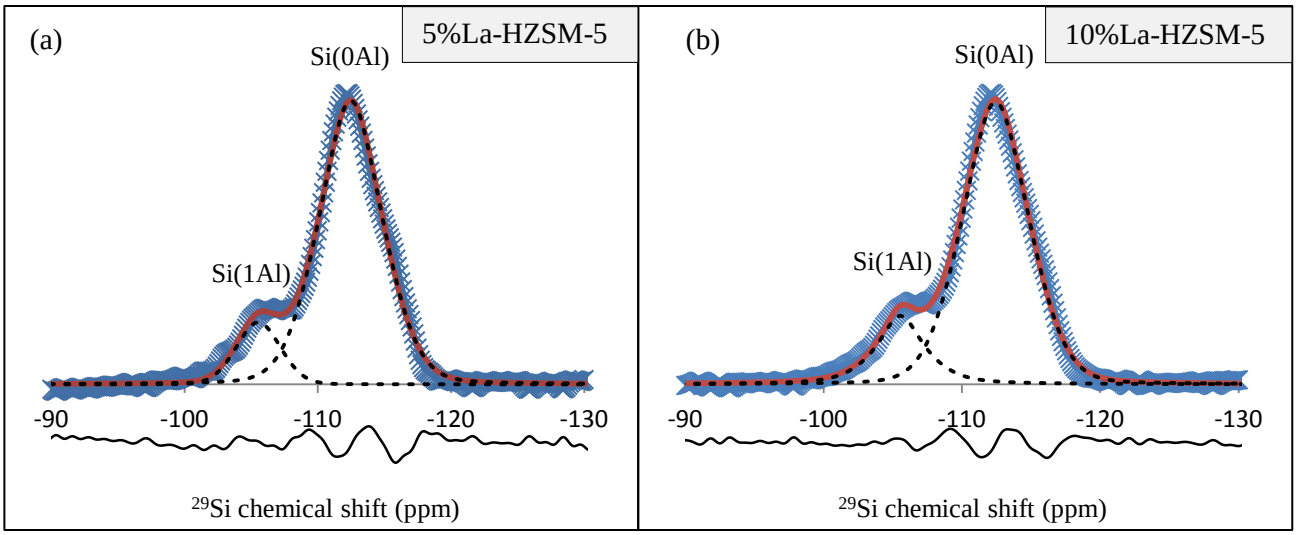


Figure 10.4 ^{29}Si MAS NMR spectra for (a) 5%La-HZSM-5 and (b) 10%La-HZSM-5.

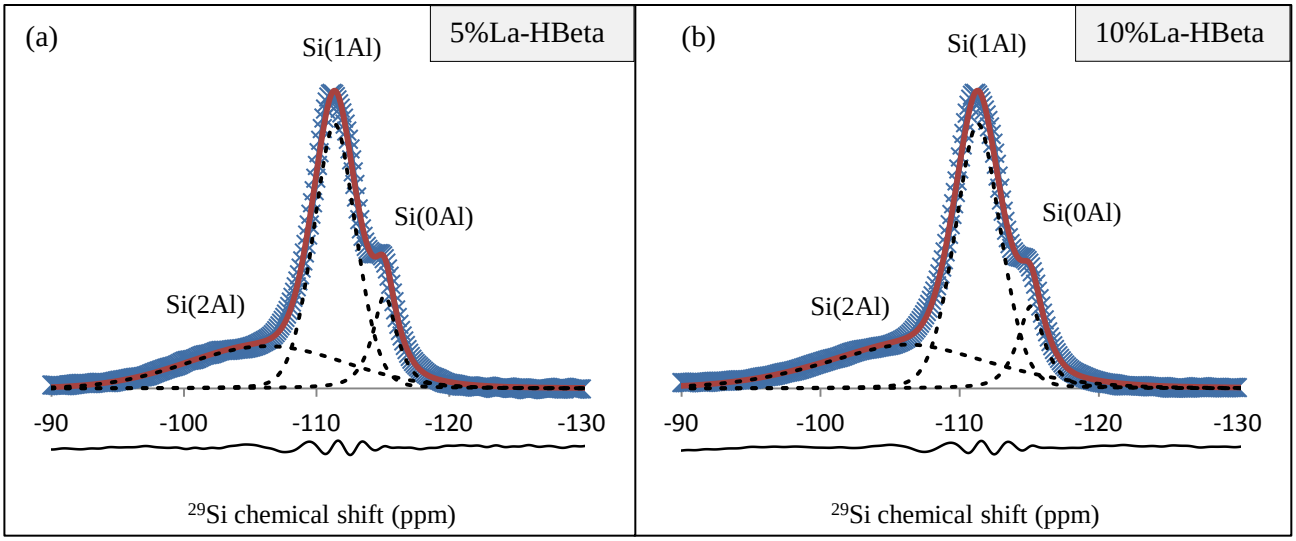


Figure 11.4 ^{29}Si MAS NMR spectra for (a) 5%La-HBeta and (b) 10%La-HBeta.

4.3.2 ^{27}Al NMR spectra

^{27}Al MAS NMR is sensitive to the local Al environments in zeolites, which can help to identify both tetrahedral and octahedral framework Al species [60,67,71]. Early work identified that a signal around 60 ppm is indicative of the tetrahedral framework aluminium in a variety of zeolites [64,68,69,70]. For ZSM-5, ^{27}Al spectrum typically show three distinct signals: an intense signal at 55 ppm corresponding to tetrahedral aluminium, two other signals appear, namely at around 35 ppm, assigned to distorted or deformed tetrahedral aluminium, and one at 0 ppm assigned to octahedrally coordinated aluminium. These are reported by Maijanen et al. [65] as arising from gradual migration of aluminium within the crystallite. Bourgeat-Lami et al. [72] have studied the state of aluminium in zeolite Beta, and they observed two ^{27}Al signals; an intense one assigned to tetrahedral aluminium and another one assigned to the formation of octahedral aluminium for HBeta zeolite.

Figure 12.4 show the ^{27}Al MAS NMR spectra of NaY, ZSM-5 and HBeta. The spectrum of NaY sample shows a single signal at 59.56 ppm assigned to tetrahedrally coordinated framework aluminium (Figure 12.4a). This is evidence that the framework Al remains intact (as tetrahedrally coordinated Al) and that the framework is not dealuminated.

^{27}Al MAS NMR spectrum of ZSM-5 (Figure 12.4b) is similar to those published previously, and shows tetrahedral aluminium signal around 55 ppm, but now additional, weak signals around 38 ppm and 0 ppm previously attributed as due to the distorted tetrahedral and octahedral aluminium ions.

The ^{27}Al MAS NMR spectrum of HBeta shows a single, sharp peak at 54 ppm assigned to tetrahedral aluminium, and a broad peak around -5 ppm due to the combination of octahedral and distorted tetrahedral aluminiums (Figure 12.4c).

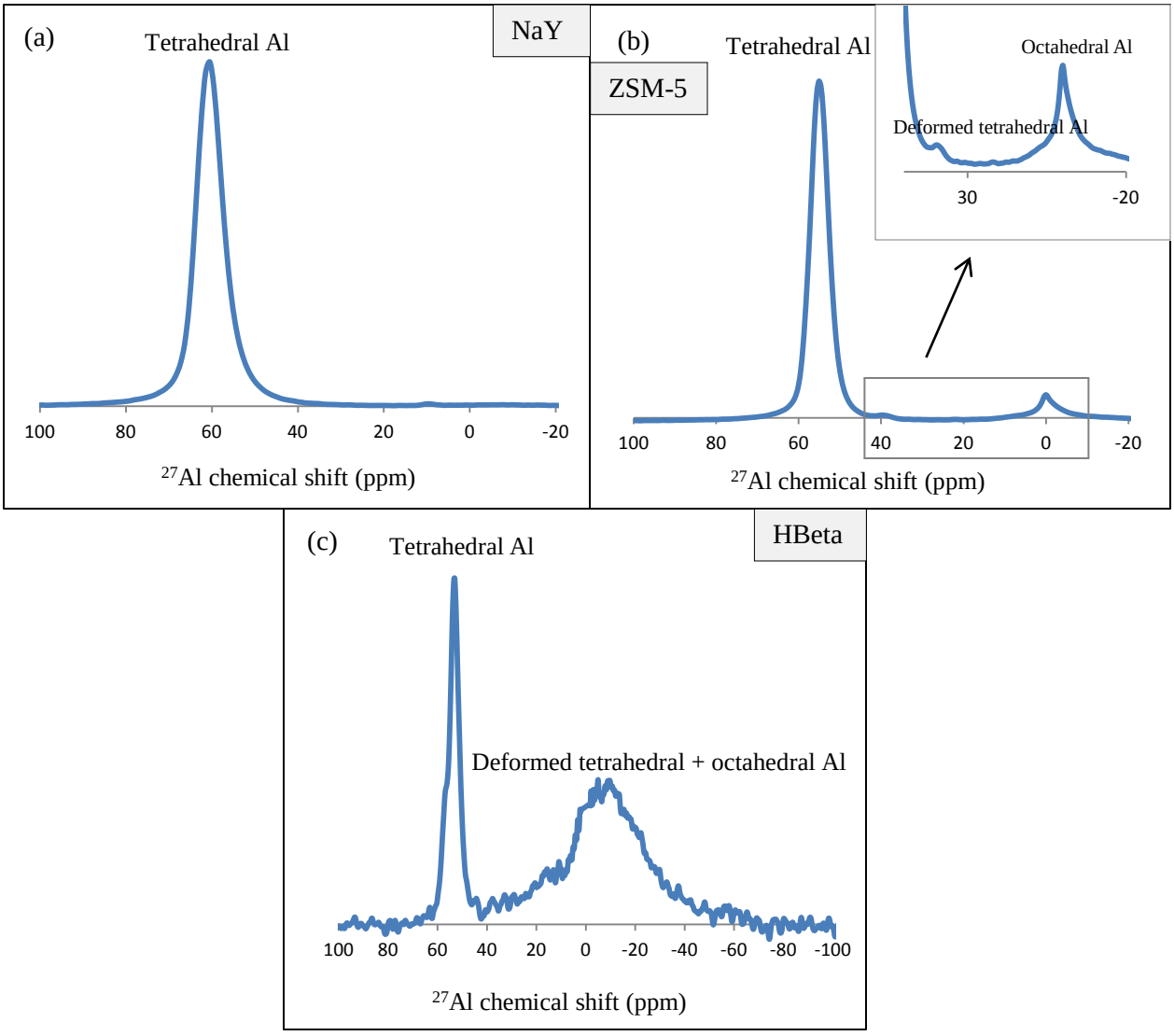


Figure 12.4 ^{27}Al MAS NMR spectra for (a) NaY, (b) ZSM-5 and (c) HBeta.

In figure 13.4 we show ^{27}Al MAS NMR spectra of the HY and HZSM-5; here the effects of ion exchange and dealumination processes gives rise to the formation of the octahedral aluminium which has been attributed as arising from so-called *"extra-framework aluminium"* close to acid sites (Figure 14.4).

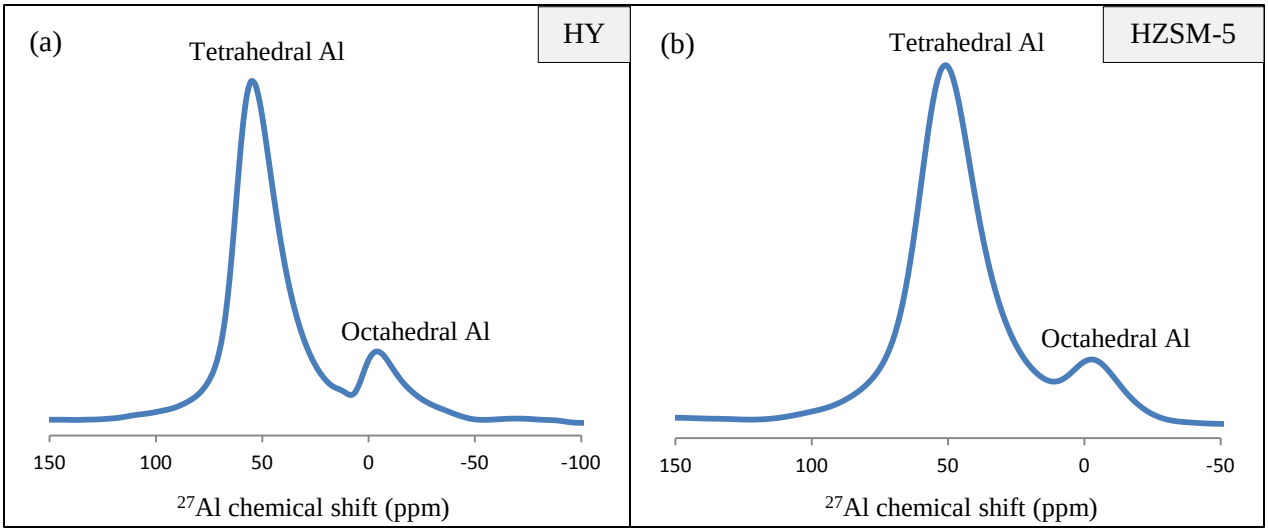


Figure 13.4 ^{27}Al MAS NMR spectra for (a) HY and (b) HZSM-5.

^{27}Al NMR spectra of rare-earth ion-exchanged zeolite catalysts are shown in figures 15.4-20.4 . All the zeolites show a strong peak around 58 ppm corresponding to tetrahedral Al. Interestingly, the intensity of the peak assigned to octahedral Al (around 0 ppm) increases on rare earth exchange when the impregnated amount is increased; this may arise from the formation of extra-framework Al upon ion exchange and subsequent high temperature activation. The additional signal at 30 ppm which appears as broad shoulder in RE-Y may be assigned to the penta-coordinated extra-framework aluminium or distorted four-coordinated aluminium [84]. It is known that, these extra-framework Al centers act as high activity Lewis acid-centers during catalytic reactions [83,89].

Another important observation is that the rare-earth ion-exchange not only increases the intensity of octahedral peak but also shifts its position. Similarly the peak position for the tetrahedral aluminium also shifted on exchange with rare earth metal ions (Table 5.4). The up-field shift in the peak position is correlated to the strain in the T-O-T framework in the presence of highly polarizing rare earth metal ions.

Table 5.4 ^{27}Al NMR Chemical shift in rare earth exchange zeolite catalysts.

	Chemical shift (ppm)				
		Ce		*La*	
Catalyst	*H-form*	*5%*	*10%*	*5%*	*10%*
Y	57.23	59.94	58.11	60.37	59.82
ZSM-5	52.6	54.54	55.52	55.97	55.49
HBeta	53.6	55.01	55.01	55.52	55.76

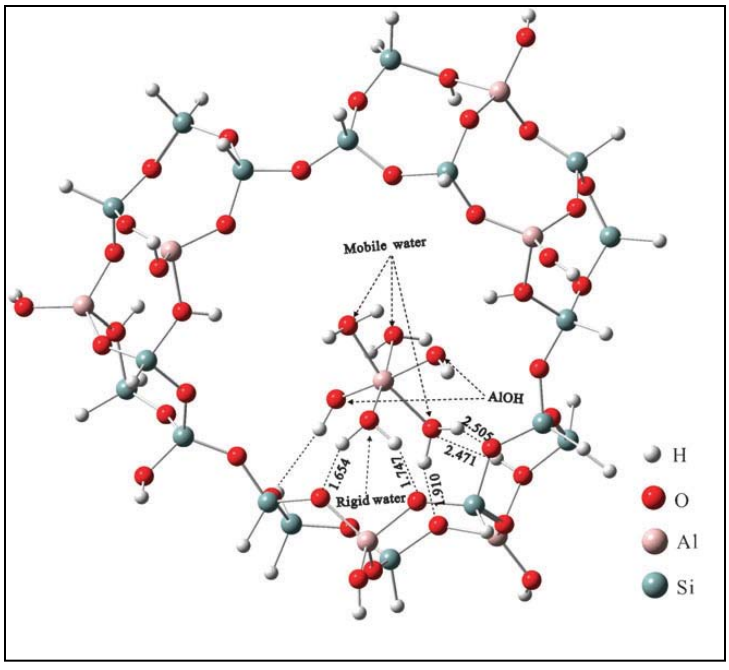


Figure 14.4 Representation of the location of octahedral extra-framework Al species in HY zeolite [89].

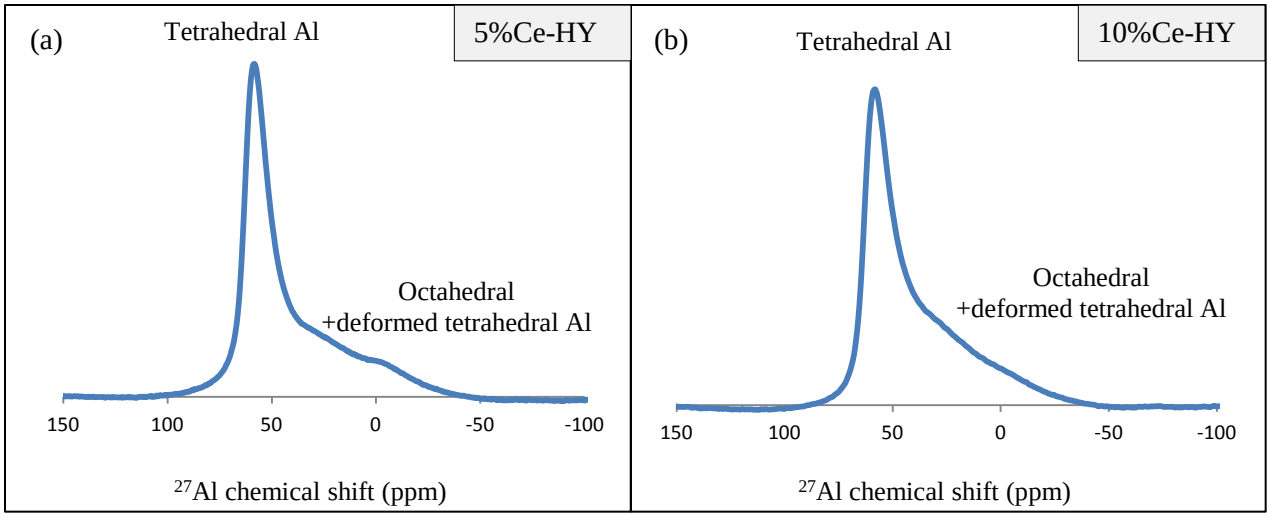


Figure 15.4 ^{27}Al MAS NMR spectra for (a) 5%Ce-HY and (b) 10%Ce-HY.

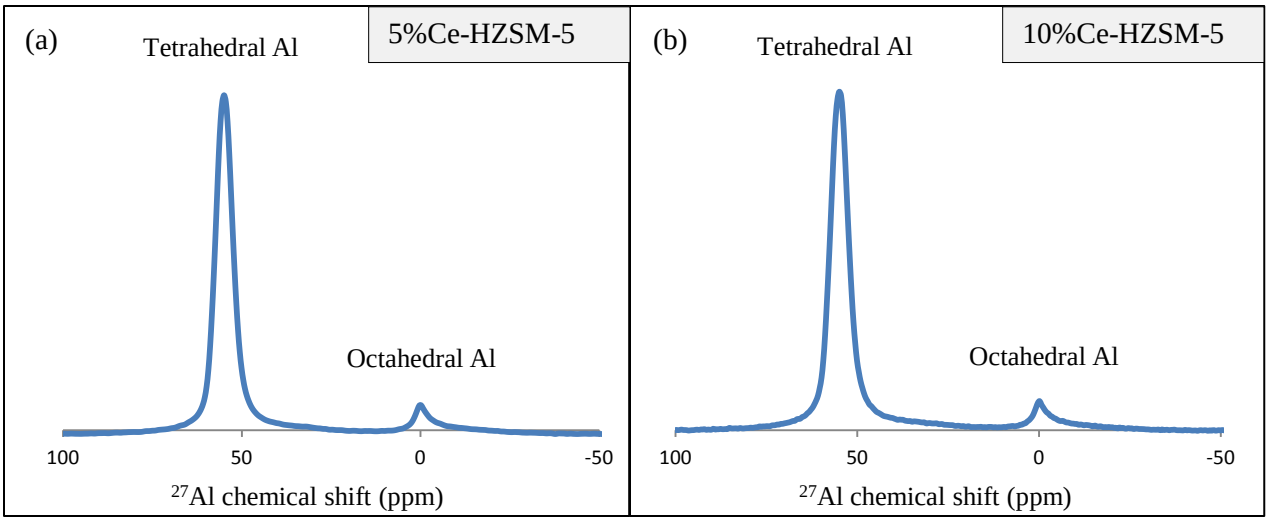


Figure 16.4 ^{27}Al MAS NMR spectra for (a) 5%Ce-HZSM-5 and (b) 10%Ce-HZSM-5.

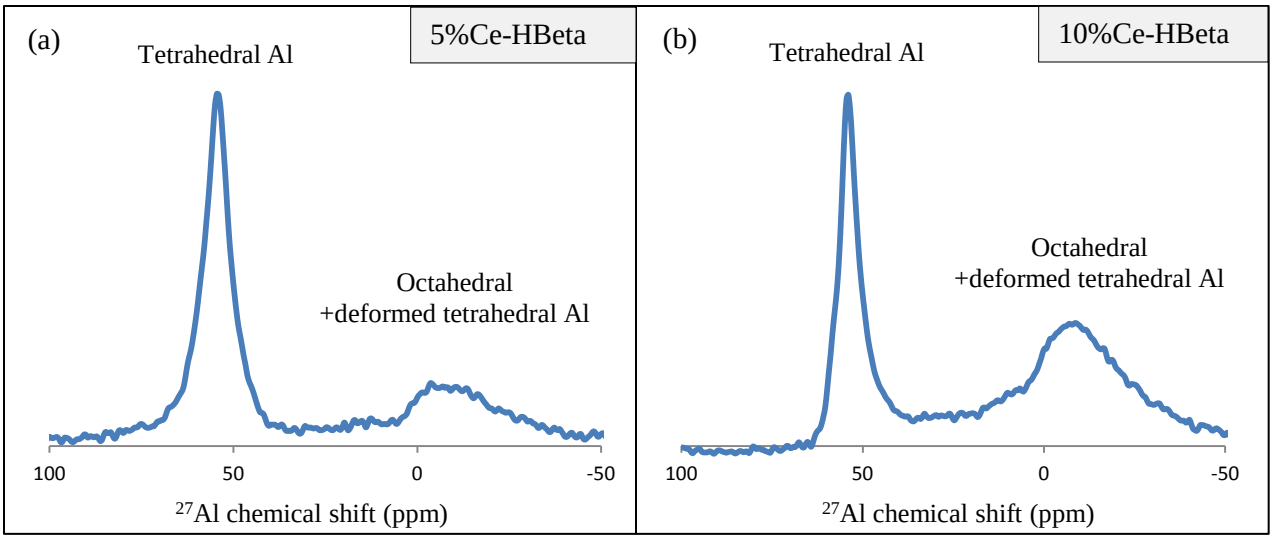


Figure 17.4 ^{27}Al MAS NMR spectra for (a) 5%Ce-HBeta and (b) 10%Ce-HBeta.

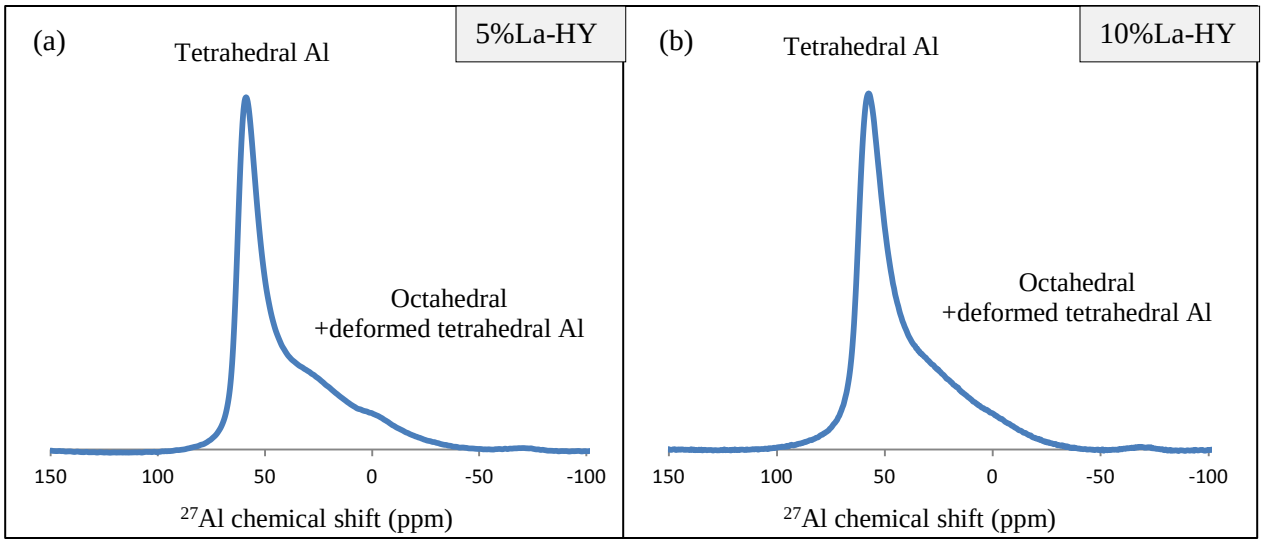


Figure 18.4 ^{27}Al MAS NMR spectra for (a) 5%La-HY and (b) 10%La-HY.

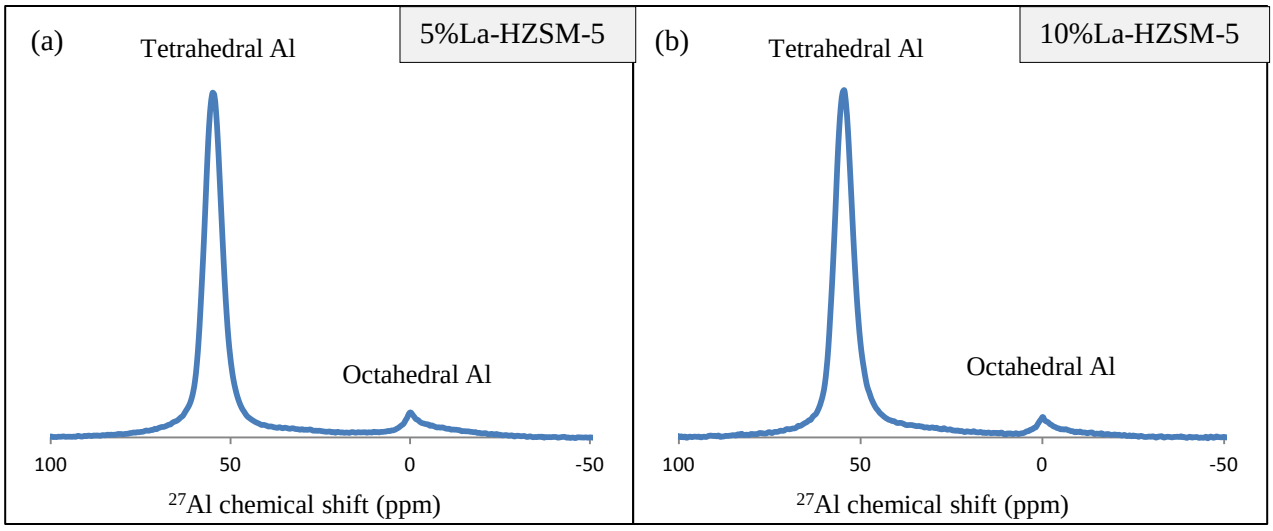


Figure 19.4 ^{27}Al MAS NMR spectra for (a) 5%La-HZSM-5 and (b) 10%La-HZSM-5.

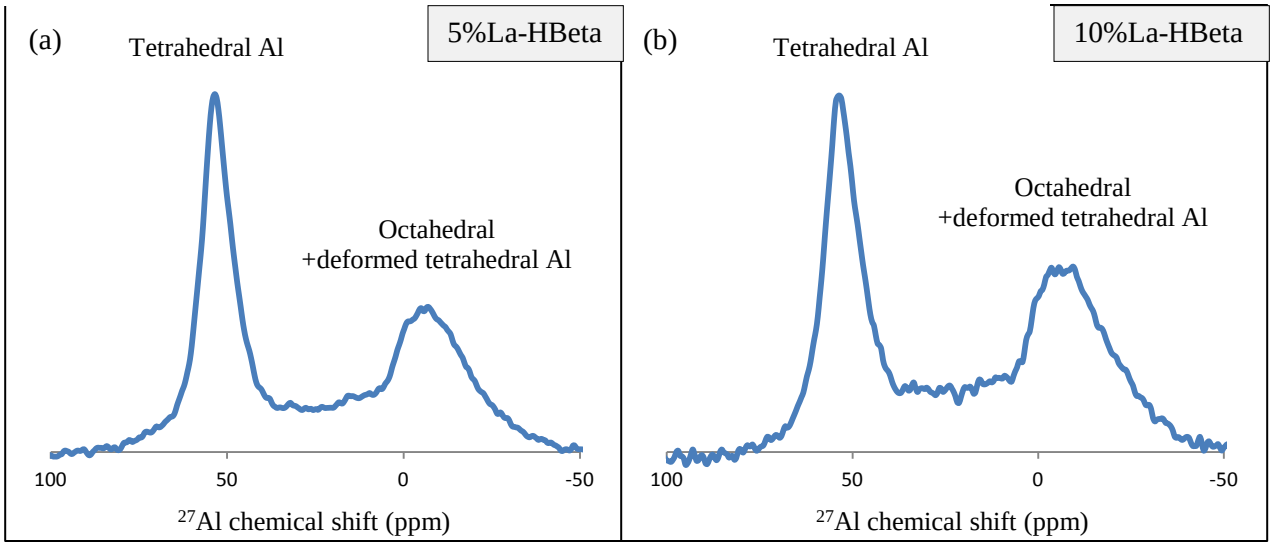


Figure 20.4 ^{27}Al MAS NMR spectra for (a) 5%La-HBeta and (b) 10%La-HBeta.

4.4 Nitrogen physisorption

One of the most widely used methods for determining the pore size and surface area of zeolites is nitrogen physisorption. From the shape of the nitrogen adsorption and desorption isotherm the presence and shape of the mesopores can be deduced. At low relative pressure ($P/P_0<0.1$) the micropores are filled, and at relative pressure above 0.95 capillary condensation in the intercrystalline voids takes place. At relative pressure between 0.1 and 0.95, multilayer adsorption on the external surface and in the mesopores takes place as well as capillary condensation in the mesopores [13].

The nitrogen adsorption and desorption isotherm for NaY, ZSM-5 and HBeta zeolites are given in figure 21.4. From these data it is clear that the mesopore system of the high-meso ZSM-5 and HBeta differs from the mesopore system in NaY zeolite regarding to the shape of the hysteresis loop. For NaY the hysteresis loop is rather flat, indicating inkbottle type pore, while the hysteresis loop of ZSM-5 and HBeta is indicative of cylindrical type pore. This observed data are similar to work done by Burevski, et al. [73] and Janssen, et al. [18]. Table 6.4 gives details of the surface area and pore structure of the different zeolite samples.

Table 6.4 Physical Properties of NaY, ZSM-5 and HBeta zeolites.

Sample	***t-Plot micropore V*** **(cm^3/g)**	***Pore size*** **(Å)**	S_{BET} **(m^2/g)**	$S_{Langmuir}$ **(m^2/g)**
NaY	0.517	20.68	123.38	162.9
ZSM-5	0.201	20.21	555.76	740.07
HBeta	0.141	30.84	491.68	656.76

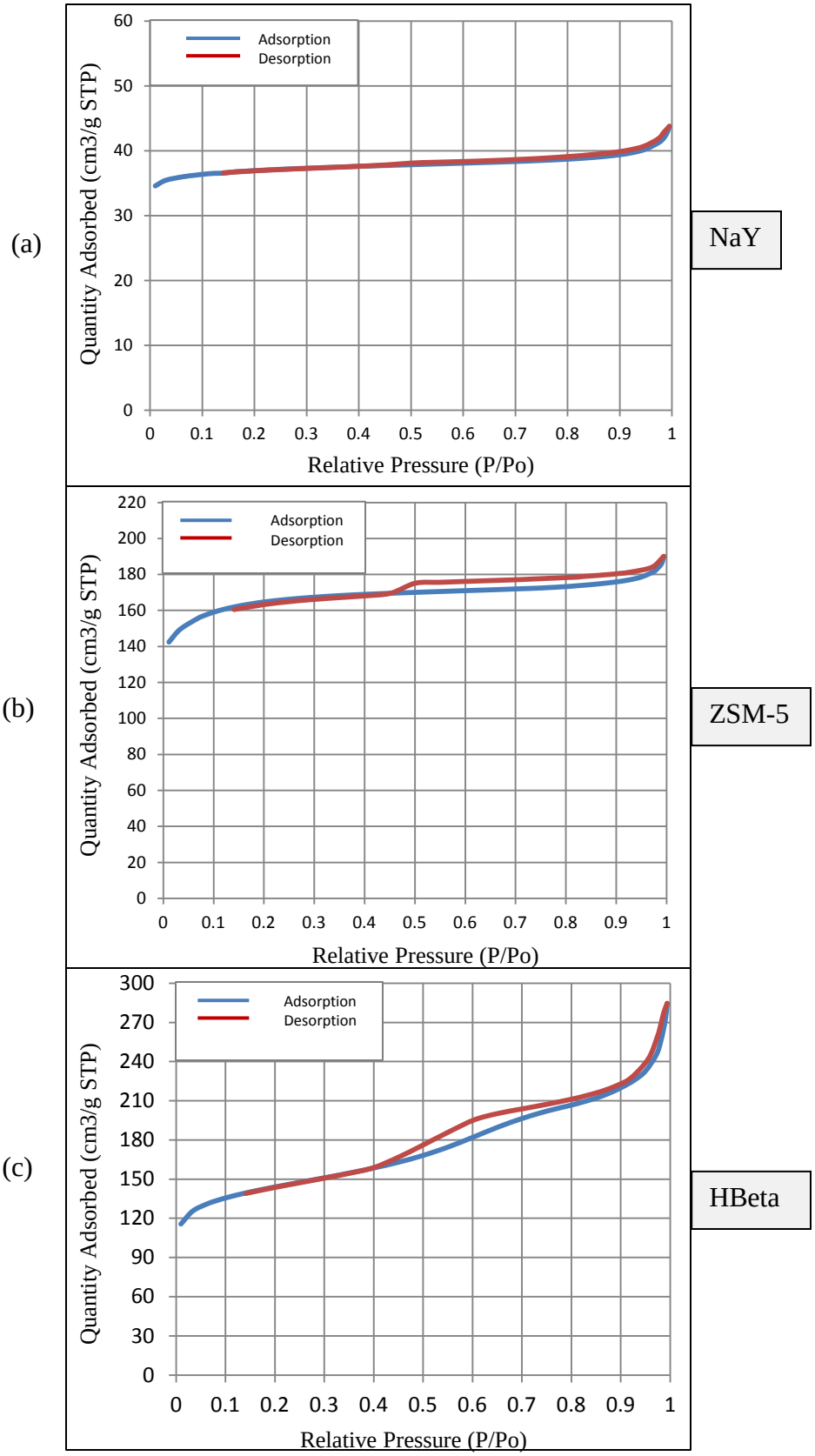


Figure 21.4 Nitrogen adsorption and desorption isotherms (relative N_2 pressure P/P_0 against adsorbed volume) for (a) NaY, (b) ZSM-5 and (c) HBeta.

4.5 Catalyst performance

The alkylation of benzene with ethylene has been widely studied and is still under focus for industrial development. Many technologies such as the Mobil-Badger, Mobil–Badger EBMax, Lummus–UOP, CDTEC, and Dow Chemical processes using zeolites have made considerable progress in recent years. The industrial-scale processes are licensed by Mobil–Badger vapor phase uses a ZSM-5 based catalyst, Mobil–Badger EBMax process uses Mobil's proprietary MCM-22 zeolite, Lummus–UOP is liquid-phase process based on a modified zeolite Y catalyst, CDTech is catalytic distillation technology uses zeolite Y, and Dow Chemical uses gallium-exchanged mordenite [28].

The vapor phase process is typically comprised of multiple fixed beds of zeolite catalyst and operates at 390−450°C with mole ratios of benzene to ethylene ranging from 7.2 to 7.6. The majority product in the reaction of ethylene with benzene is ethylbenzene. However, some undesirable byproducts are generated including xylene, diethylbenzene (DEB) isomers, triethylbenzene (TEB), and heavier aromatics through chain and side reactions. [27,74]

In previously published work, Bellussi et al. [75] found that zeolite beta is more active and more selective than zeolite Y for liquid-phase alkylation of benzene with light olefins. Yongxin et al. [76] suggested that the alkylation of benzene with diethylcarbonate over HZSM-5 (Si/Al= 200) is a convenient route for the synthesis of EB. Odedairo et al. [31] found that ethylbenzene selectivity to be highest in the ethylation reaction over ZSM-5-based catalyst as compared to its ethylation over all other zeolite catalysts which they studied.

In this work, catalytic activities were investigated on Y, ZSM-5 and Beta modified zeolite catalysts.

The conversion of benzene and selectivity of ethylbenzene were defined as follows:

$$Conversion\ of\ benzene\ (\%)\ \frac{content\ of\ benzene\ in\ the\ feedstock - content\ of\ benzene\ in\ product}{total\ benzene\ in\ the\ feedstock}\ X\ 100 \qquad (1.4)$$

$$Selectivity\ of\ ethylbenzene\ (\%)\ \frac{content\ of\ ethylbenzene\ in\ product}{total\ of\ product}\ X\ 100 \qquad (2.4)$$

4.5.1 The effect of time-on-stream

The effect of time-on-stream on benzene conversion and product selectivity was studied by collecting samples every 30 min for 2h of reaction at 250°C and 5 bar. Practically no changes are observed in benzene conversion and selectivity for EB during 120 min on stream (Figure 22.4 and 23.4). In the alkylation of benzene with ethylene the deactivation of catalysts usually occurs as active sites become blocked by coke formation. The coke results from the oligomerization of ethylene because activated ethylene easily reacts to form polymeric species. Ethylene polymerization to form coke can be avoided effectively by pumping excess benzene into the reactor to fully fill the bed before ethylene is introduced.

4.5.2 The effect of feed ratio

The effect of feed ratio on benzene conversion and product selectivity was studied by systematically varying the feed ratio (B:E) from 1:1 to 3:1 at 250°C and 5 bar. The conversion of benzene shows a significant decline as the ratio of benzene to ethylene increased from 1:1 to 3:1. A low molar ratio of benzene to ethylene is required to ensure complete conversion of benzene in the alkylation process. However, a low molar ratio of benzene to ethylene results in high conversion of benzene, but low conversion of ethylene, which may cause a large quantity of unconverted ethylene to be circulated in the industrial process, and results in increased energy consumption. Also the excess ethylene may easily polymerize over the acid site, leading to the blockage or coverage of the catalyst surface. Selectivity for EB slightly improved as the ratio of benzene to ethylene decrease. This increasing in the EB selectivity could be attributed to transalkylation of DEB isomers with benzene (Figure 24.4 and 25.4).

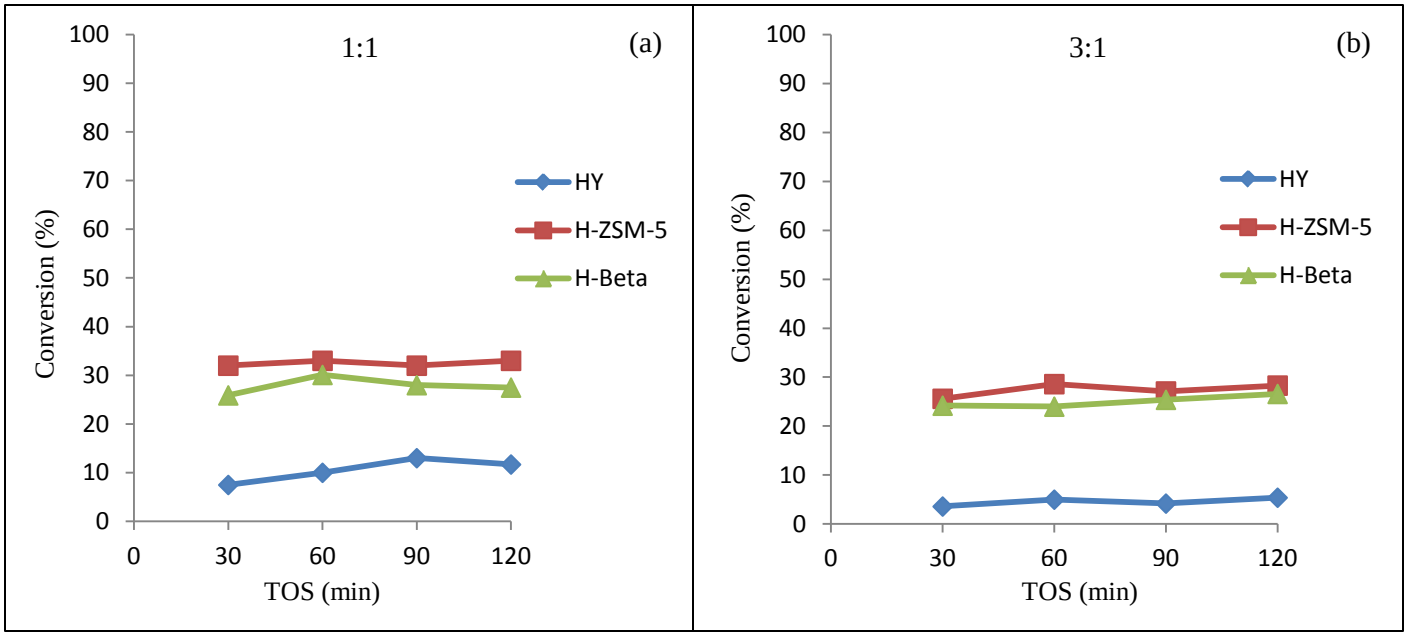


Figure 22.4 Effect of time-on-stream on benzene conversion over HY, HZSM-5 and HBeta. (a) 250°C, 5 bar, ethylene WHSV=0.5h^{-1}, feed ratio 1:1 (B:E). (b) 250°C, 5 bar, ethylene WHSV=0.5h^{-1}, feed ratio 3:1 (B:E).

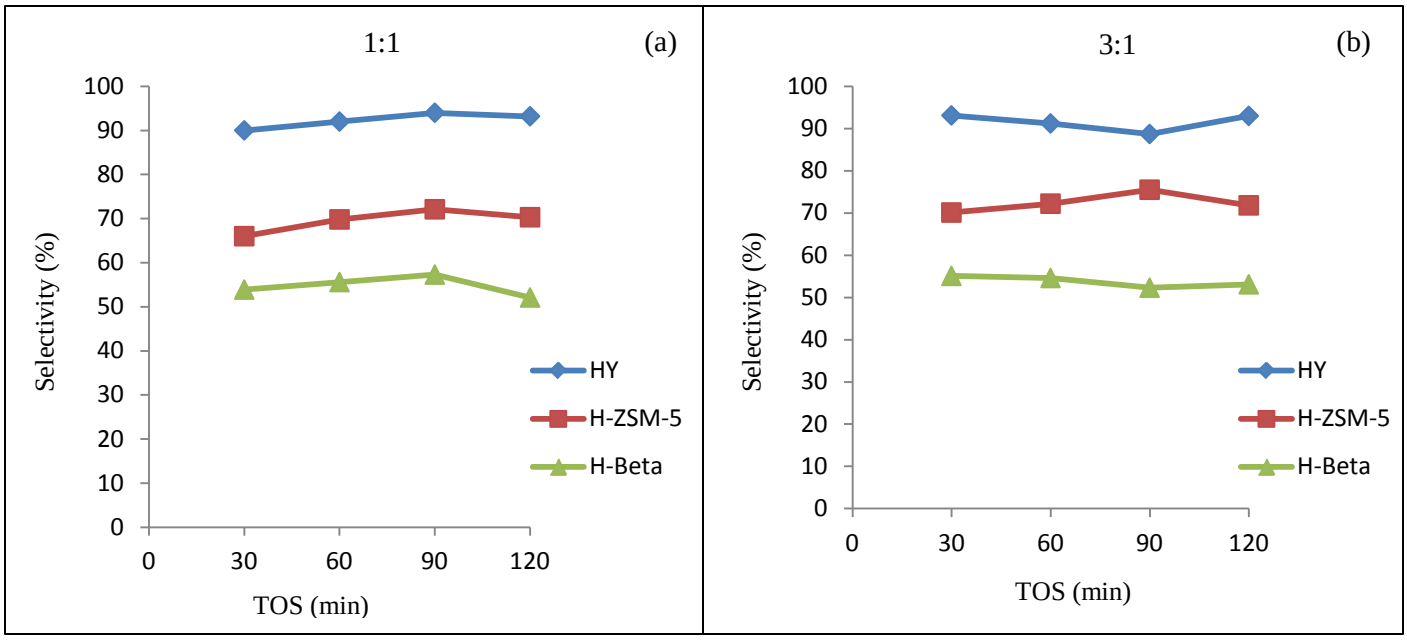


Figure 23.4 Effect of time-on-stream on selectivity for EB over HY, HZSM-5 and HBeta. (a) 250°C, 5 bar, ethylene WHSV=0.5h^{-1}, feed ratio 1:1 (B:E). (b) 250°C, 5 bar, ethylene WHSV=0.5h^{-1}, feed ratio 3:1 (B:E).

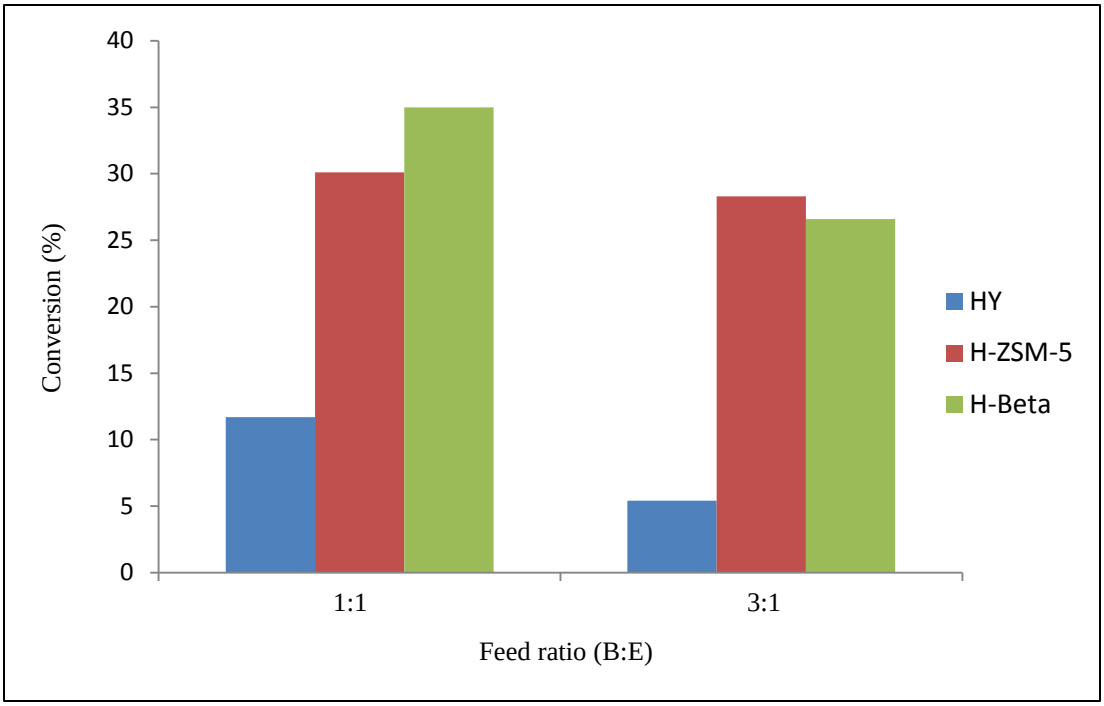


Figure 24.4 Effect of feed ratio on benzene conversion over HY, HZSM-5 and HBeta. At 250°C, 5 bar, ethylene WHSV=0.5h^{-1}, TOS=120min.

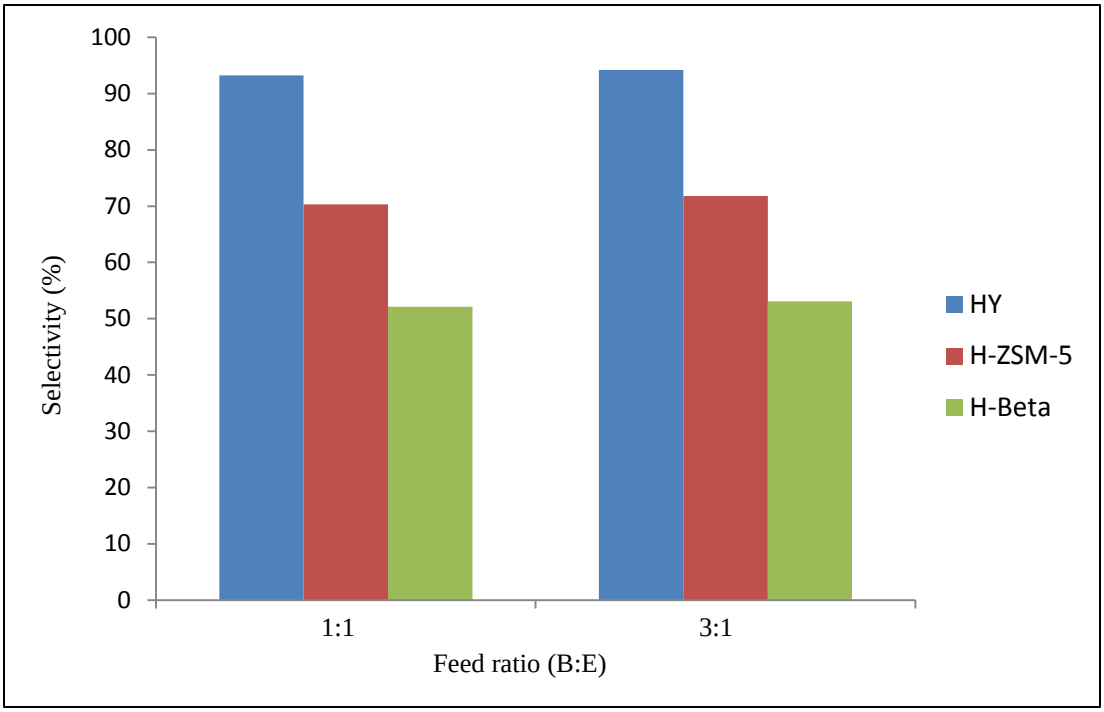


Figure 25.4 Effect of feed ratio on selectivity for EB over HY, HZSM-5 and HBeta. At 250°C, 5 bar, ethylene WHSV=0.5h^{-1}, TOS=120min.

4.5.3 The effect of rare-earth ion-exchange in HZSM-5

ZSM-5 zeolites ion-exchanged with lanthanum have attracted considerable attention and have been investigated extensively due to the adjustable acidic sites by the rare earth oxide addition. As for the influence of the lanthanum species on the hydrothermal stability and deactivation rate of the ZSM-5 zeolites, Yan et al. [77], Budi et al. [78] and Rokosz et al. [79] found that lanthanum ion-exchange can retard the dealumination and deactivation rate as well as improve the hydrothermal stability of zeolite catalysts. A significant role of the introduced La is to change the acid properties and catalytic performance of ZSM-5 zeolites. Ivanov et al. [80] found that lanthanum ion exchange only at the strongest acidic sites to generate a weaker Brønsted acid site. Moreover, they found that the addition of lanthanum does not significantly influence the strength of the acidic sites but rather only influences their concentration and distribution. In summary, the experimental studies of the lanthanum cations in ZSM-5 zeolites are still unclear [81]. To our knowledge, no comparative studies have been reported for the performance of rare-earth doped zeolites catalysts in the gas phase alkylation of benzene with ethylene.

Our data are consistent with earlier studies show that HZSM-5 zeolite is the most active of the three targeted acid zeolites for benzene/ethylene alkylation (ca 30% efficiency of benzene conversion). However, HZSM-5 does not exhibit the highest ethylbenzene selectivity (ca 70 % selectivity). In an attempt to enhance the selectivity of this zeolite having the highest benzene conversion rate, we synthesized both La and Ce ion-exchanged HZSM-5 and tested the resulting zeolites under the optimum experimental conditions of 250°C, 5 bar, ethylene WHSV=0.5h^{-1}, feed ratio 1:1 (B:E).

We find no discernable change observed in benzene conversion efficiencies upon La and Ce ion exchange, being still in range around 30-35%. Importantly however, the selectivity toward ethylbenzene formation was significantly enhanced upon La and Ce ion exchange. We attribute this increase in the ethylbenzene selectivity to the effect of the extra framework cation species (Ce and La) on the shape selectivity of HZSM-5 zeolite leading to production of primarily ethylbenzene (between 92-95%) and correspondingly smaller quantities of toluene, xylenes and diethylbenze isomers (Figure 26.4).

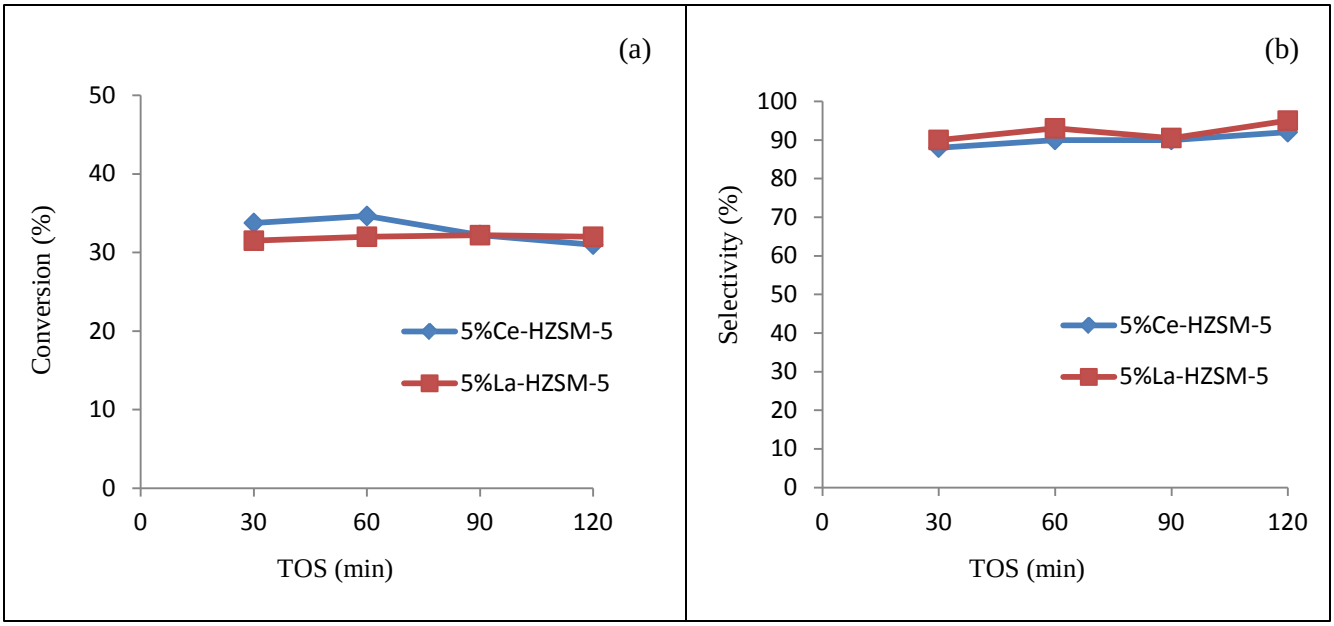


Figure 26.4 Effect of rare-earth ion-exchange of HZSM-5 on: (a) the conversion of benzene and (b) the selectivity of EB. At 250°C, 5 bar, ethylene WHSV=0.5h^{-1}, feed ratio 1:1 (B:E).

The selectivity to ethylbenzene (and hence its ultimate yield) is of course highly dependent upon the associated reactions that could occur simultaneously on the same catalyst. Alkyl benzene is typically more reactive than benzene itself in electrophilic substitution reactions and hence the formation of heavier alkylates in the product stream can finally lead to coke formation. Secondly, olefins can associate to yield oligomers.

Finally extensive alkylation and isomerization may take place on the external surface of the zeolite to give many isomers of di- and trialkylbenzene, which are not expected from the shape-selectivity considerations for chemical reactions within the pores and channels of zeolites. Further modification of the catalyst is therefore required to circumvent the major problem of non-selective reactions [82,85].

Table 2.5 summarizes the reaction performance for a variety of different zeolite catalysts. We note that the activity (conversion) of HY is the lowermost; and this may arise from two reasons: the low BET surface area (123.38 m^2/g) and the low silicon to aluminium ratio (1.92) which could result in weak acidity of the catalysts. The HBeta zeolite catalyst exhibits a higher activity but lower selectivity to ethylbenzene due to the formation of byproduct in the product stream. This is can be explained by the large pore structure which zeolite beta posses, and the high BET surface area (491.68 m^2/g).

HZSM-5 zeolite exhibits the highest benzene conversion in comparison with the other two zeolites. This may arise because it possesses the highest BET surface area (555.76 m^2/g) and the shape-selective of ZSM-5 zeolites; still there remain some undesirable by-products, but clearly not as high a concentration as those found in HBeta.

The modification of HZSM-5 by the ion-exchange of lanthanum and cerium rare-earth metals is one possible role to circumvent the problem of non-selective reactions. Taking into account that the average ionic radii of La^{3+} and Ce^{3+} cations (1.032 and 1.01 Å) are less than that of ZSM-5 pore mouth [86], it has been proposed such ion-exchanged cations may enter the main channels of ZSM-5 zeolites during the process of ion exchange -as confirmed by XRD- and act as a controller of preferential diffusion of EB by the

adjustment of pore entrance as well as by the deactivation of external acid sites. Given the high conversion and relatively high selectivity of rare-earth ion-exchanges ZSM-5 catalyst, next we focus our discussion on the Ce and La ion-exchanged HZSM-5 catalysts. Table 7.4 summarize the reaction performance for H-zeolites and 5% rare-earth HZSM-5.

Table 7.4 Reaction performance comparison between zeolite catalysts in the benzene/ethylene alkylation reaction[a].

	HY	*HZSM-5*	*HBeta*	*5%Ce-HZSM-5*	*5%La-HZSM-5*
Benzene conversion, mol%	11.71	33.27	27.52	31.13	32.07
Product Selectivity, mol%					
Ethylbenzene	93.21	70.34	52.12	92.12	95.19
Diethylbenzenes	4.63	15.19	22.39	3.84	2.96
Triethylbenzene	1.27	5.67	10.18	0.00	0.00
Tetraethylbenzene	0.63	0.86	4.35	0.00	0.00
Toluene	0.00	1.45	3.13	1.06	0.49
Xylenes	0.09	2.08	5.44	2.42	1.36
Cumene	0.17	2.60	1.03	0.56	0.00
1-methylpropylbenzene	0.00	1.81	1.36	0.00	0.00

[a] T=250°C; P= 5 bar; feed ratio 1:1 (B:E), ethylene WHSV=0.5h^{-1}, TOS=120min.

It is clear from Table 7.4 that the alkylation density over 5% Ce-, and 5% La-HZSM-5 is characterised by essentially complete ethylene conversion with very high selectivity to ethylbenzene. This monoalkylation selectivity refers to the function (percentage) of ethylene that reacts to form ethylbenzene, as opposed to the formation of polyethylated species (Di, Tri and Tetra ethylbenzenes). For the rare-earth ion-exchanged HZSM-5, there are also only very small levels of toluene and xylene byproducts originally from isomerization reactions and no evidence for cumene and methylpropylbenzene from the alkylation reaction.

It is becoming clear that the addition of lanthanum cations (via ion-exchange) affects the stability, acidic properties and catalytic behavior of ZSM-5 zeolite [81-83,85,87,88]. Our results clearly point to an enhanced shape selectivity in the product formation of the alkylation reaction.

A resent Density Functional Theory (DFT) study on the accommodation and role of La species in ZSM-5 zeolite is of direct relevance to our observations (Table 7.4). Li et al [81] confirmed earlier computational studies which showed that the straight channels in ZSM-5 in the symmetrical six-membered oxygen rings instead of the channel intersections, and that the incorporated (ion-exchanged) lanthanum ions exist as $La(OH)_2^+$ unit. A representation of the location of the $La(OH)_2^+$ cluster is given in figure below.

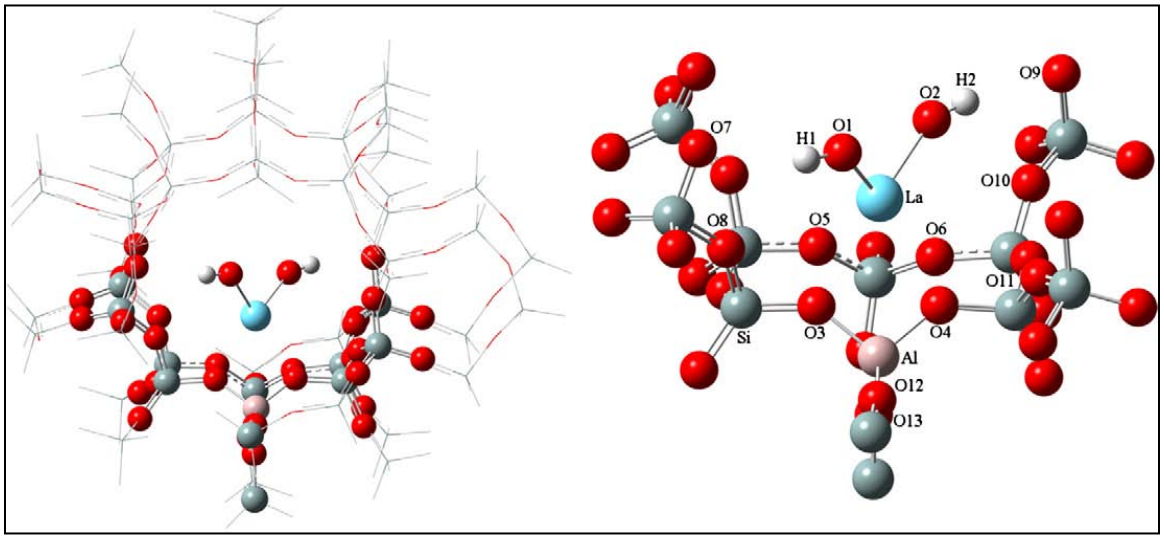


Figure 27.4 Representation of the location of the $La(OH)_2^+$ cluster in ZSM-5 zeolite [81].

Thus, a narrowing of the pore openings is achieved most effectively by the placement of $La(OH)_2^+$ in the zeolite channels; this gives rise to increased steric hindrances and an improved shape-selectivity of the zeolite. We propose that the marked enhancement in the selectivity to **only** monoalkylation arises from the spatial properties of the channel in lanthanum (and presumably cerium) modified HZSM-5 zeolite, which prevents formation of higher alkylation products (Diethylbenzene, etc, and beyond) because of restricted transition state molecular shape selectivity. This type of significant modification of the pore structure also appears to suppress other side reactions, and potentially also lowers the rate of catalyst deactivation.

Our results also suggest an enhanced hydro thermal stability of the ZSM-5 by lanthanum ion exchange which may arise from a strengthening of the Al-O bond, although more work is needed for this to be confirmed.

Chapter Five: Conclusions

The remarkable properties of zeolites have allowed the development of cleaner and more efficient processes for the large-scale production of fuels and chemicals.

In this work, we have paid particular attention for the important benzene alkylation reaction. Three important zeolite catalyst materials and their various ion-exchange derivatives were synthesised and characterized using a range of physico-chemical techniques.

X-ray diffraction studies revealed the extent of crystallinity and long-range order or periodicity in the framework structure, while solid state NMR was shown to be a highly sensitive probe of the local environment of a particular atom in the zeolite structure. We hope to have illustrated the great complementarity of the techniques in providing detailed information on the structure of a variety of zeolites.

The catalytic activities for the benzene/ethylene alkylation reaction of the three zeolites in various ion-exchange forms was investigated using a bench-top flow reactor, constructed in the KOPRC laboratories in the Inorganic Chemistry Laboratory.

Particularly promising results were obtained for lanthanum and cerium ion-exchanged zeolites used as catalysts in the benzene/ethylene alkylation reaction.

Most notable is the significant enhancement in product selectivity – viz, ethylbenzene selectivity- for La and Ce ion-exchanged HZSM-5 zeolite catalysts, showing a 30% + increase in selectivity for the alkylation reaction after rare-earth ion exchange.

These studies highlight the importance of ion-exchange with rare earth cations as a powerful method to control the local structural and catalytic properties of zeolites, and also to enhance the acid properties upon rare earth exchange.

In the case of our ^{27}Al NMR studies (Figures 15.4-20.4) the intensity of the octahedral and deformed tetrahedral Al peak increase noticeably on rare earth exchange of all three zeolites.

Rare earth exchange not only increases the intensities of the octahedral peak but also shift the position arising from strains included in the aluminosilicate framework in the presence of highly polarizing La^{3+} and Ce^{3+} cations.

The enhanced selectivity for monoalkylation for La-HZSM-5 is attributed to migration of the La^{3+} ions to specific sites in the zeolite channels. DFT calculations reported in the literature point to the occurrence of $La(OH)_2^+$ clusters, now effectively inhibiting the formation and diffusion of bulky alkylated products.

Complete confirmation of the proposed mechanisms will require an extensive study of structural and vibrational properties of the rare-earth ion-exchange acid zeolites to probe the $La(OH)_2^+$ species – and their interaction with framework Al-O-Si sites.

Similarly, the proposal that the introduced La cations may also affect the Brønsted acid sites (Si-OH-Al) could also be probed by advanced vibrational spectroscopies. For example, can one identify Si-O$La(OH)_2$ –Al species?

We also have tentative evidence that the hydrothermal stability of ZSM-5 is improved by lanthanum ion-exchange. This important aspect also requires further details investigations.

Advanced structural – and vibrational – information can also be obtained from high resolution neutron and X-ray diffraction studies to investigate the accommodation and role of La and Ce species in three zeolites, notably HZSM-5.

Critically important also would be DFT calculations to understand the energetic stabilization for La and Ce cations in the zeolites and the role of changes in the framework bounding and steric hindrances, potential enhanced acidities and acid site locations.

References

1. Marcilly C. (2003), *"Present status and future trends in catalysis for refining and petrochemicals"*, J Catal, **216**: 47-62.
2. Armor J. (2011), *"A history of industrial catalysis"*, Catal Today, **163**: 3-9.
3. Coons R., *"Catalysts: seeking the next big thing"*, Chem Week, (2009).
4. Vermeiren W. and Gilson J. P. (2009), *"Impact of zeolites on the petroleum and petrochemical industry"*, Top Catal, **52**(9): 1131-1161.
5. Wilson K. and Clark J. (2000), "*Solid acids and their use as environmentally friendly catalysts in organic synthesis"*, Pure Appl Chem, **72**(7): 1313-1319.
6. Michel G. and Jean G., *"Zeolites for cleaner technologies"*, Catalytic Science Series (2002).
7. Perego C. and Ingallina P. (2004), *"Combining alkylation and transalkylation for alkylaromatic production"*, Green Chem, **6**: 274-279.
8. Rao L. (2007), *"Solid acid catalysts in Green Chemistry"*, Resonance, **12**(10): 30-36.
9. Corma A. (1997), *"Solid acid catalysts"*, Curr Opin Solid St M, **2**(1): 63-75.
10. Corma A. (1995), *"Inorganic solid acid and their use in acid catalyzed hydrocarbon reactions"*, Chem Rev, **95**: 559-614.
11. Corma A. and Garcia H. (1997), *"Organic reactions catalyzed over solid acids"*, Catal Today, **38**(3): 257-308.
12. Subhash B., *"Zeolite catalysis: principles and applications"*, CRC Press, Inc., Boca Raton, Florida (1990).
13. Santi K., *"Zeolites in industrial separation and catalysis"*, Wiley, (2010).
14. Thomas J.M. (1992), *"Solid acid catalysts"*, Sci Am, April: 112-118.
15. Gates B., *"Catalytic Chemistry"*, Wiley (1992).
16. Dyer A., *"An introduction to zeolite molecular sieves"*, Wiley, (1990).
17. Corma A. (2003), *"State of the art and future challenges of zeolites as catalysts"*, J Catal, **216**(1-2): 298-312.
18. Janssen A. et al. (2002), *"On the shape of the mesopores in zeolite Y"*, J Phys Chem B, **106**: 11905-11909.

19. Karami D. and Rohani S. (2009). *"Synthesis of pure zeolite Y using soluble silicate, a two-level factorial experimental design"*, Chem Eng Process, **48**(8): 1288-1292.
20. Kumar N. et al. (2002), *"Effect of synthesis time and mode of stirring on physico-chemical and catalytic properties of ZSM-5 zeolite catalysts"*, Appl Catal A-Gen, **235**(1-2): 113-123.
21. Chen X. et al. (2007), *"Optimal feed ratio of benzene-propylene binary mixtures for alkylation in ZSM-5 by molecular simulation"*, Fluid Phase Equilibria, **260**(1): 146-152.
22. Caullet P. et al. (1992), *"Synthesis of zeolite beta from nonalkaline fluoride aqueous aluminosilicate gels"*, Zeolites, **12**(3): 240-250.
23. *"Database of zeolite structures"*, www.iza-structure.org.
24. David T. (2007), *"Zeolite-earliest solid state acids"*, Au Journal, **11**(1): 36-41.
25. British Zeolite Association (BZA), www.bza.org.
26. Corma A. and Martinez A. (2005), *"Zeolites in refining and petrochemistry"*, Stud Surf Sci Catal, **157**: 337-366.
27. Perego C. (2002), *"Recent advances in the industrial alkylation of aromatics: new catalysts and new processes"*, Catal Today, **73**: 3-22.
28. Degnan T. et al. (2001), *"Alkylation of aromatics with ethylene and propylene: recent developments in commercial processes"*, Appl Catal A-Gen, **221**: 283-294.
29. Du Y., et al. (2002), *"Study on alkylation of benzene with ethylene over beta-zeolite catalyst to ethylbenzene by in situ IR"*, J Mol Catal A-Chem, **179**(1-2): 353-261.
30. Liu S. et al. (2009), *"Highly selective ethylbenzene production through alkylation of dilute ethylene with gas phase-liquid phase benzene and transalkylation feed"*, J Nat Gas Chem, **18**: 21-24.
31. Odedairo T. and Al-Khattaf S. (2010), *"Ethylation of benzene: effect of zeolite acidity and structure"*, Appl Catal A-Gen, **385**: 31-45.
32. Cavani F. and Trifiro F. (1995), *"Alternative processes for the production of styrene"*, Appl Catal A-Gen, **113**: 219-239.
33. CMAI: Chemical Market Associates, Inc. (www.cmaiglobal.com).
34. Dann S., *"Reaction and characterization of solid"*, The royal science of chemistry, (2000).

35. Sanders J. et al., *"Modern NMR spectroscopy - a workbook of chemical problems"*, Oxford university press, (1989).
36. Iggo J., *"NMR spectroscopy in inorganic chemistry"*, Oxford university press, (1999).
37. W O Parker JR (2000), *"NMR spectroscopy applied to zeolite catalysis: progress and prospects"*, Comment Inorg Chem, **22**: 1, 31-73.
38. Weitkamp J. and Puppe L. *"Catalysis and zeolites: fundamentals and applications"*, Springer, (1999).
39. Hargreaves J. (2005), *"Powder X-ray diffraction and heterogeneous catalysis"*, Crystallography reviews, **11**: 21-34.
40. Zhuang J. et al. (2004), *"Solid-state MAS NMR studies on the hydrothermal stability of the zeolite catalysts for residual oil selective catalytic cracking"*, J Catal, **228**: 234–242.
41. Brunauer S. et al. (1938), *"Adsorption of gases in multimolecular layers"*, J. Am. Chem. Soc., **60**: 309-19.
42. Sing K. et al. (1985), *"Reporting physisorption data for gas/solid system with special reference to the determination of surface area and porosity"*, Pure & Appl. Chem., **57**(4): 603-619.
43. Karasek F. And Clement R., *"Basic gas chromatography-mass spectrometry"*, Elsevier, (1988).
44. Settle F., *"Gas chromatography mass spectrometry"*, Handbook of Instrumental Techniques for Analytical Chemistry, Hites A., Prentice Hall, (1997).
45. Occelli M.L. and Robson H.F. (1992). *"Synthesis of microporous materials"*. Molecular Sieves. Ginter D. e. al. New York, Van Nostrand Reinhold. **1**
46. Robson H. (2001), *"Verified syntheses of zeolitic materials"* Elsevier **2:**159-160.
47. Joyner R. et al. (1999), *"Preparation, characterization, and performance of Fe-ZSM-5 Catalysts"*, J Phys Chem B, **103**: 5963-5976.
48. Siffert S. et al. (2000), *"Alkylation of benzene by propene on a series of Beta zeolites: toward a better understanding of the mechanisms"*, J Mol Catal A-Chem, **153**: 267-279.

49. Gopal V. et al. (2002), *"Vapor-phase alkylation of indole with methanol over zeolites"*, Appl Catal A-Gen, **224**: 121–128.
50. Lutz W. et al. (2007), *"Siliceous extra-framework species in dealuminated Y zeolites generated by steaming"*, Micropor Mesopor Mat, **104**: 171-178.
51. Morales P. et al. (2011), *"Synthesis of FAU(Y)- and MFI(ZSM5)-nanosized crystallites for catalytic cracking of 1,3,5-triisopropylbenzene"*, Catal Today, **166**(1): 25-38.
52. Akbar S. (2010), *"Characterization of beta zeolites by x-ray diffraction, scanning electron microscope, and refractive index techniques"*, J Chem Soc Pakistan, **32**: 592-598.
53. Holland T. and Redfern S. (1997), *"Unit cell refinement from powder diffraction data; the use of regression diagnostics"*, Mineral Mag, **61**: 65-77.
54. Treacy M. and Higgins J. (2001),*"Collection of Simulated XRD Powder Patterns for Zeolites"* Elsevier, Fourth Revised Edition.
55. Turner S. et al. (2008), *"Characterization of chemical properties, unit cell parameters and particle size distribution of three zeolite reference materials"*, Micropor Mesopor Mat, **107**: 252−267.
56. Thomas B. et al. (2006), *"Rare earth exchange (Ce^{3+}, La^{3+} and RE^{3+}) H-Y zeolites as solid acid catalysts for synthesis of linear alkyl benzenes"*, Micropor Mesopor Mat, **95**: 329-338.
57. Ren L. et al. (2007), *"ZSM-5 catalysts modified with lanthanum for catalytic cracking of C4-olefins to propylene"*, Industrial Catalysis **3**: 30-34.
58. Wang J. et al. (2001), *"Aromatization of Propane over La/HZSM-5 Catalyst"*, J. Chin. Rare Earth Soc. **19**: 103-106.
59. Lippmaa E. et al. (1981), *"Investigation of the structure of zeolites by solid-state high-resolution silicon-29 NMR spectroscopy"*, J Am Chem Soc, **103**(17): 4992-4996.
60. Yan Z. et al. (2003), *"On the acid-dealumination of USY zeolite: a solid state NMR investigation"*, J Mol Catal A-Chem, **194** (1-2): 153-167.
61. Klinowski J. (1993), *"Applications of solid-state NMR for the study of molecular sieves"*, Analytica Chimica Acta, **283**(3): 929-965.

62. Klinowski J. (1988), *"Recent advances in solid-state NMR of zeolites"*, Annu Rev Mater Sci, **18**: 189-218.
63. Engelhardt G. et al. (1982), *"High resolution ^{29}Si n.m.r of dealuminated and ultrastable Y-zeolites"*, Zeolites, **2**: 59-62.
64. Hannus I. et al. (1998), *"Solid state MAS NMR investigation of Y-type zeolites reacted with chlorofluorocarbons"*, Appl Catal B-Environ, **17**(1-2): 157-166.
65. Maijanen A. et al. (1994), *"FT-IR and solid-state NMR investigation of surface hydroxyl groups on dealuminated ZSM-5"*, Appl Surf Sci, **75**(1-4): 204-212.
66. Kuehl G. and Timken (2000), *"Acid sites in zeolite beta: effects of ammonium exchange and steaming"*, Micropor Mesopor Mat, **35-36**: 531-532.
67. Nagy J. and Derouane (1988), *"NMR spectroscopy and zeolite chemistry"*, perspectives in molecular sieve science, **368**: 2-31.
68. Jiao J. et al. (2006*)," ^{29}Si and ^{27}Al MAS NMR characterization of non-hydrated zeolites Y upon adsorption of ammonia"*, Micropor Mesopor Mat, **90**(1-3): 246-250.
69. Xu B. et al. (2006), *"Reversibility of structural collapse in zeolite Y: Alkane cracking and characterization"*, J Catal, **241**(1): 66-73.
70. Xu B. et al. (2007), *"Effect of framework Si/Al ratio and extra-framework aluminium on the catalytic activity of Y zeolite"*, Appl Catal A-Gen, **333**(2): 245-253.
71. Wallace O. (2000), *"NMR Spectroscopy applied to zeolite catalysis: progress and prospects"*, Comment Inorg Chem, **22**(1-2): 31-73.
72. Bourgeat-Lami E., et al. (1991), *"Study of the state of aluminium in zeolite beta"*, Appl Catal, **72**(1):139-152.
73. Burevski D. et al. (1994), *"Adsorption on nitrogen on NaX, CaNaX and NaY zeolites"*, Bulletin of the chemists and technology of Macedonia, **13**: 15-18.
74. Ebrahimi A. et al. (2001), *"Modification and optimization of benzene alkylation process for production of ethylbenzene"*, Chem Eng Process, **50**: 31-36.
75. Bellussi G. et al. (1995), *"Liquid-phase alkylation of benzene with light olefins catalyzed by β zeolites"*, J Catal, **157**: 227-234.
76. Yongxin L. et al. (2009), *"Catalytic synthesis of ethylbenzene by alkylation of benzene with diethyl carbonate over HZSM-5"*, Catal Commun, **10**: 702-707.

77. Yan J. et al. (1997), *"Effect of Cu loading and addition of modifiers on the stability of Cu/ZSM-5 in lean NO_x reduction catalysis"*, Catal Today, **33**: 279-290.
78. Ivanov A. et al. (1999), *"Stabilization of CuZSM-5 NOx reduction catalysts with lanthanum"*, Catal Lett, **41**: 47-53.
79. Rokosz M. et al. (1997), *"Spectroscopic studies of the stability of zeolitic deNOx catalysts "*, Catal Today **35**: 65-73.
80. Ivanov A. et al. (1999), *"Adsorption of hydrocarbons by ZSM-5 zeolites with different SiO_2/Al_2O_3 ratios: a combined FTIR and gravimetric study"*, Appl Catal B- Environ, **21**: 243-258.
81. Yanfeng L. et al. (2011), *"DFT study on the accommodation and role of La species in ZSM-5 zeolites"*, Micropor Mesopor Mat, **142**: 621-628.
82. Sugi Y. et al. (2006), *"Shape-selective alkylation and related reactions of mononuclear aromatic hydrocarbons over H-ZSM-5 zeolites modified with lanthanum and cerium oxides"*, Appl Catal A-Gen, **299**: 157-166.
83. Zhao Z. et al. (2006), *"Alkylation of α-methylnaphthalene with long-chain olefins catalyzed by rare earth lanthanum modified HY zeolite"*, J Mol Catal A-Chem, **250**: 50-56.
84. Ding C. et al. (2007), *"Characterization and catalytic alkylation of hydrothermally dealuminated nanoscale ZSM-5 zeolite catalyst"*, Catal Commun, **9**: 487-493.
85. Zhang Y. et al. (2007), *"Effect of La addition on catalytic performance of PtSnNa/ZSM-5 catalyst for propane dehydrogenation"*, Appl Catal A-Gen, **333**: 202-210.
86. Ramaswamy A. (2003), *"Catalysts selectivity: shape selective catalysis over* zeolites", Bulletin of the Catalysis Society of India, **2**: 140-156.
87. Ping L. et al. (2011), *"Rare earth metals ion-exchanged β-zeolites as supports of platinum catalysts for hydroisomerization of n-heptane"*, Chinese J Chem Eng, 19(2): 278-284.
88. Xiaoning W. et al. (2007), *"Effects of light rare earth on acidity and catalytic performance of HZSM-5 zeolite for catalytic cracking of butane to light olefins"*, J Rare Earth, **25**: 321-328.

89. Li S. et al. (2010), *"Extra-framework aluminium species in hydrated faujasite zeolite as investigated by two-dimensional solid-state NMR spectroscopy and theoretical calculations"*, Phys Chem Chem Phys, **12**: 3895-3903.
90. Purdue University SEM Web Site.
91. University of Oxford Surface Analysis Facility Web Site.

Appendix A: XRD peak position

Table A1. Peak position for zeolite Y catalysts.

Index	*NaY*	*NH_4Y*	*HY*	*5%Ce-HY*	*10%Ce-HY*	*5%La-HY*	*10%La-HY*
111	6.31	6.22	6.26	6.21	6.22	6.168	6.24
220	10.23	10.13	10.17	10.09	-	10.06	-
311	11.98	11.88	11.94	11.86	11.79	11.81	11.86
331	15.78	15.61	15.66	15.62	15.61	15.57	15.62
511	18.76	18.68	18.69	18.65	18.64	18.57	18.62
440	20.46	20.31	20.36	20.31	20.32	20.25	20.29
620	22.86	22.71	22.76	22.71	22.74	22.66	22.72
533	23.74	23.57	23.62	23.58	23.59	23.52	23.56
444	24.99	24.94	24.97	24.91	24.93	24.85	24.84
551	25.82	25.69	25.73	25.75	25.74	25.65	25.69
642	27.12	26.95	27.01	26.96	26.99	26.89	26.93
733	29.68	29.53	29.61	29.56	29.58	29.46	29.43
660	30.82	30.64	30.71	30.66	30.69	30.58	30.61
555	31.47	31.28	31.35	31.29	31.31	31.22	31.25
840	32.52	32.34	32.39	32.36	32.36	32.26	32.29
664	34.13	33.95	34.04	34.21	33.98	33.88	33.95
666	37.93	37.74	37.84	37.79	37.04	37.66	37.53

Table A2. Peak position for ZSM-5 zeolite catalysts

Index	*ZSM-5*	*NH_4Z5M-5*	*HZSM-5*	*5%Ce-HZSM-5*	*10%Ce-HZSM-5*	*5%La-HZSM-5*	*10%La-HZSM-5*
101	7.98	7.91	7.93	7.95	7.97	7.93	7.95
200	8.84	8.78	8.79	8.91	8.93	8.89	8.82
020	8.97	9.06	9.07	9.09	9.13	9.08	9.11
210	9.68	9.73	9.75	9.78	9.82	9.76	9.77
102	13.93	13.89	13.91	13.93	13.96	13.91	13.93
112	14.77	14.75	14.76	14.78	14.81	14.76	14.78
103	20.32	20.29	20.32	20.35	20.37	20.34	20.34
013	20.66	20.82	20.83	20.88	20.87	20.82	20.85
123	22.15	22.12	22.15	22.23	22.18	22.14	22.17
501	23.09	23.04	23.05	23.08	23.10	23.05	23.07
051	23.15	23.24	23.26	23.28	23.31	23.26	23.29
303	23.91	23.86	23.89	23.91	23.93	23.89	23.91
133	24.39	24.34	24.37	24.39	24.42	24.37	24.38
432	25.86	25.85	25.86	25.88	25.91	25.84	25.88
352	29.24	29.22	29.24	29.26	29.28	29.24	29.25

Table A3. Peak position of HBeta zeolite catalysts.

Index	***HBeta***	***10%La-HBeta***	***5%La-HBeta***	***10%Ce-HBeta***	***10%Ce-HBeta***
101	7.74	7.89	7.96	7.87	7.89
004	13.51	13.54	13.65	13.58	13.56
201	14.76	14.83	14.74	14.79	14.68
205	21.84	21.53	21.66	21.81	21.68
302	22.85	22.64	22.69	22.66	22.65
216	25.61	25.62	25.45	25.53	25.36
008	27.31	27.24	27.32	27.23	27.29
306	28.58	28.75	28.86	28.49	28.62
209	33.35	33.37	33.14	33.18	33.22
432	36.19	36.51	36.31	36.38	36.42
600	43.73	43.74	43.76	43.73	43.81

Appendix B: Unit-cell parameters

Table B1. Unit-cell parameters of zeolite Y catalysts (Crystal system: cubic).

Catalyst	*a=b=c* (Å)	*Error*	*V* (Å^3)	*Error V*
NaY	24.60003	0.00115	14886.9915	2.0884
NH_4Y	24.73541	0.00116	15134.1312	2.1356
HY	24.68245	0.00116	15037.1238	2.1171
5%Ce-HY	24.70445	0.00116	15077.3763	2.1248
10%Ce-HY	24.77999	0.00117	15216.1075	2.1612
5%La-HY	24.79601	0.00117	15245.6398	2.1570
10%La-HY	24.78033	0.00117	15216.7348	2.1613

Table B2. Unit-cell parameters of ZSM-5 zeolite catalysts. (Crystal system: orthorhombic).

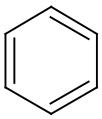
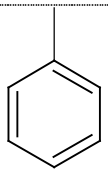
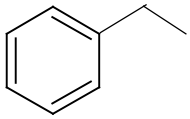
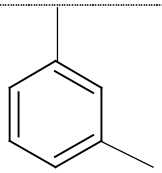
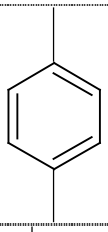
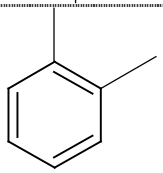
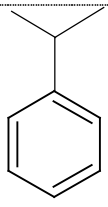
Catalyst	*a* (Å)	*Error a*	*b* (Å)	*Error b*	*c* (Å)	*Error c*	*V* (Å^3)	*Error V*
ZSM-5	20.21843	0.00369	20.05305	0.00343	13.2113	0.00153	5356.4438	1.1456
NH_4ZSM-5	20.19927	0.00368	19.93584	0.00338	13.35765	0.00157	5378.9848	1.1457
HZSM-5	20.18467	0.00367	19.91926	0.00338	13.34348	0.00157	5364.9275	1.1418
5%Ce	20.14289	0.00365	19.90687	0.00337	13.32358	0.00156	5342.5154	1.1354
10%Ce	20.11041	0.00364	19.88685	0.00337	13.31626	0.00156	5325.6085	1.1301
5%La	20.17225	0.00366	19.92222	0.00338	13.34467	0.00157	5362.9022	1.1410
10%La	20.16587	0.00366	19.90247	0.00337	13.32875	0.00156	5349.5037	1.1375

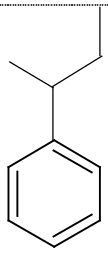
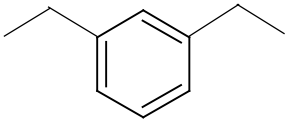
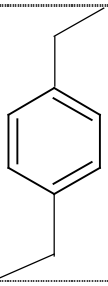
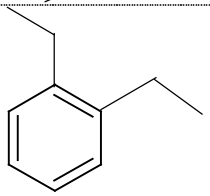
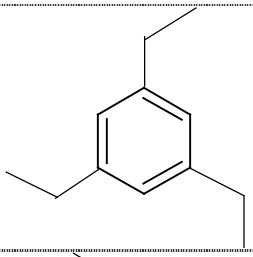
Table B3. Unit-cell parameters of HBeta zeolite catalysts (Crystal system: tetragonal).

Catalyst	*a=b* (Å)	*Error*	*c* (Å)	*Error c*	*Volume* (Å^3)	*Error V*
HBeta	12.48165	0.00095	26.47509	0.00280	4124.596	0.6724
5%Ce	12.48972	0.00095	26.70683	0.00285	4166.082	0.6812
10%Ce	12.4495	0.00095	26.57487	0.00282	4118.838	0.6708
5%La	12.48522	0.00095	26.66051	0.00284	4155.857	0.6790
10%La	12.46823	0.00095	26.64485	0.00284	4142.122	0.5759

Appendix C: GC/MS data

Table C1. The GC/MS retention time of the B/E alkylation products.

	Component	***Retention time (min)***	***Structure***
1	Benzene	2.1	
2	Toluene	3.045	
3	Ethylbenzene	4.26	
4	m-Xylene	4.414	
5	p-Xylene	4.425	
6	o-Xylene	4.76	
7	Cumene	5.2	

8	1-methylpropylbenzene	6.57	
9	1,3 diethylbenzene	7.18	
10	1,4 diethylbenzene	7.34	
11	1,2 diethylbenzene	7.38	
12	1,3,5 triethylbenzene	10.09	
13	1,2,4,5 tetraethylbenzene	12.36	